

Sheffield Hallam University

Evaluation of the Raman spectroscopy technique for in situ corrosion studies.

LARROUMET, Damien.

Available from the Sheffield Hallam University Research Archive (SHURA) at:

<http://shura.shu.ac.uk/19941/>

A Sheffield Hallam University thesis

This thesis is protected by copyright which belongs to the author.

The content must not be changed in any way or sold commercially in any format or medium without the formal permission of the author.

When referring to this work, full bibliographic details including the author, title, awarding institution and date of the thesis must be given.

Please visit <http://shura.shu.ac.uk/19941/> and <http://shura.shu.ac.uk/information.html> for further details about copyright and re-use permissions.

Adsetts Centre City Campus
Sheffield S1 1WB

101 810 716 9



Return to Learning Centre of issue
Fines are charged at 50p per hour

REFERENCE

ProQuest Number: 10697247

All rights reserved

INFORMATION TO ALL USERS

The quality of this reproduction is dependent upon the quality of the copy submitted.

In the unlikely event that the author did not send a complete manuscript and there are missing pages, these will be noted. Also, if material had to be removed, a note will indicate the deletion.



ProQuest 10697247

Published by ProQuest LLC (2017). Copyright of the Dissertation is held by the Author.

All rights reserved.

This work is protected against unauthorized copying under Title 17, United States Code
Microform Edition © ProQuest LLC.

ProQuest LLC.
789 East Eisenhower Parkway
P.O. Box 1346
Ann Arbor, MI 48106 – 1346

**Evaluation of the Raman spectroscopy technique
for in situ corrosion studies**

By

Damien Larroumet

A thesis submitted in partial fulfilment of the requirements
of Sheffield Hallam University
for the degree of Doctor of Philosophy



April 2005

Contents

ABSTRACT	VI
CHAPTER 1. INTRODUCTION	1
1.1. OBJECTIVES	1
1.1.1. <i>'In situ' investigation without using SERS</i>	1
1.1.2. <i>Localised corrosion studies</i>	2
1.1.3. <i>Corrosion kinetics investigation</i>	2
1.1.4. <i>Observation of different corrosion behaviour</i>	3
1.2. HOW THE THESIS IS CONSTRUCTED.....	3
1.3. REFERENCES	4
CHAPTER 2. RAMAN SPECTROSCOPY	7
2.1. INTRODUCTION AND HISTORY	7
2.2. THE RAMAN EFFECT	8
2.3. QUANTUM MECHANICAL THEORY	9
2.3.1. <i>Classical theory; Molecular Polarisability</i>	10
2.3.2. <i>Selection rules and intensity</i>	11
2.3.2.1. Selection rules	11
2.3.2.2. Intensity	12
2.3.3. <i>Resonance effect</i>	14
2.3.4. <i>Fluorescence</i>	14
2.3.5. <i>Surface Enhanced Raman Spectroscopy (SERS)</i>	15
2.4. DATA COLLECTION AND ANALYSIS	16
2.4.1. <i>Experimental Raman Spectrum</i>	16
2.4.2. <i>Spectra analysis</i>	18
2.4.2.1. Spectra smoothing	18
2.4.2.2. Band fitting.....	20
2.5. THE RAMAN MICROSCOPE SYSTEM.....	21
2.5.1. <i>System overview</i>	22
2.5.2. <i>Laser</i>	23
2.5.3. <i>Holographic Notch Filters</i>	23
2.5.4. <i>Microscope objective</i>	24
2.5.4.1. Focal point.....	24
2.5.4.2. Long working distance objectives.....	25

2.5.5. <i>Diffraction gratings</i>	25
2.5.6. <i>Charged Couple Device (CCD) detector</i>	25
2.5.7. <i>Software parameters</i>	26
2.5.7.1. <i>Scanning mode and spectral range</i>	26
2.5.7.2. <i>Exposure time and laser power</i>	27
2.6. REFERENCES	27
CHAPTER 3. CORROSION	30
3.1. INTRODUCTION AND DEFINITION.....	30
3.2. BASIC ELECTROCHEMICAL CONCEPTS.....	31
3.2.1. <i>Behaviour of metal in an environment</i>	31
3.2.2. <i>The corrosion cell</i>	31
3.2.3. <i>Electrochemical reactions</i>	32
3.2.4. <i>Electrode Potential and Polarisation</i>	32
3.3. THE DIFFERENT TYPES OF CORROSION.....	33
3.3.1. <i>Uniform corrosion</i>	33
3.3.2. <i>Galvanic corrosion</i>	33
3.3.3. <i>Pitting corrosion</i>	34
3.4. THEORETICAL POTENTIAL-PH DIAGRAMS (POURBAIX DIAGRAM)	35
3.5. TECHNIQUES USED TO EVALUATE AND STUDY CORROSION	36
3.5.1. <i>Intrusive techniques</i>	37
3.5.1.1. <i>Tafel plot</i>	37
3.5.1.2. <i>Polarisation resistance</i>	38
3.5.1.3. <i>Potentiodynamic anodic polarisation</i>	38
3.5.1.4. <i>Cyclic polarisation</i>	39
3.5.2. <i>Scanning electrode techniques</i>	39
3.5.2.1. <i>Scanning reference electrode technique</i>	39
3.5.2.2. <i>Scanning vibrating electrode technique</i>	40
3.5.2.3. <i>Scanning Kelvin Probe (SKP)</i>	40
3.5.3. <i>Imaging techniques for corrosion analysis</i>	40
3.5.3.1. <i>Electron microscopy techniques</i>	40
3.5.3.2. <i>Atomic Force Microscopy (AFM)</i>	41
3.6. COMPARISON BETWEEN RAMAN SPECTROSCOPY AND OTHER CONVENTIONAL TECHNIQUES FOR CORROSION STUDIES.	41

3.7. APPLICATION OF RAMAN TO CORROSION STUDIES	42
3.7.1. <i>Product identification</i>	42
3.7.1.1. Iron oxides and oxyhydroxides	42
3.7.1.2. Green rust	44
3.7.1.3. Mixture identification.....	45
3.7.2. <i>Quantitative information and mapping</i>	45
3.7.3. <i>Raman and Corrosion conditions</i>	46
3.7.4. <i>Utilisation of SERS for corrosion studies</i>	47
3.8. REFERENCES	48

CHAPTER 4. EXPERIMENTAL APPROACHES AND TECHNICAL CHALLENGES.. 52

4.1. TECHNICAL CHALLENGES.....	52
4.1.1. <i>Sample degradation</i>	52
4.1.1.1. Introduction	52
4.1.1.2. Transformation of magnetite under laser excitation.....	53
4.1.1.3. Temperature calculations (Stokes / Anti Stokes ratio).....	55
4.1.2. <i>Compound identification and quantification</i>	58
4.1.2.1. Calibration set preparation	58
4.1.2.2. Results and discussion.....	59
4.1.2.3. Conclusions	62
4.1.3. <i>In-situ experiment</i>	63
4.1.4. <i>Effect of the electrochemical factors</i>	64
4.1.4.1. Chloride contamination	64
4.1.4.2. Effect of the scan rate on potentiodynamic studies	64
4.1.5. <i>Nature and size of the working electrode</i>	67
4.1.5.1. Experimental	67
4.1.5.2. In situ analysis	68
4.1.5.3. Ex situ analysis	70
4.1.5.4. System assessment	71
4.2. EXPERIMENTAL.....	73
4.2.1. <i>Iron in 3.5% NaCl solution</i>	73
4.2.1.1. Simple iron wire system (25 μm)	73
4.2.1.2. Twin iron wire model system.....	74
4.2.2. <i>Iron in buffer solution</i>	75
4.2.2.1. Sample.....	75

4.2.2.2. Solutions.....	76
4.2.2.3. Cyclic polarisation.....	76
4.3. REFERENCES	76
CHAPTER 5. IRON MODEL SYSTEMS IN SODIUM CHLORIDE SOLUTION	77
5.1. SIMPLE IRON WIRE MODEL SYSTEM	78
5.1.1. <i>Open circuit potential analysis</i>	78
5.1.1.1. Raman investigation.....	78
5.1.1.2. Comparison between Raman and OCP data.....	79
5.1.2. <i>Polarisation</i>	81
5.1.3. <i>Corrosion processes</i>	84
5.2. TWIN IRON WIRE MODEL SYSTEM	85
5.2.1. <i>Evolution of the electrodes surfaces with time</i>	86
5.2.1.1. Raman analysis.....	86
5.2.1.2. Optical analysis	88
5.2.2. <i>Effect of the potential applied</i>	90
5.2.2.1. The overlapping band system.....	90
5.2.2.2. Fitting process	91
5.2.2.3. Results interpretation.....	95
5.2.3. <i>Dry sample analysis</i>	96
5.3. SUMMARY AND CONCLUSIONS.....	99
5.3.1. <i>Simple iron model system</i>	99
5.3.2. <i>Twin iron model system</i>	100
5.4. REFERENCES	100
CHAPTER 6. IRON DISC IN BUFFER SOLUTIONS	101
6.1. IRON IN BORATE BUFFER SOLUTION	101
6.1.1. <i>Open circuit potential</i>	102
6.1.2. <i>Anodic oxidation</i>	104
6.1.2.1. Cyclic voltammograms.....	104
6.1.2.2. Cyclic voltammograms interpretation.....	107
6.1.2.3. Interpretation of the lack of Raman activity.....	108
6.2. IRON IN CARBONATE/BICARBONATE BUFFER SOLUTION	111
6.2.1. <i>Open circuit potential</i>	111
6.2.2. <i>Cyclic polarisation</i>	115
6.2.3. <i>Anodic waves (-700 mV and -320 mV)</i>	121

6.2.4. <i>Model representation of the passive film formation</i>	122
6.3. IRON IN POTASSIUM PHOSPHATE BUFFER SOLUTION	124
6.3.1. <i>Oxidation at Open Circuit Potential (OCP)</i>	124
6.3.1.1. Raman data	124
6.3.1.2. Potential evolution.....	125
6.3.1.3. Optical analysis	127
6.3.1.4. Dry sample analysis.....	128
6.3.2. <i>Cyclic polarisation</i>	130
6.3.3. <i>Anodic waves identification.</i>	132
6.3.3.1. Raman data	132
6.3.3.2. Band integration	134
6.3.3.3. Current evolution.....	135
6.3.4. <i>Pitting experiment</i>	136
6.4. SUMMARY	140
6.5. REFERENCES	141
CHAPTER 7. GENERAL DISCUSSION	144
7.1. POTENTIAL ADVANTAGES OF THE RAMAN TECHNIQUE.....	145
7.2. CHALLENGES OF USING RAMAN SPECTROSCOPY	145
7.3. STUDY OF PURE IRON OXIDATION PROCESSES IN DIFFERENT SOLUTIONS.	147
7.3.1. <i>Iron in Sodium Chloride solution</i>	147
7.3.1.1. Simple iron wire model system	147
7.3.1.2. Twin iron model system	148
7.3.2. <i>Iron in borate buffer solution</i>	149
7.3.3. <i>Iron in carbonate buffer solution</i>	149
7.3.4. <i>Iron in phosphate buffer solution</i>	150
7.4. FUTURE WORK	150
7.4.1. <i>Sample heterogeneity</i>	151
7.4.2. <i>Study of Stress corrosion cracking</i>	151
7.4.3. <i>Study of alternative conversion coatings for aluminium</i>	151
7.4.4. <i>Coupling of Raman spectroscopy and ESEM</i>	152

Abstract

Laser Raman spectroscopy has been widely used for corrosion studies but it appeared that, in most of the cases, the sample under investigation was removed from the media in which it has been corroded prior the Raman investigation. The necessity of running 'ex situ' analysis was often due to the poor Raman response due to the absorption of the scattered light by the solution. A large number of studies have previously been conducted after increasing the amount of scattered light by using surface enhanced Raman spectroscopy. Unfortunately, removing the sample from the media in which it has been corroded, or applying metal islands onto the sample under investigation may have a significant effect on the sample's electrochemical reactions. Therefore, the objective of the current work was to evaluate the *possibility of using conventional Raman spectroscopy for 'in situ' corrosion studies.*

The first stage of the research was *to identify the potential advantages and the limitations of the technique* itself. Once these parameters were identified, it was necessary to *assess the technique* through different experimental tests. Two model systems, both based on pure iron wires, were exposed to 3.5 % NaCl solution. From both systems, we showed that first a layer of lepidocrocite (γ -FeOOH) was developing with time at open circuit potential and second that the anodic reaction started with the formation of magnetite which later oxidised to lepidocrocite. Further experiments on iron, performed in three different buffer solutions (borate, carbonate and phosphate) permitted us to observe different oxidation reactions. Although no Raman data could be obtained from the iron sample immersed in borate solution, it was possible firstly to identify the reactions associated to the anodic / cathodic waves visible on the cyclic voltammograms and second to follow the development of the oxide layers and propose a model representation of the passive film. The passive film developed in phosphate buffer solution was identified as a mixture of $Fe_3(PO_4)_2 \cdot 8H_2O$ and $FePO_4 \cdot xH_2O$. Further pitting experimental tests examined the electrochemical resistance of the passive film developed in such solution. It has therefore been shown through the series of experiments describe here that conventional Raman spectroscopy is an appropriate tool to study, in situ, corrosion processes.

The large number of publications which discuss about the use of Raman for corrosion studies (1-11) have showed that laser Raman spectroscopy has the potential to be an important tool for the study of electrochemical systems and processes. The large utilisation of such technique for corrosion studies is mainly due to the molecular specific information that it provides on the structure of the compounds generated at the substrate / solution interface, and the capability of analysing compounds on a microscopic scale.

1.1. Objectives

1.1.1. 'In situ' investigation without using SERS

Used predominantly on samples removed from the media, in which they have been corroded, Raman spectroscopy can be used 'in situ' by focusing a laser source onto the sample studied, through a solution (3,12-17). Unfortunately, the presence of the solution above the sample drastically reduces the amount of scattered light collected by the spectrometer.

Therefore, to improve the quality of the signal, several studies have been achieved in and ex situ, by employing surface enhanced Raman spectroscopy (SERS) (6,8,18-23). The surface enhancement is achieved by depositing a layer of silver, gold or copper onto the sample. Even if these SERS studies gave a large amount of information, they were limited by a certain number of drawbacks, such as the creation of a galvanic cell that can affect the corrosion behaviour of the sample studied (section 3.7.4 and 6.1.2.3).

Consequently, it became difficult to predict whether the corrosion processes were real or affected by the analysis method. Therefore, it appeared clear to us that if the Raman spectroscopy technique had to be used to its full potential, it was necessary to evaluate the possibility to run *in situ analysis without using surface enhancement* and obtain the maximum information from the data recorded.

1.1.2. Localised corrosion studies

One of the main advantages of the Raman spectroscopy technique is the ability to study a surface on a microscopic scale. This advantage is due to the utilisation of an optical microscope through which the laser light is focused onto the sample studied. As shown in chapter 3, different types of corrosion can occur. These types of corrosion are strongly linked to the nature of the metal and the environment in which it is susceptible to corrode. Therefore, the use of Raman spectroscopy allows the evolution of particular surfaces to be studied. It is then possible to follow the formation of corrosion products onto an isolated anodic site and observe localised corrosion phenomenon such as pitting corrosion (section 3.3.3). Moreover, since the Raman microscope is equipped with a two dimensional mapping stage, it is possible to analyse a particular corroded area and create a map showing the spatial distribution of the different oxides. An introduction to the experiments used to achieve the observation of localised corrosion processes is presented in section 1.2.

1.1.3. Corrosion kinetics investigation

As identified above, the main advantage of Raman spectroscopy is its ability to identify the different oxides present on a sample. Moreover, since the intensity of the Raman spectrum recorded is directly linked to the amount of product under investigation, Raman spectroscopy permits both a qualitative and a quantitative analysis of the system under investigation. Applied to the analysis of a system in constant evolution, such as a corroding metal, the record of successive spectra permits to follow with time, the formation / conversion of particular molecular species. To evaluate the possibility to obtain information about the kinetics of the corrosion reactions, different model systems, based on pure iron, have been used.

Two different approaches were taken to change the kinetic of the corrosion reactions. First, electrochemical drivers were used. These drivers consisted in accelerating / reducing the surface evolution with time by driving the current through the electrode studied. It was then possible to put the sample in conditions in which the oxidation or reduction reactions could occur, allowing the formation / conversion of the corrosion product to be studied.

Second, the introduction of chloride ions into the solution allowed us to increase the corrosion rate and develop the local activity of the sample studied. This has been

achieved here in section 6.3.4, where the pitting behaviour of iron in phosphate buffer solution has been studied

1.1.4. Observation of different corrosion behaviour

As shown in chapter 3, and more particularly in the Pourbaix diagram (figure 3.3), a metal immersed in solution can react in three different ways. It can stay immune, active or passivate. When it stays immune, no oxidation reactions are occurring on the surface, and it is then impossible to follow any change by Raman spectroscopy, since no product is developing at the sample surface. When it is active or, when the metal passivates, the corrosion activity can be picked up by Raman and it is then possible to follow the evolution of the surface and the development of a passive film. The behaviour of the system under investigation depends on the nature of the environment to which it is exposed. Therefore, the choice of the solution (e.g. the pH, the nature of the ions present, etc...) will have a significant effect on the sample behaviour. This has been showed in chapter 6 where an iron disc electrode has been exposed to three different solutions in which the corrosion processes were entirely different.

1.2. *How the thesis is constructed*

Since the objectives had to be tackled by taking into account two different approaches (Raman and corrosion), it was necessary to present the Raman technique separately. This has been achieved in chapter 2 where, a brief history of the technique is introduced. Once the Raman effect, as well as the quantum mechanical theory had been explained, a presentation of the data collection and the spectral analysis is given, before introducing the metal/electrolyte systems used for the current work.

In chapter 3, the basic electrochemical concepts and the different types of corrosion are presented. This is followed by an introduction to the Pourbaix diagram and a presentation of the different corrosion analysis techniques. Once the comparison between the conventional techniques and Raman spectroscopy is achieved, a summary of the previous work by different research groups is presented.

Before starting to investigate the different corrosion behaviour by Raman, the technical challenges associated to the use of Raman spectroscopy had to be identified. These challenges, presented in chapter 4, are particularly related to:

- The possible sample degradation due to the heating effect produced by the laser.
- The identification and quantification of the oxide in situ (sometimes difficult, due to the fact that the sample studied were subject to Resonance enhancement)
- The challenges created by the analysis on a microscopic scale of a large and inhomogeneous system.

To evaluate the feasibility of analysing corrosion reactions using 'in situ' Raman spectroscopy, a pure iron system was immersed in different solutions. The analysis conducted in sodium chloride allowed the growth or breakdown of a passive film to be studied at open circuit potential and during anodic polarisation at -300 mV. A further set of experiments using a "twin iron model system" allowed the isolation of the anodic and cathodic sites, from which a study of the evolution of corrosion product with time was possible.

Once the corrosion reaction of iron in sodium chloride was analysed, the behaviour of iron in three different buffer solutions (borate, carbonate and phosphate solutions) was studied. The behaviour of iron in these different solutions has been initially studied at open circuit potential and then by polarising at different potentials, identified by cyclic voltammetry. The results and interpretation of such systems are presented in chapter 5 and 6.

Finally, in chapter 7, the results and conclusions of the work described in this thesis are presented. These results permitted us to show that conventional Raman spectroscopy is an appropriate technique for in situ corrosion studies. Despite the difficulties associated with the technique, the molecular information obtained, in situ, from pure iron model systems allowed the formation, identification and conversion of the different oxides to be made with time. Therefore it is possible to run 'in situ' (without using SERS) conventional Raman spectroscopy to obtain information on the kinetics, the spatial distribution of the corrosion products and reaction processes of a metal immersed in solution.

1.3. References

- (1) Tomandl A, Wolpers M, Ogle K. The alkaline stability of phosphate coatings II: in situ Raman spectroscopy. *Corrosion Science* 2004 4; 46 (4): pp. 997-1011.

- (2) Odziemkowski MS, Jedral W, Bonin PML. Response to discussion on "Electrochemical and Raman spectroscopic studies of the influence of chlorinated solvents on the corrosion behaviour of iron in borate buffer and in simulated groundwater" [Corrosion Science 42 (2000) 1921-1939]. Corrosion Science 2002 5; 44 (5): pp. 1159-1162.
- (3) Maslar JE, Hurst WS, Bowers WJ, Hendricks JH. In situ Raman spectroscopic investigation of zirconium-niobium alloy corrosion under hydrothermal conditions. Journal of Nuclear Materials 2001 10; 298 (3): pp. 239-247.
- (4) Ramsey JD, Xia L, Kendig MW, McCreery, R.L. . Raman spectroscopic analysis of the speciation of dilute chromate solutions. Corrosion Science 2001 8; 43 (8): pp. 1557-1572.
- (5) Huang BX, Tornatore P, Li Y. IR and Raman spectro electrochemical studies of corrosion films on tin. Electrochimica Acta 2001 1/1; 46 (5): pp. 671-679.
- (6) Melendres CA, Pankuch M, Li YS, Knight RL. Surface enhanced Raman spectroelectrochemical studies of the corrosion films on iron and chromium in aqueous solution environments. Electrochimica Acta 1992 12; 37 (15): pp. 2747-2754.
- (7) Thierry D, Persson D, Leygraf C, Boucherit N, Hugot-le Goff A. Raman spectroscopy and XPS investigations of anodic corrosion films formed on Fe-Mo alloys in alkaline solutions. Corrosion Science 1991; 32 (3): pp. 273-281.
- (8) Oblonsky LJ, Devine TM. A Surface enhanced Raman spectroscopic study of the passive films formed in borate buffer on iron, nickel, chromium and stainless-steel. Corrosion Science 1995 JAN; 37 (1): pp. 17-41.
- (9) Maslar JE, Hurst WS, Bowers WJ, Hendricks JH, Aquino MI. In situ Raman spectroscopic investigation of aqueous iron corrosion at elevated temperatures and pressures. Journal of the Electrochemical Society 2000 JUL; 147 (7): pp. 2532-2542.
- (10) Ohtsuka T, Matsuda M. In situ Raman spectroscopy for corrosion products of zinc in humidified atmosphere in the presence of sodium chloride precipitate. Corrosion 2003 MAY; 59 (5): pp. 407-413.
- (11) Boucherit N, Hugot-Le Goff A, Joiret S. Influence of Ni, Mo, and Cr on Pitting Corrosion of Steels Studied by Raman-Spectroscopy. Corrosion 1992 JUL; 48 (7): pp. 569-579.
- (12) Sourisseau C, Cruege F, Gorochov O. In-situ Raman investigation of photo-corrosion processes at p- and n-type WS₂ electrodes in acid solutions. Journal of Electroanalytical Chemistry 1991 6/25; 308 (1-2): pp. 239-253.
- (13) Thanos ICG. In situ Raman and other studies of electrochemically oxidized iron and iron-9% chromium alloy. Electrochimica Acta 1986 7; 31 (7): pp. 811-820.
- (14) Perardi A, Zoppi A, Castellucci E. Micro-Raman spectroscopy for standard and in situ characterisation of painting materials. Journal of Cultural Heritage 2000 8/1; 1 (Supplement 1): pp. S269-S272.
- (15) Simard S, Odziemkowski MS, Irish DE, Brossard L, Menard H. In situ micro-Raman spectroscopy to investigate pitting corrosion product of 1024 mild steel in phosphate and bicarbonate solutions containing chloride and sulfate ions. Journal of Applied Electrochemistry 2001 AUG; 31 (8): pp. 913-920.

- (16) Fanigliulo A, Bozzini B. An electrochemical and in-situ Raman investigation of the electrodeposition of gold from sulphite electrolyte. *Trans IMF* 2002; 80 (4): pp. 132-136.
- (17) Threthewey KR, Chamberlain J. *Corrosion for students of science and engineering*. 3rd ed. Singapore: Longman Scientific & Technical; 1992.
- (18) Baek W-, Kang T, Sohn H-, Kho YT. In situ surface enhanced Raman spectroscopic study on the effect of dissolved oxygen on the corrosion film on low carbon steel in 0.01 M NaCl solution. *Electrochimica Acta* 2001 4/ 30; 46 (15): pp. 2321-2325.
- (19) Simpson LJ, Melendres CA. Temperature dependence of the surface enhanced Raman spectroelectrochemistry of iron in aqueous solutions. *Electrochimica Acta* 1996, 41 (10): pp. 1727-1730.
- (20) Gui J, Devine TM. The influence of sulphate ions on the surface enhanced Raman spectra of passive films formed on iron. *Corrosion Science* 1994 MAR; 36 (3): pp. 441-462.
- (21) Rubim JC, Dunnwald J. Enhanced Raman scattering from passive film on silver-coated iron electrodes. *Journal of electroanalytical chemistry* 1989; 258: pp. 327-344.
- (22) Aramaki K, Uehara J. The surface enhanced Raman scattering spectra of pyridine adsorbed on an iron surface. *Journal of Electrochemical society* 1990; 137 (1): pp. 185-187.
- (23) Gui J, Devine TM. Obtaining surface enhanced Raman spectra from the passive film on iron. *Journal of the electrochemical society* 1991; 138 (5): pp. 1376-1384.

Chapter 2. Raman Spectroscopy

2.1. Introduction and history

First predicted in 1922 by Brillouin (1) and in 1923 by A. Smekal (2), the Raman effect, a light-scattering phenomenon, was observed five years later by C.V. Raman and K.S. Krishanan (3). The first experiments were carried out using focussed sunlight and filters and relied on visual observation of colour changes in the scattered light. Later, C. Raman, recorded spectra of several liquids including benzene and carbon tetrachloride using a mercury lamp and a spectrograph. The experiments used 600 mL of sample and required a 24 hour exposure to obtain measurable spectra (4). In 1931, Raman was awarded the Nobel Prize in Physics for the discovery and exploration of the phenomenon.

Due to the relatively weak effect (10^{-8} of the intensity of the incident exciting radiation) and to the low stability and intensity of the source, Raman spectroscopy was very difficult to realise, particularly in comparison with the faster and less expensive infrared spectroscopy. Therefore, it was not until the 1960's, when a major improvement occurred, that the application of Raman spectroscopy analysis increased considerably. By January 1969, 500 to 600 papers had been published (5). The development of high intensity visible laser source, producing a monochromatic, coherent, narrow beam source, offered the possibility to easily analyse small samples, solids, liquids and gases, as well as samples at high temperature, in dilute solution and in a variety of other non standard conditions.

Since then, optics and microelectronics development have further improved the technique. Coupling of a microscope to the spectrometer (6), utilisation of holographic notch filters, charge coupled device detector, digital data acquisition and computer processing have replaced cameras and photographic plates. Nowadays, a Raman spectrum, can be recorded from micrometer-sized particles in few seconds and the reduction of the acquisition time, on the top of being a help to routine analysis, opens up the possibility of time resolved spectroscopy and kinetic studies. The technique may also be used for 2 dimensional analysis like mapping and imaging (7-10).

Even if Raman spectroscopy is mainly considered as a research tool, the evolution of the technology, giving user friendly spectrometers is now becoming standard technique in academic and industrial analytical laboratories, and industrial plants.

Raman spectroscopy theory has been largely presented in the literature. Therefore, the approach taken here is a simplified outline, permitting the understanding of the essential nature of the technique. Nevertheless, some points essential to the understanding of the application of the process to the corrosion studies will be developed in more details in this chapter (resonance, fluorescence, etc.). Approaches used by others in reviewing this material have been used, principally those of Long (11), Grasselli and Bulkin (12), Skoog and West (13) or Banwell (14).

2.2. The Raman Effect

Raman spectroscopy depends on the frequency of the light scattered by molecules as they undergo rotations and vibrations. When monochromatic light of frequency ν_0 , too low in energy to excite an electronic transition, is directed at a cell containing a dust-free transparent substance, most of the light passes through unaffected. Some of the light however is scattered by the sample molecules in all direction.

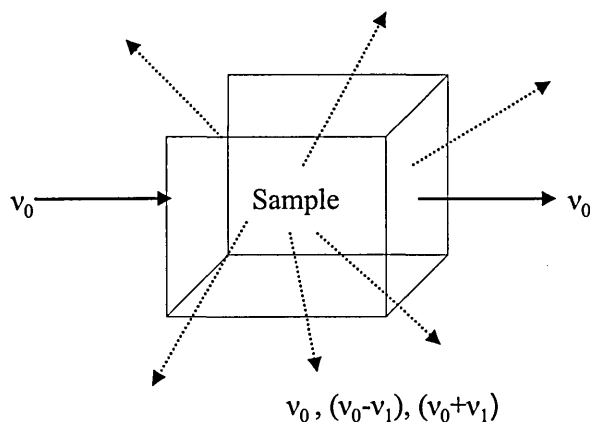


Figure 2.1. Appearance of scattered light with frequencies ν_0 , $(\nu_0 + \nu_1)$ and $(\nu_0 - \nu_1)$.

The scattered light, less than 0.1% of the original radiation, contains photons which have the same frequency ν_0 as the incident light (elastic scattering), but in addition the emergent radiation contains other frequencies due to inelastic scattering such as $(\nu_0 + \nu_1)$

and $(\nu_0 - \nu_1)$ where $\pm \nu_1$ are frequencies of the transition between the ground state and the first vibrational state (see Figure 2.1).

2.3. Quantum mechanical theory

The quantum theory is by far the simplest way of thinking about the mechanism of Raman spectroscopy. When a photon of energy $h\nu_0$ interacts with a molecule having vibrational energy levels, $\nu_0, \nu_1 \dots \nu_n$, (see Figure 2.2) it is transmitted, refracted, reflected or even scattered and a small portion of the energy is lost to the energy levels of the molecule. The Raman effect is a scattering process where the molecule can gain or lose amounts of energy only in accordance with the quantum laws; i.e., its energy change, ΔE joules, must be the difference in energy between two of its allowed states. In order to return to a more stable state (lower energy level), a molecule will release photons in two different ways. Firstly, it can return directly to the ground state emitting light of same energy (Rayleigh scattering) as the excitation source (or frequency since energy and frequency are linked by the Planck constant: $E=h\nu_0$) and secondly, it can relax producing two different types of inelastic scattering: Stokes and anti-Stokes scattered lines.

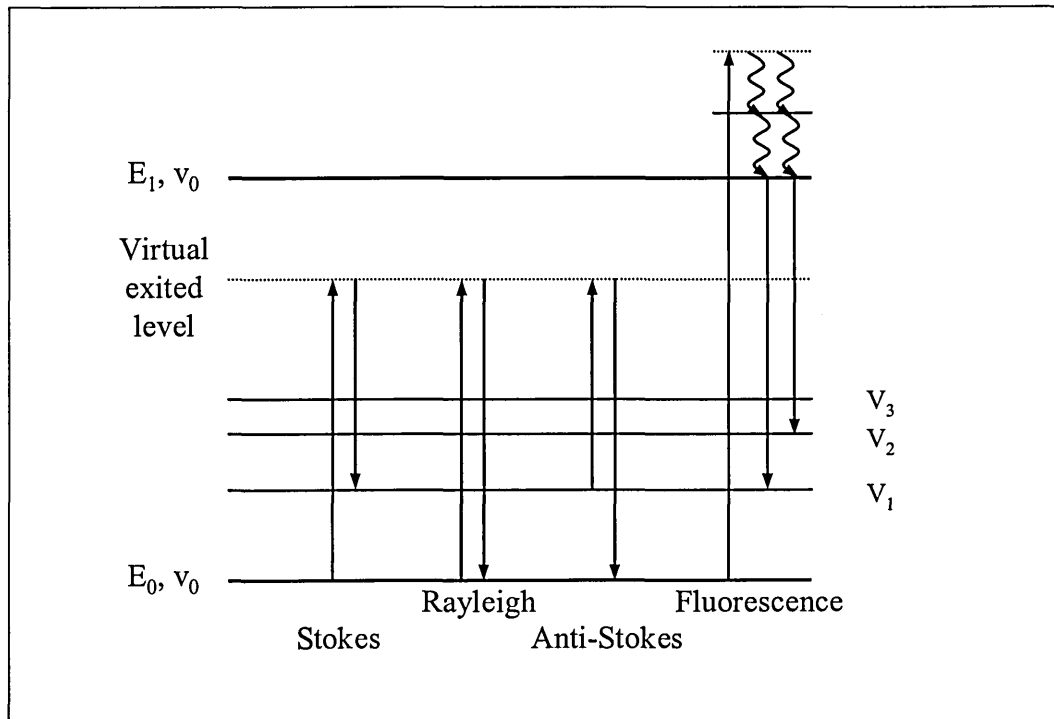


Figure 2.2. Diagrammatic representation of an energy model of the different possible scattering

Stokes and anti-Stokes lines are symmetrically shifted either side of the Rayleigh line (ν_0). Stokes lines to lower energy ($\nu_0 - \nu_{\text{vib}}$) are more intense than anti-Stokes lines ($\nu_0 + \nu_{\text{vib}}$) because the scattered photons are coming from the ground state which is more populated at ambient temperature.

If the energy produced by the monochromatic source corresponds with the energy difference between the ground level (E_0) and the first electronic excited state (E_1), fluorescence occurs. This phenomenon, much stronger than Raman scattering, is presented in section 2.3.4.

2.3.1. Classical theory; Molecular Polarisability

In all spectroscopies, there is a mechanism by which the incident radiation interacts with the molecular energy levels. For IR absorption spectroscopy, it is the change in the dipole moment during the vibration. For Raman spectroscopy, the mechanism originates from the general phenomenon of light scattering, in which the electromagnetic radiation interacts with a deformable electron cloud.

When a diatomic molecule is placed into an electric field it suffers some distortion. The positively charged nuclei are then attracted towards the negative pole of the field and the electrons are attracted to the positive pole. Suppose that the incident electric field associated with the light, which is a wave phenomenon is represented in equation 2.1.

$$E = E_0 \sin 2\pi\nu_0 t \quad (\text{Eq. 2.1})$$

where E is the time dependent intensity, E_0 the maximum amplitude, and ν_0 the frequency of the electric field. This field induces a dipole μ expressed by the equation 2.2 where α , the proportionality constant, is the polarisability of the molecule.

$$\mu = \alpha E = \alpha E_0 \sin 2\pi\nu_0 t \quad (\text{Eq. 2.2})$$

Such an oscillating dipole emits radiation of its own oscillation frequency (ν_0) explaining the Rayleigh scattering. If on the top of that, the molecule undergoes some internal motion, such as vibration or rotation, the polarisability will change periodically altering the oscillating dipole.

Consider now a vibration of frequency ν_{vib} which changes the polarisability. The new polarisability can be expressed by the equation 2.3 where α_0 is the equilibrium polarisability and β ($\beta = \frac{\partial \alpha}{\partial r}$) represents the rate of change of the polarisability with the vibration.

$$\alpha = \alpha_0 + \beta \sin 2\pi\nu_{\text{vib}}t \quad (\text{Eq. 2.3})$$

Combining equations 2.2 and 2.3, the dipole moment (μ) can then be expressed as follow:

$$\mu = \alpha E = (\alpha_0 + \beta \sin 2\pi\nu_{\text{vib}}t)E_0 \sin 2\pi\nu_0t \quad (\text{Eq. 2.4})$$

Expanding and using the following trigonometric relation (Eq. 2.5), it can then be expressed as presented in equation 2.6.

$$\sin A \sin B = \frac{1}{2} \{ \cos(A - B) - \cos(A + B) \} \quad (\text{Eq. 2.5})$$

$$\mu = \alpha E_0 \sin 2\pi\nu_0t + \frac{1}{2} \beta E_0 \{ \cos 2\pi(\nu_0 - \nu_{\text{vib}})t - \cos 2\pi(\nu_0 + \nu_{\text{vib}})t \} \quad (\text{Eq. 2.6})$$

Hence, the oscillating dipole has frequency components $\nu_0 \pm \nu_{\text{vib}}$, as well as the exciting frequency ν_0 . It should be noted that if the vibration does not alter the polarisability of the molecule then β , the rate of change of the polarisability will be equal to zero and the molecule will then oscillate only at the frequency of the incident radiation ν_0 . In other words, to be Raman active, a molecular rotation or vibration must cause some changes in a component of the molecular polarisability.

2.3.2. Selection rules and intensity

2.3.2.1. Selection rules

As it has just been shown, the Raman effect is due to a change in the polarisability of the molecule but the number of Raman bands due to modes of vibration can be predicted using the theory of molecular symmetry (15). It has been established that a N-atomic molecule has $3N-5$ normal modes of vibrations if it is linear and $3N-6$ if it is non-linear.

In the case of the non linear molecule, the calculation follows from each atom having three degrees of freedom due to the need to specify three coordinate (x, y, z) to define

their positions. Then, of the total of $3N$ degrees of freedom for the molecule three degrees represent the translation of the molecule as a whole along the three axes and another three represent rotation of the molecule about each of these axes. Finally, the remaining $3N-6$ degrees of freedom represent the motion of all the atoms with respect to each other. In the case of a linear molecule, there is no degree of freedom corresponding to the rotation of the molecule around the inter-nuclear axis so the number of degrees of freedom (and then the number of Raman bands) can be calculated using the $3N-5$ equation.

It is important to note that only a certain number of the modes of vibration will be Raman active. For example, the benzene, C_6H_6 has 30 modes of vibrations but the Raman spectrum shows only 7 fundamental bands.

Additionally, if a molecule has a large number of symmetry elements, it is a very straightforward matter to decide whether its vibrational modes will be Raman active or inactive. When the molecule has little or no symmetry it is not always easy to make the decision whether or not the polarisability changes during the vibration. Finally a further extremely important general rule has been established: if a molecule has a centre of symmetry then the Raman active vibrations are infra-red inactive, and vice versa. If there is no centre of symmetry then some vibrations may be both Raman and infra-red active. This is one of the reasons why Raman and infra-red are two complementary and not competitive, techniques.

2.3.2.2. Intensity

As for the Raman effect, the intensity of a Raman band can be justified using two different approaches. Once again, they can both be explained using respectively the quantum molecular theory, where the intensity of the Raman bands depend on the population of the initial state at a fixed temperature and the classical theory of Raman, based on the change of the polarisability of the molecule.

a. Quantum molecular approach and Boltzmann distribution

The intensity of a Raman band is directly linked to the number of molecules with a considered energy level. The most populated state is the ground state where the energy level of the molecule will be the lowest. Then vibrational bands coming from the ground state (Stokes) will be more intense than vibrational bands from an excited state (anti-Stokes) as it can be seen in Figure 2.3.

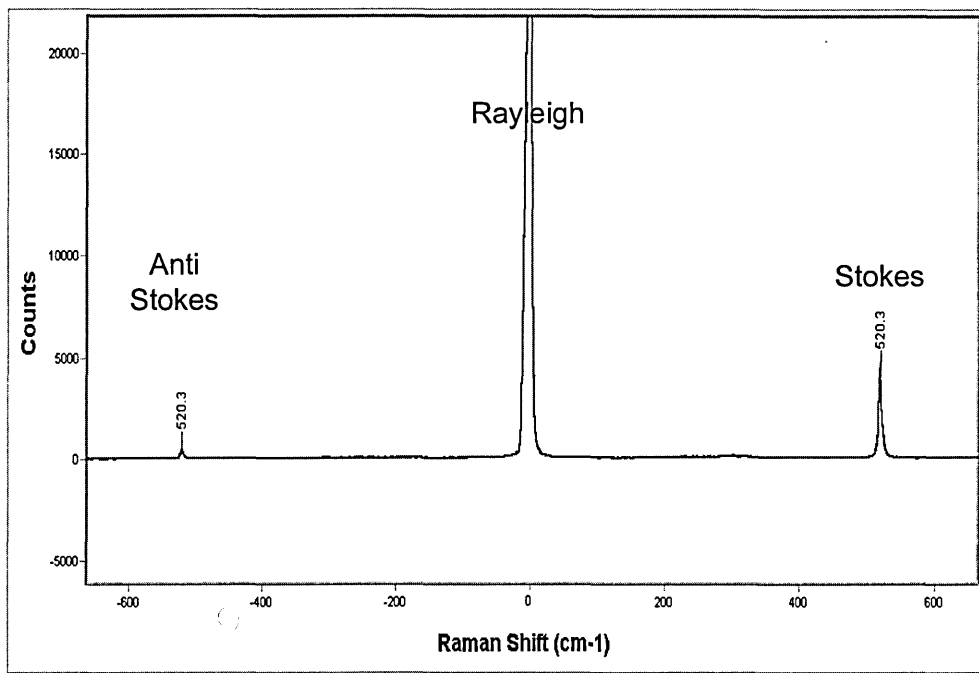


Figure 2.3. Raman spectrum of Silicon showing the different scattering modes and their relative intensities

If the temperature of a molecule is increased, the populations of the vibrationally excited states will rise and the anti-Stokes bands will become more intense. The ratio between the intensities of the anti-Stokes (I_{AS}) and Stokes (I_S) lines in the spectra should (in the absence of resonance effects) follow the expected populations of the vibrational ground and first excited state. These are expressed by the Boltzmann distribution law (equation 2.7) where ΔE is the energy difference between the initial and final energy levels, T is the microscopic temperature of the sample (in degrees Kelvin), k is the Boltzmann constant and g_v and g_0 are the degeneracies of the two vibrational states.

$$\frac{I_{AS}}{I_S} \equiv \frac{N_{v=1}}{N_{v=0}} = \frac{g_v}{g_0} \exp\left(-\frac{\Delta E}{kT}\right) \quad (\text{Eq. 2.7})$$

By inverting the equation and then using the band intensities, the sample's temperature can be calculated. This non contact technique has been used in order to avoid perturbing the system thereby leading to external temperature changes (16). It has been used as well in the current work to evaluate the influence of the laser on the sample and the damage it can generate.

b. Classical theory and polarisability.

Scattering intensity is proportional to the square of the induced dipole moment (μ') which is proportional to the square of the polarisability derivative (equation 2.8). If a

vibration does not greatly change the polarisability (α), then the polarisability derivative ($\partial\alpha/\partial Q$) will be near zero, and the intensity (I) of the Raman band will be low.

$$I \propto \mu^2 \Leftrightarrow I \propto \left(\frac{\partial\alpha}{\partial Q}\right)^2 \quad (\text{Eq. 2.8})$$

Typical strong Raman scatterers are bonds with distributed electron clouds, such as carbon-carbon double bonds. The pi-electron cloud of the double bond is easily distorted in an external electric field. Bending or stretching the bond changes the distribution of electron density substantially and causes a large change in induced dipole moment and then a high intensity Raman band.

2.3.3. Resonance effect

Up to this point, a major simplification in the theory of the Raman effect has been made; namely, that no electronic transitions were close to the energy of the excitation beam. The main consequence from this omission is that in the expression of the Raman intensities the polarisability tensor α did not contain terms such as $(\nu_{el}-\nu_0)$ where ν_{el} is the frequency of an electronic transition (see Long (11) for more details on the equations). When the frequency of the exciting line (ν_0) is far from the frequency of electronic transitions (ν_{el}), then these differences are large and such terms are negligible. As the exciting frequency approaches that of electronic transitions, however, these terms dominate the Raman scattering, and the observed spectrum changes dramatically, showing a resonance enhancement of intensity of certain vibrational modes.

There are certain circumstances in which the normally weak Raman signal may be dramatically enhanced (typically in the range of 3 to 6 orders of magnitude). For example, in a complex substituted aromatic species, there might be a considerable enhancement of ring modes and very little of vibrational modes associated with aliphatic substituent. The resonance enhancement is often observed on oxides due to the fact that the compounds studied are coloured. This phenomenon is discussed in more details in section 4.1.

2.3.4. Fluorescence

Fluorescence occurs when the incident light source excites the species beyond the vibrational energy levels to actual excited electronic states (Figure 2.2). As a

phenomenon, fluorescence is approximately 10^6 to 10^8 stronger and is present in the same frequency range as the Raman scattering (13). Often, when one tries to excite a Raman spectrum, fluorescence is the only phenomenon observed. Trace impurities, coating on polymers, additives, etc., may fluoresce so strongly that it is impossible to observe the Raman spectrum of a major component.

The negative aspect of fluorescence on Raman measurement has received considerable attention. Different approaches have been used to tackle the problem from chemical to physical manipulation of the sample (addition of quenchers, cleanup of the sample or burnout or the fluorescence by preliminary exposure to high-intensity radiation) but such approaches are incompatible with the goal of rapid routine analysis and may even some time damage the sample analysed (17).

Another way to reduce the fluorescence will be to choose a different excitation laser source such as UV laser, which is further away from the excitation frequencies, or using a phase sensitive detection technique (18). Such method is based on the fact that the fluorescence typical lifetime is 10^{-9} to 10^{-7} second while the average lifetime of a vibrationally excited molecule is only $\sim 10^{-13}$ second, a period that is significantly shorter than the average lifetime of an electronically excited state.

A similar approach but this time using a picosecond laser pulse coupled with a 'gateable' multichannel detector (19) permits to significantly improve the Raman spectra of highly fluorescent solutions and solid films. Unfortunately, the cost of the equipment and the difficulty to obtain decent spectra from powder due to multiple scattering, make the technique difficult to operate in practice.

Finally a simpler approach (20-25) consists in shifting the spectrometer grating (see 2.5.5) slightly and recording a spectrum twice. Then by a non trivial mathematical process it is possible, in some cases, to remove fluorescence.

2.3.5. Surface Enhanced Raman Spectroscopy (SERS)

In general the Raman technique suffers from the drawback of a lack of sensitivity. In some cases, however, the sensitivity can be greatly increased by taking advantage of the surface enhanced effects.

In 1974 Fleischmann *et al.* (26) reported very intense bands from pyridine absorbed onto an anodised silver surface and attributed this strong signal to the presence of a

large number of pyridine molecules present at the highly roughened electrode surface. This early work marked the advent of what is known today as the SERS effect.

The origin of the phenomenon is still not fully understood, despite intensive theoretical and experimental research. The theories put forward fall into two categories: the electromagnetic enhancement and the chemical enhancement.

While the electromagnetic enhancement results in the magnification of Raman scattering of species located within a distance of the metal-solution interface, that is on the order of the wavelength of the incident radiation, the chemical enhancement is operative over distances on the order of atomic dimensions.

The electromagnetic enhancement occurs when a beam of incident electromagnetic radiation illuminates the surface of a metal with resonant electromagnetic modes. The beam causes an oscillatory fluctuation of the surface electron density (surface plasmon) in the metal surface that may, in turn, lead to a strong local electromagnetic field.

The chemical enhancement involves the incident radiation striking the roughened metallic surface resulting in a photon being excited within the metal to higher energy level. From this excited state, a charge transfer takes place toward a vibrational level of the similar energy within the target molecule analysed. Variations in vibrational energy states occur, resulting in the transfer of a photon of different frequency to the metallic energy levels before returning to the ground state of the metal (27).

Since the SERS effect is exhibited most strongly by four metal substrates, silver, gold, copper and nickel, it has been largely used for corrosion analysis (28-35). The reason why SERS has not been used in the current work is because the introduction of a different metal onto the sample will not be compatible to in-situ corrosion studies since it will create a galvanic cell and affect the sample behaviour.

2.4. *Data Collection and Analysis*

2.4.1. *Experimental Raman Spectrum*

As explained in section 2.2, the Raman effect permits the number of scattered photons after the excitation by a monochromatic source to be recorded. The Stokes and anti-Stokes vibrational bands can be both analysed but due to their greater intensity, in

most of the cases, only the Stokes bands are studied. A typical Raman spectrum will show a set of bands where the position, shape, and intensity will produce a large amount of information. Raman spectra are represented by a display of the intensity using an arbitrary unit (number of counts or relative intensity) with respect to relative Raman shift (wave number). See Figure 2.4.

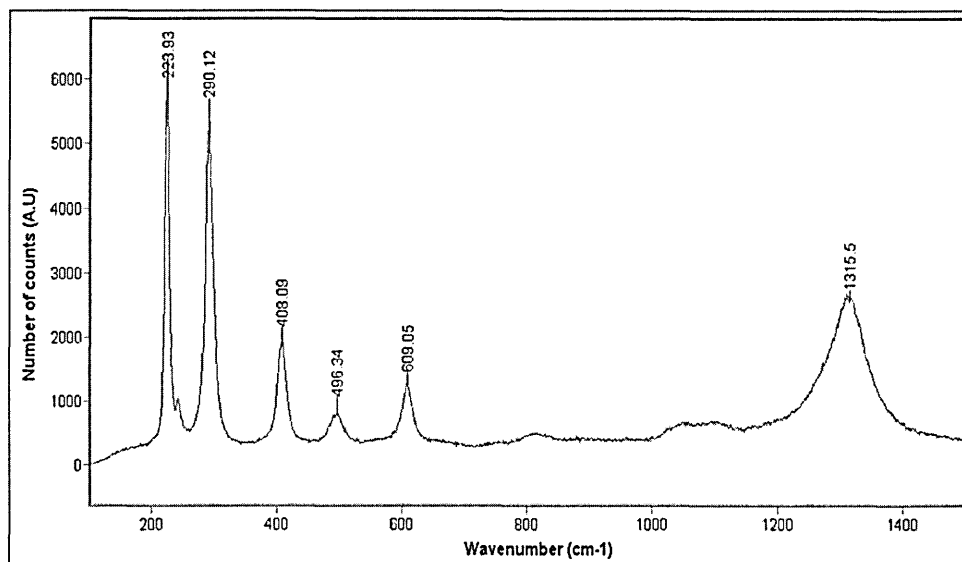


Figure 2.4. Raman spectrum of a Fe₂O₃ powder showing the number of counts recorded by the spectrometer detector with respect to Raman shift in wavenumber (cm⁻¹)

Since a Raman spectrum shows the energy difference between each vibrational transition and the excitation energy, the spectrum recorded is specific to the analysed species. A Raman spectrum is then a fingerprint of the molecule where the number of bands, their positions, and relative intensities should be constant. However, when resonance occurs, the band relative intensities can be affected (see section 4.1).

The shape of the band can as well give some information on the nature of the sample tested. In crystalline solids, the Raman bands are relatively sharp, the widths being due primarily to the anharmonicity of the molecular vibrations. Thus, the bandwidths increase approximately linearly with increasing the temperature. However, the presence of impurities, vacancies or other imperfections in the crystal lattice results in additional broadening of the Raman band. In particular, the vibrational Raman spectra of amorphous material are characterised by very broad features, which have quite generally resisted attempts at quantitative interpretation.

The intensity of a Raman spectrum also depends on the concentration of each active group (see section 2.3.2). In the case of a mixture, Raman bands from each product will be present in the spectrum recorded from the mixture. The relative intensities between bands from different species will give quantitative information and the ratio of each compound within the mixture can be determined. For quantitative analysis, chemometrics techniques like principal linear regression (PLR) or principal component analysis (PCA) can be used (36).

Due to certain issues and difficulties to apply chemometrics to spectra analysis (see section 4.1.2) only more conventional techniques, presented below, have been used to fulfil the current work.

2.4.2. Spectra analysis

The following spectra analysis methods, based on mathematical calculation are the ones offered by the Grams 32 Software produced by Galactic Industries. A basic understanding of the routines is necessary in order to be able to evaluate the treated data.

2.4.2.1. Spectra smoothing

When the signal/noise ratio is low, the determination of the position of the centre of a band, the width or even the area become difficult and the data interpretation can not be achieved without smoothing the spectra. The smoothing process is usually, on poor quality spectra, the first step to data analysis.

Three different methods are available in Grams 32 software package: Fourier, Savitsky-Golay and binomial smoothing. Even if the three techniques are introduced, only the binomial method will be developed in detail since it is the one that has been used as a standard smoothing technique.

a. Fourier smoothing

Fourier smoothing is accomplished by Fourier transforming the data, applying a filter function, and then reverse Fourier transforming the data. A triangular filter function is applied with the apodization value reaching zero at a specified cut-off point (expressed in the software by a percentage value). One of the drawbacks of the Fourier processing is it can sometimes introduce artefacts. These are usually seen as high frequency periodic signals imposed on the smoothed data.

b. Savitzky-Golay smoothing

With a different mathematical approach, Savitzky-Golay smoothing does not introduce artefacts into the data like Fourier smoothing does. Savitzky-Golay algorithm is based on the methods described by Steiner *et al.* (37) and Madden (38) performing a least squares linear regression fit of a polynomial. This smoothing technique, on the top of truncating the spectrum analysed on both ends (by $(n-1)/2$ data points where n is the number of points used in the convolution function) leaves the smoothing parameter data dependent and arbitrary.

c. Binomial smoothing

In the binomial smoothing technique (39) the value (y_k) of each point k in the spectrum is replaced by a value equal to the weighted average of some of the points nearby (\bar{y}_k).

Each point in the binomial filter is given a weight according to the binomial distribution (equation 2.9) so that the points further from the point of interest have a decreasing effect.

$$\bar{y}_k = \frac{1}{2^{2s}} \sum_{i=0}^{2s} \left(\frac{2s!}{i!(2s-i)!} \right) y_{k-s+i} \quad (\text{Eq. 2.9})$$

Where : y_k = original data from the spectrum

$2s$ = the total number of points selected for the fit

\bar{y}_k = smoothed value of the data

An example of the raw and smoothed data can be seen in figure (Figure 2.5)

The only parameter that can be chosen in binomial smoothing is the width of the smoothing window ($2s$).

As a general purpose smoothing technique, the binomial process is perhaps the easiest to implement and it usually gives good results. But if the data points are not equally spaced then it can run into trouble and other smoothing techniques have to be considered. Since it is not the case for the Raman data, binomial smoothing is the filtering technique that has been used here for the data analysis.

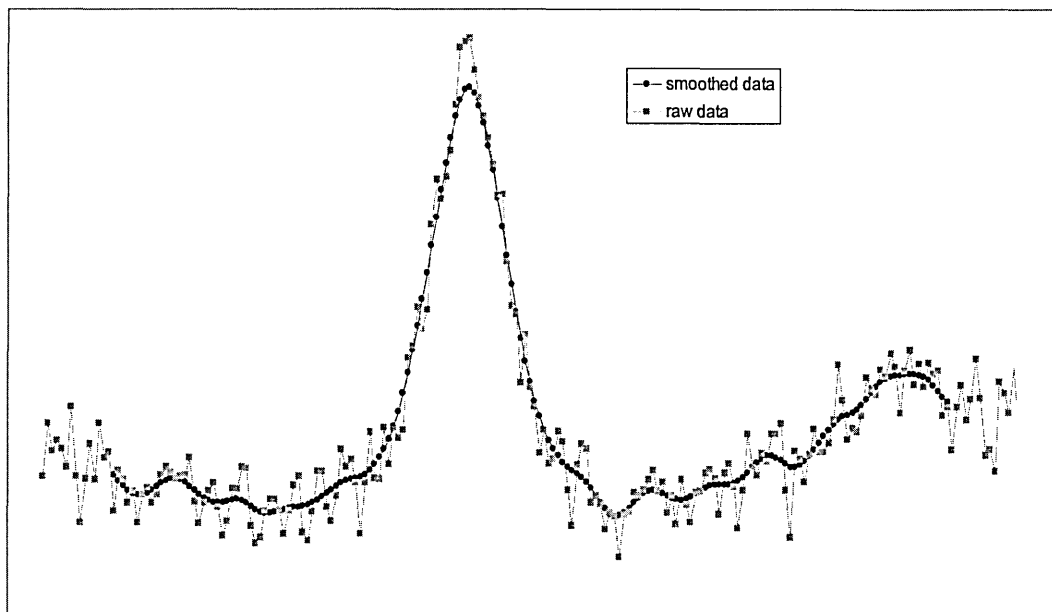


Figure 2.5. Effect of the binomial smoothing on a data set containing 176 data point and using a smoothing window of 30 points. This explains then the fact that the 15 first and last data points are not present in the smoothed curve.

2.4.2.2. Band fitting

Once the spectra have been smoothed and the data are clear of noise, a very efficient way to compare two similar bands within two different spectra is to fit the bands using a band fitting process. This is achieved running a mathematical calculation in order to determine the polynomial equation that matches best with the actual data recorded. The area, intensity, width at half maximum or the centre of the band can then be calculated. All these data then give information on the evolution of the quantity of product measured or on the chemical structure of the sample.

The fitting process is not a straight forward method but the determination of the best fit is achieved by trying a series of combinations of values until the least square possible solution is reached. When fitting the peaks of interest, it is imperative to begin with a line shape that closely models the data, since this will result not only in faster convergence, but also in a more accurate fit.

Even if the natural band shape in spectroscopy is Lorentzian, the starting band shape used for peak fitting can either be Gaussian (eq. 2.10), Lorentzian (eq. 2.11) or a sum of both types of bands (eq. 2.12).

$$Y_G = a \exp(-x^2) \quad (\text{Eq. 2.10})$$

$$Y_L = b(1 + x^2)^{-1} \quad (\text{Eq. 2.11})$$

$$Y(x) = (1 - M)Y_G + M(Y_L) \quad (\text{Eq. 2.12})$$

The parameter M , used in equation 12, is the mixture coefficient that reflects the contribution of the Lorentzian equation in the fitting process. It is expressed in the final result as a percentage.

The interest of using the two different type of fitting band is explained by the difference in the band shape and particularly on the shape of the wings. Lorentzian line is characterised by having most of the intensity of the peak located in the wings which extend to infinity. The Gaussian line tends to have smaller wings and greater intensity under the centre peak (see Figure 2.6).

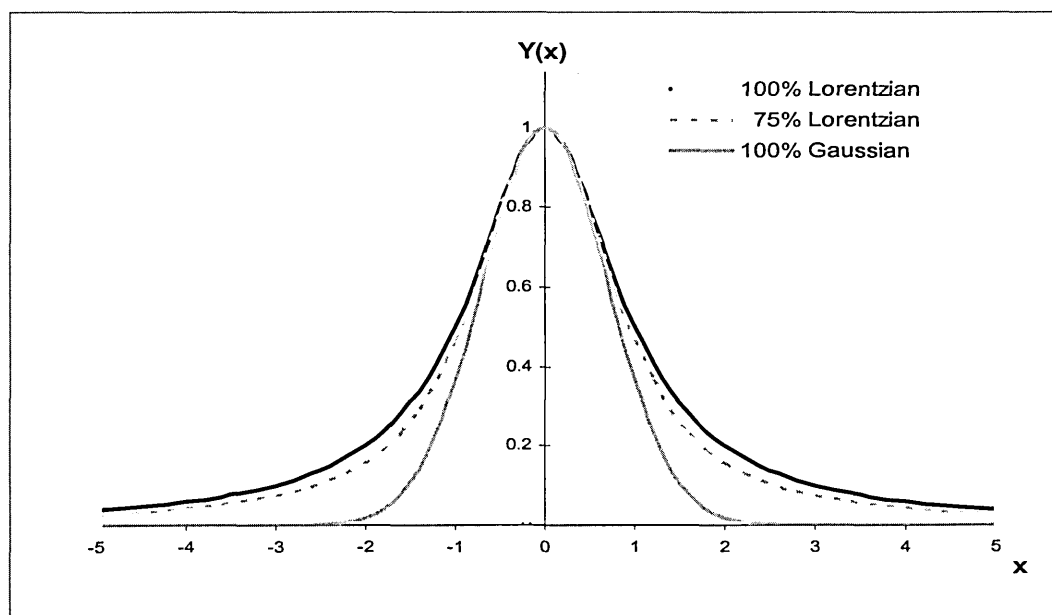


Figure 2.6. Plot of the fitting equation $Y(x)$ using $a=b=1$ and $M=1$ (100% Lorentzian), $M=0.75$ (75% Lorentzian) and $M=0$ (100% Gaussian)

2.5. The Raman microscope system

Broken down into its basic components, a Raman spectrometer consists of a light source, a series of filters, a set of collection optics, a slit, a dispersing optical element, and a detection system. Each of these different parts will be briefly reviewed in the following paragraphs.

2.5.1. System overview

The Raman spectrometer used for the project was a Renishaw Raman system 1000. Before studying in more detail each element, it is necessary, in order to understand the arrangement of the different parts, to follow the path of the laser light through the spectrometer. See Figure 2.7.

Just before entering the spectrometer the light is delivered onto a *beam attenuation wheel*. The wheel permits to select the intensity of the light used to excite the sample and then gives the operator the choice between 100%, 50%, 25%, 10% and 1% of the laser power. This laser power selection is crucial since in some cases, the sample can be damaged by a too intense laser source.

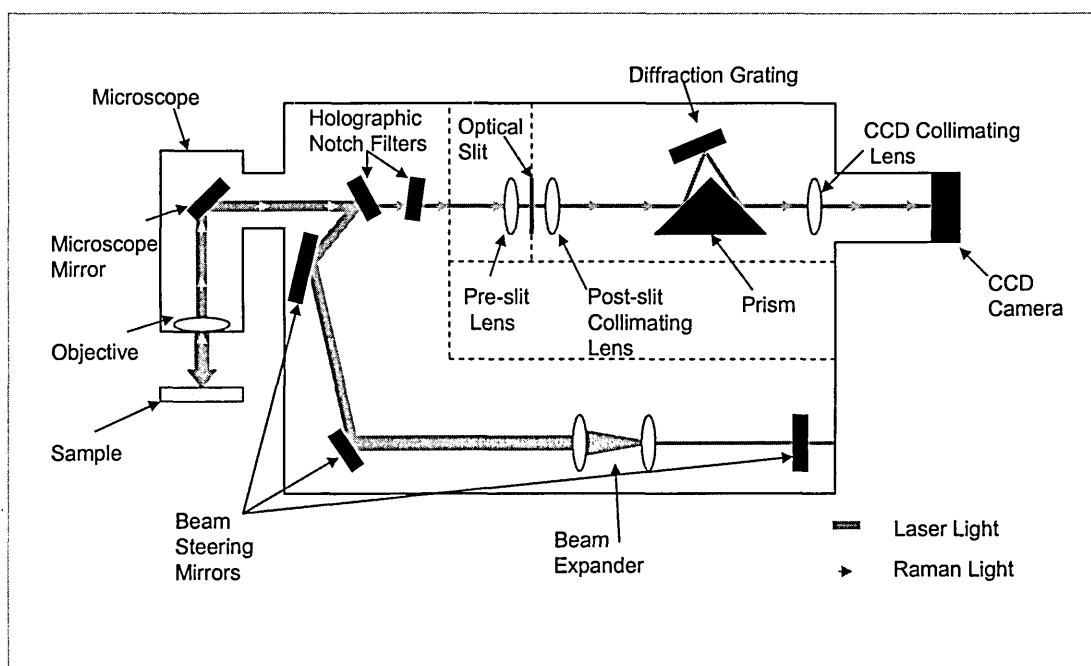


Figure 2.7. Schematic representation of the Renishaw Raman microscope system 1000 and a display of the path of the laser light and the Raman light

Once the power has been selected, the light travels through the first optic within the system: a *plasma line rejection filter* that removes the laser lines which would be detected and mistaken for Raman bands. After travelling via an alignment mirror (*beam steering mirror*) the beam hits the *beam expander* which has the effect of increasing the size of the beam from 1 mm to a 6 mm diameter collimated beam. The beam is then angled off two *steering mirrors* onto the first of two *holographic notch filters* and reflected into the *optical microscope* where it is focused onto the sample via the *microscope objective*.

The Raman light and the laser light are both reflected back into the microscope via the *objective*. From there, the beam returns back into the *notch filters* in order to block the laser radiation of travelling any further. Next, the Raman light is focused through an *optical slit* which produces a sharp image, and then it is recollimated via the *post slit collimating lens*. The Raman light is then directed on the *diffraction grating* via a *prism* in order to separate the scattered light into the different component frequencies before being focused onto the *CCD detector*.

2.5.2. Laser

Even if it may be possible to obtain satisfactory Raman spectra from some materials using light sources other than lasers, there is no doubt that the laser is currently the only excitation source that is realistically worth considering. Three different lasers were available with the Raman system in order to give a larger range of excitation wavelength and intensity.

The first source available is a 25 mW He/Ne which is the most common laser used in Raman spectroscopy because of its relatively low price and very robust nature. It gives an output of 632.8 nm and produces a power of 2-3 mW over a 2 μm diameter spot through a standard $\times 50$ objective. The second laser, a 25 mW Argon laser, offers a green excitation with a wavelength of 514.5 nm. In the case of the Ar^+ , the power can be increased up to 40 mW but this is not recommended since it will reduce significantly the lifetime of the source. Finally, a much more powerful diode laser (782 nm) is also available. It permits to excite the sample using a $5 \times 20 \mu\text{m}^2$ line with a much higher power (up to 300 mW). Unfortunately, at such wavelengths, the laser is not visible and it becomes difficult to focus it onto the sample. Moreover, the fact that it is a line and not a spot makes the local analysis more difficult than when a laser spot is used.

2.5.3. Holographic Notch Filters

Holographic notch filters are an expensive, but essential, part of a spectrometer, since their main function is to remove the Rayleigh light. The notch filters can then be described as wavelength specific mirrors and they reflect light of a narrow band of wavelengths with a high degree of efficiency. The notch filters are made of photosensitive organic material sandwiched between transparent substrates. A laser beam is used to write a hologram into the material to produce sinusoidal variation in the refractive index through the material. The change in the refractive index is necessary to

2.5.4.2. Long working distance objectives

The working distance of an objective lens is the distance from the front surface of the lens to the focal point. High magnification lenses necessarily have shorter working distances, sometimes making it difficult to examine samples with very rough surfaces, or sample in solution. Long working distance objectives are more suitable for in-situ corrosion studies for two main reasons. First, if a conventional working distance objective is used, it will be partially immersed in a corrosive environment and that will not be suitable for the objective. Second, introducing a metallic object in the corrosion cell will disturb the corrosion processes and might alter the behaviour of the sample studied.

2.5.5. Diffraction gratings

A grating is an optical device which the surface is made of a series of n parallel lines or "grooves" spaced from each other by the same value d . The role of the grating is to disperse the incident polychromatic light into its constituent wavelengths. Each wavelength in the dispersed output beam leaves the grating at a slightly different angle to every other wavelength before being collimated by a field lens. The number of grooves to some extent determines the resolution of the spectrometer. The more groove per millimeter are on the grating, the better is the dispersion and so the higher the resolution. As a large number of grooves permits to increase the resolution, it reduces dramatically the region of the spectrum monitored at one time.

2.5.6. Charged Couple Device (CCD) detector

Until fifteen years ago, the only alternatives for Raman detection were photo multiplier tubes and diode arrays. Nowadays, the most commonly used detection technique is the CCD detector. In order to collect and count the number of photons scattered from the sample, an array detector composed of 578×385 individual detector elements (pixels), is situated at the focal plane of the field lens. Each wavelength will in principle fall onto the array detector at a different place onto a separate and distinct array element. The pixels are exposed to the dispersed light and photo electrons are generated, proportional to the intensity of the light.

One of the great advantages of the CCD detectors is that they can be utilised, on the top of the conventional use, for Raman imaging. In this application a selected frequency of the light scattered from a portion of the sample can be recorded using the

diffract the light. The hologram can then be written in order to reflect or reject a narrow band of wavelengths.

2.5.4. Microscope objective

In all Raman microscopes, the laser beam is focused onto the sample using a microscope lens. A large range of microscope objective with different magnification and working distance can be used.

2.5.4.1. Focal point

The focal point of the exciting beam is usually adjusted to coincide with the surface of the sample. At this point, the diameter of the beam is not zero but is in reality limited by aberration effect and fundamentally by the diffraction limit, which is a function of the wavelength of the light (λ). It is therefore more realistic to consider the focal region to be approximately cylindrical (Figure 2.8).

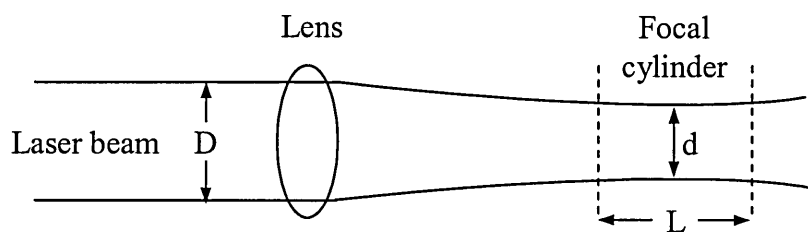


Figure 2.8. Focusing of a laser beam onto the optical lens (4)

The diameter (d) and the length (L) of the focal cylinder are given by equations 2.13 and 2.14 where f is the focal length of the objective and D the diameter of the laser beam (Figure 2.8). A 6 mm laser, focused onto a $\times 20$ objective with 633 nm laser source will give a focal cylinder of 24 μm diameter by 25 μm long. (4)

$$d = \frac{4\lambda f}{\pi D} \quad (\text{Eq. 2.13})$$

$$L = \frac{16\lambda f^2}{\pi D^2} \quad (\text{Eq. 2.14})$$

The fact that the focus is a cylinder and not a point is important for the interpretation of Raman spectra recorded from 'in-situ' corrosion experiments. This then explains why the Raman spectra recorded from the sample's surface will always contains bands from the solution.

two dimensions of the detector offering the possibility to map the sample. The image obtained reflects the evolution of the intensity of the studied band all over the area analysed. This type of application can be of a great interest for corrosion studies where a corroded surface is rarely made of a single oxide or corrosion product, but the time needed for point by point data acquisition makes it incompatible with kinetic experiments.

2.5.7. Software parameters

All the elements described above are essential parts of the spectrometer but computer software are necessary to run the system. The one used to run the spectrometer is Grams 32 version 4.11. Developed by Galactic Industries, it permits a series of parameters to be set, especially the spectral range, the scanning mode, the laser power and the exposure time.

2.5.7.1. Scanning mode and spectral range

Two different modes of acquisition can be selected to record a Raman spectrum.

The static mode, where the grating position does not change during the experiment, is used to acquire Raman spectra where the central value is chosen by the operator and the spectral window is fixed (since it's dependent on the number of grooves on the grating). In the Renishaw system used, the spectra window is centred at a value ν and has a width of $\pm 275 \text{ cm}^{-1}$.

In the continuous extended scanning mode, the user determines the scan range limits. Usually, the scan range depends on the material under investigation. For inorganic material, a reasonable range will be between 150 and 2000 cm^{-1} and between 400 and 3600 cm^{-1} for organic materials. The desired scan range and exposure time are entered into the software, the grating is rotated such that the lower Raman shift limit will be incident in the pixel furthest from the output-register. Then, the shutter is opened and the grating is continuously rotated. The time taken for the first wavelength to traverse the CCD chip is equal to the exposure time. When the last wavelength has finally traversed the chip onto the read about register, the camera shutter closes, the scan finishes and the results are then displayed. Since each wavelength spends the set exposure time traversing the CCD, the total exposure time is much larger than the set exposure time.

Both modes are very different and the choice of one over the other depends entirely on the operator and the type of data needed. Since there is no mechanical motion during the static scan it is much quicker to acquire a spectrum than using the continuous extended scanning mode. Therefore, the static mode will be more convenient for corrosion time dependent experiment. But as soon as the data range has to be larger than 550 cm^{-1} , the continuous extended scanning has to be used.

2.5.7.2. Exposure time and laser power

Exposure time and laser power are both important parameters that have a key effect on the signal to noise ratio of the final spectra. The more powerful the laser and the longer the acquisition time, the stronger will be the Raman scattering and then the better will be the signal to noise ratio.

But using a too high laser power can produce fluorescence or even damage the sample. Moreover, using a very long exposure time increases dramatically the acquisition time and makes the setting incompatible with fast acquisition for kinetic experiment. The choices of the laser power and exposure time have to be selected wisely in order to find the best compromise between spectrum quality and acquisition time without of course affecting the sample.

2.6. References

- (1) Brillouin L. *Analytical Physics* 1922; 88: p.17.
- (2) Smekal A. *Naturwissenschaften* 1923; 11: p.873.
- (3) Raman CV, Krishnan KS. A new type of secondary radiation. *Nature* 1928; 121: p. 501.
- (4) Gardiner DJ, Graves PR. *Practical Raman Spectroscopy*. 1989.
- (5) Durig JR. *Vibrational spectra and structure*. 1975.
- (6) Delhaye M, Dhamelin court P. *Journal of Raman Spectroscopy* 1975; 3: p. 33.
- (7) Treado PJ, Morris MD. *Infrared and Raman Spectroscopy Imaging. Practical spectroscopy*; 1993. pp. 71-108.
- (8) Delhaye M, Turrell G, Dhamelin court P. *Raman Microscopy Developments and applications*. London: Academic Press Limited; 1966.
- (9) Gardiner DJ, Littleton CJ, Bowden M. Automated Mapping of High-Temperature Corrosion Products on Iron Chromium-Alloy using Raman Microscopy. *Applied Spectroscopy* 1988 JAN; 42(1): 15-19.
- (10) Gardiner DJ, Bowden M. Mapping and imaging applications of Raman microscopy. *Microscopy and analysis* 1990 (November): pp.27-29.

- (11) Long DA. Raman Spectroscopy. : McGraw-Hill International Book company; 1977.
- (12) Grasselli JG, Bulkin BJ. Analytical Raman Spectroscopy. 1st ed. United states: Wiley Interscience; 1991.
- (13) Skoog DA, Holler FJ, Nieman TA. Principles of instrumental Analysis. 5th ed. London: Saunder College Publishing; 1998.
- (14) Banwell CN. Fundamentals of molecular spectroscopy. 3rd ed. UK: MC Crow-Hill Book company ltd; 1983.
- (15) Hollas JM. Modern Spectroscopy. 2nd edition ed. New York: John Wiley & Sons; 1992.
- (16) Walrafen GE, Fisher MR, Hokmabadi MS, Yang WH. Temperature-Dependence of the Low-Frequency and High-Frequency Raman-Scattering from Liquid Water. Journal of Chemical Physics 1986 DEC 15; 85 (12): pp. 6970-6982.
- (17) De Faria DLA, Venancio Silva S, de Oliveira MT. Raman Microspectroscopy of some iron oxides and oxyhydroxides. Journal of Raman spectroscopy 1997; 28: pp. 873-878.
- (18) Genack AZ. Phase-sensitive detection of emission and scattering by electro-optic demodulation. Journal of Luminescence 1984 12; 31-32 (Part 2): pp. 696-698.
- (19) Everall N, Hahn TM,P, Parker AW, Towrie M. Picosecond Time-resolved Raman spectroscopy of Solids: Capabilities and limitations for Fluorescence Rejection and the influence of Diffuse Reflectance. Applied Spectroscopy 2001; 55 (12).
- (20) Bell SEJ, Bourguignon ESO, Dennis AC. Analysis of luminescent samples using the subtracted shifted Raman spectroscopy (SSRS) method . Analyst 1998; 123: pp. 1729-1734.
- (21) Xie CG, Li YQ. Confocal micro-Raman spectroscopy of single biological cells using optical trapping and shifted excitation difference techniques. Journal of Applied Physics 2003 MAR 1;93(5): pp. 2982-2986.
- (22) O'Grady A, Dennis AC, Denvir D, McGarvey JJ, Bell SEJ. Quantitative Raman spectroscopy of highly fluorescent samples using pseudosecond derivatives and multivariate analysis. Analytical Chemistry 2001 MAY 1; 73 (9): pp. 2058-2065.
- (23) Bell SEJ, Bourguignon ESO, Dennis AC, Fields JA, McGarvey JJ, Seddon KR. Identification of dyes on ancient Chinese paper samples using the subtracted shifted Raman spectroscopy method. Analytical Chemistry 2000 JAN 1; 72 (1): pp. 234-239.
- (24) Mosierboss PA, Lieberman SH, Newbery R. Fluorescence rejection in Raman spectroscopy by shifted-spectra, edge-detection, and Fft Filtering Techniques. Applied Spectroscopy 1995 MAY; 49 (5): pp. 630-638.
- (25) Shreve AP, Cherepy NJ, Mathies RA. Effective rejection of fluorescence interference in Raman spectroscopy using a shifted excitation difference technique. Applied Spectroscopy 1992 APR; 46 (4): pp. 707-711.
- (26) Fleischmann M, Hendra PJ, McQuillan AJ. Raman spectra of pyridine adsorbed at a silver electrode. Chemical Physics Letters 1974 5/15;26 (2): pp. 163-166.
- (27) Spectroscopy of surfaces, Vol 16 - Advances in spectroscopy. Clark and Hester editors; 1988.

- (28) Baek W, Kang T, Sohn H-, Kho YT. In situ surface enhanced Raman spectroscopic study on the effect of dissolved oxygen on the corrosion film on low carbon steel in 0.01 M NaCl solution. *Electrochimica Acta* 2001 4/30; 46 (15): pp. 2321-2325.
- (29) Simpson LJ, Melendres CA. Temperature dependence of the surface enhanced Raman spectroelectrochemistry of iron in aqueous solutions. *Electrochimica Acta* 1996 6; 41 (10): pp. 1727-1730.
- (30) Melendres CA, Pankuch M, Li YS, Knight RL. Surface enhanced Raman spectroelectrochemical studies of the corrosion films on iron and chromium in aqueous solution environments. *Electrochimica Acta* 1992 12; 37(15): pp. 2747-2754.
- (31) Oblonsky LJ, Devine TM. A Surface enhanced Raman spectroscopic study of the passive films formed in borate buffer on iron, nickel, chromium and stainless-steel. *Corrosion Science* 1995 JAN; 37 (1): pp. 17-41.
- (32) Gui J, Devine TM. The Influence of sulphate ions on the surface enhanced Raman spectra of passive films formed on iron. *Corrosion Science* 1994 MAR; 36 (3): pp. 441-462.
- (33) Mengoli G, Musiani MM, Fleischmann M, Mao B, Tian ZQ. Enhanced Raman-scattering from iron electrodes. *Electrochimica Acta* 1987 AUG; 32 (8): pp. 1239-1245.
- (34) Rubim JC, Dunnwald J. Enhanced Raman scattering from passive film on silver-coated iron electrodes. *Journal of electroanalytical chemistry* 1989; 258: pp. 327-344.
- (35) Aramaki K, Uehara J. A SERS study on adsorption of some organic compounds on iron. *Journal of electrochemical society* 1989; 136 (5): pp. 1299-1303.
- (36) Galactic. PLSplus / IQ User's guide. USA: Galactic Industries corporation; 1991.
- (37) Steiner J, Termonia Y, Deltour J. Smoothing and differentiation of data by simplified least square procedure. *Analytical Chemistry* 1972; 44 (11): pp. 1906-1909.
- (38) Madden HH. Comments on the Savitzky-Golay convolution method for least-squares-fit smoothing and differentiation of digital data. *Analytical Chemistry* 1978; 50 (9): pp. 1383-1386.
- (39) Delamar M. Binomial smoothing for electron spectroscopies. *Journal of Electron Spectroscopy and Related Phenomena* 1990;53: pp. c1-c4.

Chapter 3. Corrosion

3.1. Introduction and Definition

Corrosion can be defined as the degradation of a metallic material. Since it involves production and movement of electrical charges, corrosion processes are always electrochemical. The result of electrochemical reactions is a “corrosion effect” which can be useful but is generally detrimental. If the disintegration of scrap metal such as empty cans and abandoned cars are examples of useful corrosion, corrosion attack can produce a contamination of the environment with corrosion products and functional impairment of the system. Generally, corrosion is a deleterious process and causes a great deal of destruction and inconvenience.

The cost of corrosion has been estimated in the USA as \$276 bn per year¹. This figure groups all direct and indirect costs caused by material failure, corrosion prevention etc... It affects all branches of industry, from production and manufacturing to transportation and commerce. A good understanding of corrosion processes is essential to reduce these costs through the development of new anti-corrosion.

The corrosion behaviour of a material cannot be described unless the operating conditions to which the material is subjected are identified. Physical state, chemical composition, temperature and mechanical stress are some of the factors that influence a material's performance.

Corrosion is an interdisciplinary subject that combines elements of physics, metallurgy, electronics, engineering and chemistry. In this respect different emphasis can be given to the different aspects of the subject. The following contents of this chapter provide a brief presentation of electrochemical concepts and an overview of the possible forms of corrosion. It is then followed by a presentation of the conventional DC electrochemical analysis and some more recent novel techniques before introducing the use of Raman spectroscopy for corrosion studies.

¹ Report published by NACE international on the 15th of August 2000 (Corrosion costs and preventing strategies in the United States). The 276 billions of dollars are shared between the following categories: Production and manufacturing (12.8%), Government (14.6%), Infrastructure (16.4%), Transportation (21.5%) and Utilities (34.7%)

3.2. Basic Electrochemical concepts

3.2.1. Behaviour of metal in an environment

When a metal is exposed to an aqueous environment, it can behave in three different ways. The first possibility is that the metal is *immune*, where there is no reaction between the metal and the environment and no corrosion occurs. This *immune* behaviour results from the metal being thermodynamically stable in the particular environment.

The second possibility is that the metal is *active* and corrodes in the environment. This kind of behaviour is characterised by a change in the weight of the metal as the system tends toward its lowest energy state through the development of chemical compounds, e.g. corrosion products.

Finally in the third case, the metal begins to corrode but a state of *passive* behaviour results due to the formation of an insoluble protective film. This protective film limits the reaction rate to very low levels.

3.2.2. The corrosion cell

Corrosion science involves a study of electrochemical processes that occur at metal-liquid interfaces.

An electrochemical half-cell reaction is characterised by the simultaneous exchange of electrons occurring at the surface of a metallic material, leading to the development of anodic and cathodic sites. The sites of the anodes and cathodes are not fixed, rather they form an ever shifting pattern of electrochemical reactions.

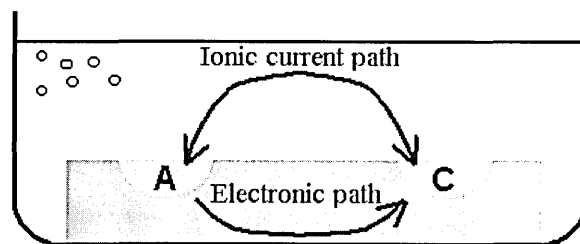


Figure 3.1. The four requirements of an electrochemical corrosion cell

Figure 3.1 presents the four elements required in forming a corrosion cell. The corrosion cell necessitates a cathode (C), where electrons are consumed and an anode

(A), where electrons are generated. The anode and cathode are in electrical contact via an electronic path through the material and by an ionic path through the environment.

3.2.3. Electrochemical reactions

The anode is where metal dissolution occurs, that is, where the metal liberates ions into the solution. The anodic reaction ($M \rightarrow M^{n+} + ne^{-}$) is an oxidation reaction which produces electrons that travel through the metal to the cathode. At the cathode, the electrons are consumed by a reduction reaction. Such a reaction is schematically represented in equation 3.1 where Red is a reducing agent (electron donor), Ox is an oxidising agent (electron acceptor) and n is the number of electrons (e^{-}) that take part in the reaction.



3.2.4. Electrode Potential and Polarisation

As an electrochemical reaction induces a flow of electrons and ions, the transfer of charges creates an electrical current and the electrode, where Redox reactions occur, has an electrical potential.

The electrode potential depends on the redox potential (E_0) and on the concentration of reactants and products. This electrode potential (E) can be calculated using the Nernst equation (eq. 3.2).

$$E = E_0 - \frac{RT}{nF} \ln \frac{[\text{red}]}{[\text{ox}]} \quad (\text{Eq. 3.2})$$

Where E_0 is the standard electrode potential (at 25°C, 1 bar), R is the gas constant ($\text{J}\cdot\text{mol}^{-1}\cdot\text{K}^{-1}$), n is the number of electrons involved in the reaction, F is the Faraday constant ($\text{C}\cdot\text{mol}^{-1}$) and [red] and [ox] are the respective concentrations of species present during the electrochemical reaction.

3.3. The different types of corrosion

It is convenient to classify corrosion by the forms in which it manifests itself, the basis for this classification being the appearance of the corroded metal. Each form can be identified by visual observation. In most cases the naked eye is sufficient, but sometimes magnification is helpful or required.

The number of forms of corrosion and the method of classification varies from one book to another. The order in which they are presented is arbitrary and reflects the personal preference of the authors (1-7). In the following paragraphs, only the three main types of corrosion (uniform, galvanic, pitting) will be introduced while some types of corrosion behaviour like stress corrosion cracking, crevice, erosion or intergranular corrosion, not related to the current work, will not be treated here.

3.3.1. Uniform corrosion

Uniform corrosion is the most common form of corrosion and is characterised by an equal corrosion rate over the whole surface of the metal exposed to the corrosive environment. In order for uniform corrosion to occur, the corrosive environment must have the same access to all parts of the metal surface and the metal itself must be metallurgically and compositionally uniform.

Despite the fact that this form of corrosion represents the greatest destruction of metal on a tonnage basis, uniform corrosion is not too great a concern from the technical point of view because the rate of damage and hence the life of the equipment can, generally, be accurately estimated.

3.3.2. Galvanic corrosion

Bimetallic or galvanic corrosion occurs when two metals of different electrochemical potential are in electrical contact and immersed in a corrosive environment. The potential difference existing between the two metals creates an electron flow and produces oxidation of the less corrosion resistant metal. The less resistant metal becomes anodic and the more resistant one becomes cathodic.

Corrosion due to galvanic effects is usually greater near the junction of the two metals, with attack decreasing with distance from that point. An important factor in

galvanic corrosion is the area ratio between the anode and the cathode. If the cathode is much larger than the anode, the current density at the surface of the anode (for a given current) will be much larger than at the surface of the cathode and the corrosion rate of the anode will be higher.

The galvanic effect can be used, in some cases as a corrosion protection process. A sacrificial anode made of a less noble metal (e.g. use of zinc to protect steel) is attached to the material that must be protected and corrosion will then occurs on the anode.

3.3.3. Pitting corrosion

Pits are generally described as a cavity or hole having a surface diameter about the same as or less than the depth. This form of corrosion is one of the most destructive and insidious since it causes equipment to fail because of perforation with only a small percent weight loss of the entire structure. Pitting corrosion usually takes place in corrosion cells with clearly separated anode and cathode sites and above a certain potential called the *pitting potential*.

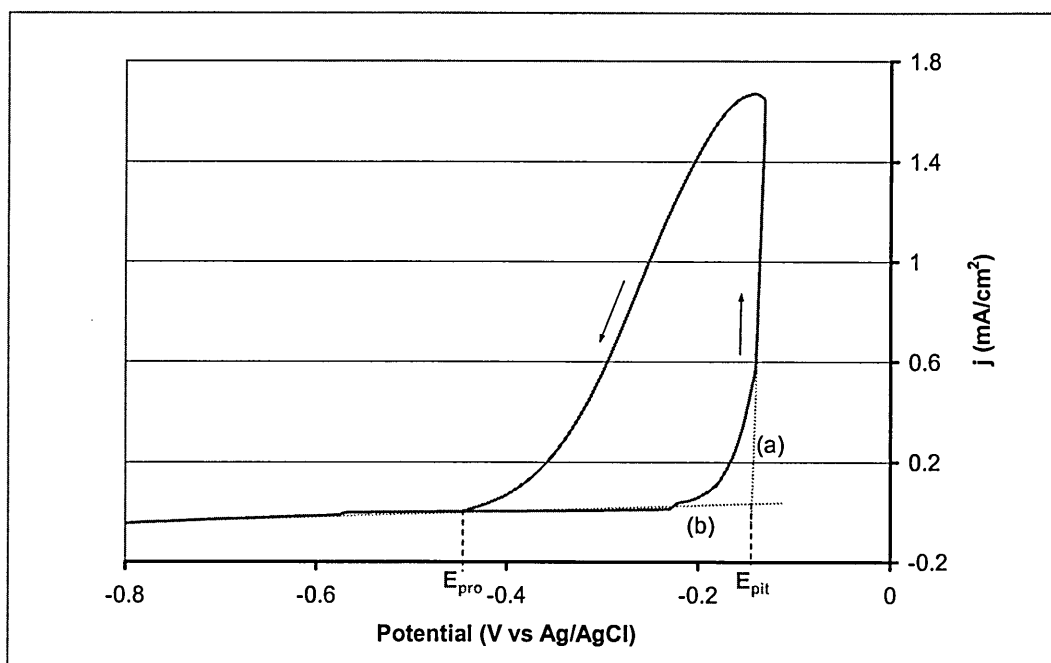


Figure 3.2. Pitting hysteresis polarisation scan of a pure iron sample in 0.1 M sodium chloride solution. The two arrows represent the direction the scan and the lines (a) and (b) are the two tangents used to determine the pitting potential.

The pitting potential can be calculated after running a pitting hysteresis polarisation (or pitting) scan where the current is measured and recorded versus the imposed

potential. An example of the determination of the pitting potential of a pure iron sample in a 0.1 M sodium chloride solution is presented in Figure 3.2.

Two types of information can be obtained from a pitting scan. Firstly, two tangents (a) and (b) can be added on the anodic scan of the curve. The pitting potential (E_{pit}) can then be directly read from the abscissa of the intersection of the tangents (a) and (b). The higher the pitting potential, the more resistant to pitting will be the material. Secondly, the protection potential (E_{pro}) corresponds to the potential at which the loop closes on the reverse scan. If the protection potential is more negative than the pitting potential, pitting could occur.

Finally, the size of the loop will indicate the tendency of the material to pit (1). A large area of the loop will indicate a poor resistance to pitting. The ideal material will show no pitting hysteresis loop due to the instantaneous repassivation of the pits during the cathodic scan.

3.4. Theoretical potential-pH diagrams (Pourbaix diagram)

Marcel Pourbaix (8) designed a theoretical tool having the ability to describe the stable species generated on a metal immersed in water. The result of his work is a chart of each metal showing the condition under which it will corrode, passivate or remain immune. Calculated for pure water, Pourbaix diagrams refer only to pure metals but their construction, based on simple principles, requires numerous calculations.

These diagrams can be used to predict which species are likely to be present on the surface of a metal for a given pH / electrode potential combination. Since the 1950's, a large number of studies have been carried out in order to adapt the initial Pourbaix diagrams to different systems at different temperatures. From these studies a wide range of diagrams can be found in the literature (9-11).

Pourbaix diagrams include boundary lines based upon the concentration of ions in solution and are plotted between the stable species. These lines are arbitrarily set at a value of 10^{-6} g/mol. For example in Figure 3.3 the line at -0.6 V separates the active and immune states of Fe; below the line the concentration of the Fe^{2+} ions in solution is less than 10^{-6} g/mol, above this line it is greater than 10^{-6} g/mol. When the corrosion product is insoluble in the electrolyte, for example Fe_2O_3 in the case of iron, the oxide

forms a passive film on the metal and prevents further reaction at the surface of the electrode.

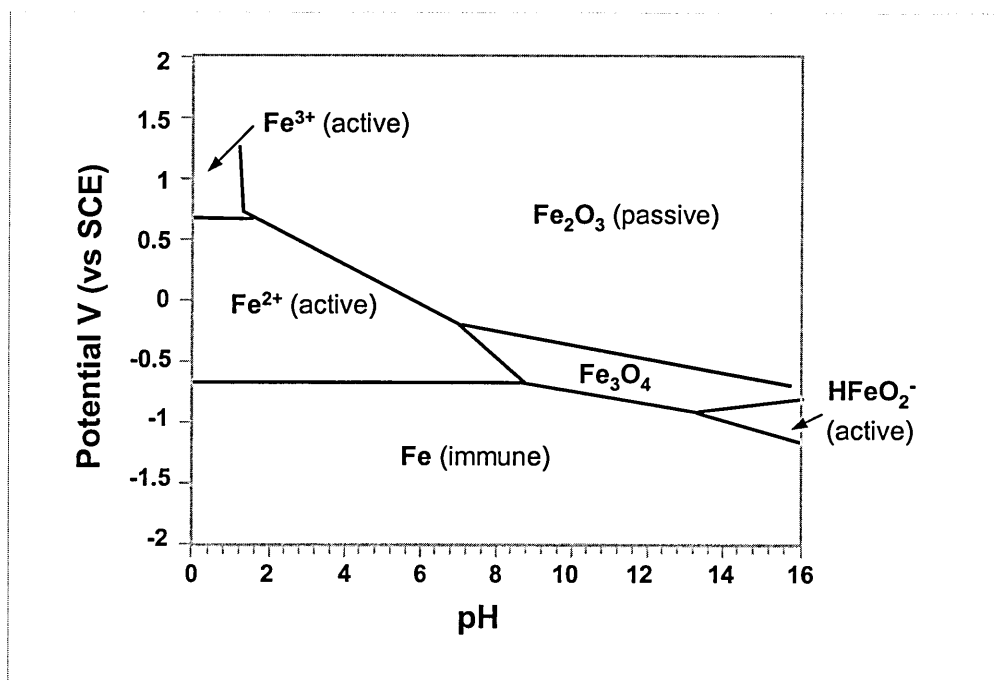


Figure 3.3. Pourbaix diagram (9) for Fe-H₂O system at 25 °C. (pH of solution against electrode potential with respect to Saturated Calomel Electrode (SCE) in volts)

It is important to note that the Pourbaix diagram presented above is not an exact description of the system. In fact, one single system can have several different potential-pH equilibrium diagrams depending on the solid substances considered. For example, the diagram shown in Figure 3.3 does not take into account the passivation of the iron surface by Fe(OH)₂ or by γ -FeOOH.

Finally, another essential limitation of the Pourbaix diagram is that it does not take into account many of the environmental factors such as flow rate, oxygen concentration or temperature and does not give kinetic information.

3.5. Techniques used to evaluate and study corrosion

When designing a component of a structure to operate in a corrosion environment, it is essential to understand the nature and rates of any corrosion reactions that may take place. The selection of the techniques used to evaluate and study corrosion depends on the type of corrosion going on. Investigation of corrosion can be achieved using several

different techniques giving different information. The techniques can be classified into two categories: intrusive and non-intrusive methods.

Intrusive methods involve the system being stimulated externally and the response of the system to the perturbation is measured. In non intrusive methods, the corrosion activity is measured without introducing any type of perturbation. Furthermore, the non intrusive techniques may be further split into two categories: scanning techniques and imaging techniques.

3.5.1. Intrusive techniques

3.5.1.1. Tafel plot

The purpose of the Tafel plot technique is to measure the corrosion rate (i_{corr}) via calculation of the Tafel constants β_A and β_C . A Tafel plot is generated after scanning the potential of a specimen from, for example, 250 mV below the free corrosion potential (E_{corr}) to 250 mV above at a typical scan rate of 5 mV/min (12).

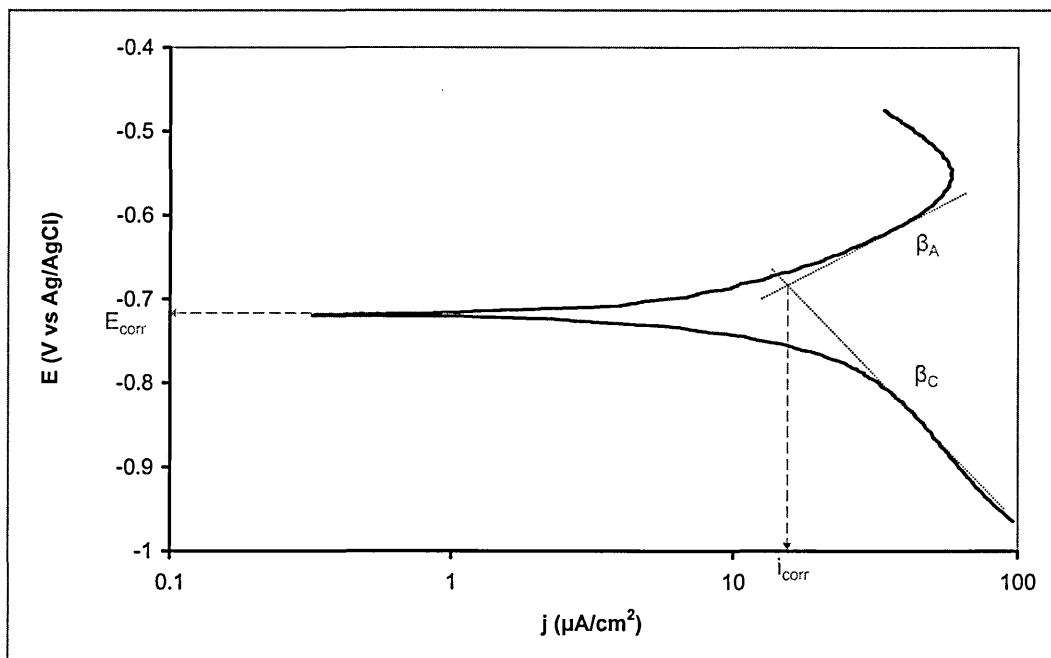


Figure 3.4. Tafel plot of a 10 mm iron disc in pH=7.5 borate buffer solution

The resulting curve is a plot of the applied potential versus the measured current (plotted on a log scale) as shown in Figure 3.4 where E_{corr} is the free corrosion potential of the specimen, i_{corr} the corrosion current and β_A and β_C are respectively the anodic and cathodic Tafel constants. The Tafel constants are the slopes of the straight line that fit

the linear region of the anodic and cathodic branches of the Tafel plot. These constants are then used to calculate the polarisation resistance (Eq. 3.3).

3.5.1.2. Polarisation resistance

The polarisation resistance (R_p) is defined as the resistance of the specimen to oxidation during the application of an external potential. Consequently, the higher the value of R_p , the more corrosion resistant is the material.

To calculate the R_p the potential is scanned over a range of ± 20 mV about the free corrosion potential at a typical scan rate of about 5 mV/min (12). Once the current response is recorded, the potential versus current curve is plotted. The polarisation resistance is then determined by calculating the slope of the linear region of the plot. The reason why the value R_p is called the polarisation resistance is due to the unit (Ohms) of the calculated slope ($R_p = \Delta E / \Delta i$). The Tafel constants described in the previous part are linked to the polarisation resistance and the corrosion current by equation 3.3.

$$\Delta E / \Delta i = R_p = \frac{\beta_A \beta_C}{2.3(i_{corr})(\beta_A + \beta_C)} \quad (\text{Eq. 3.3})$$

Although more information may be obtained from the Tafel plot than from the polarisation resistance experiment, R_p has two main advantages. First, determination of R_p takes a much shorter time and second, the samples are exposed to smaller voltages and therefore the sample surface is less susceptible to damage.

3.5.1.3. Potentiodynamic anodic polarisation

As shown by the Pourbaix diagram (section 3.4), a metal can show different responses (immune, active or passive) in a set environment depending on the potential applied. The aim of the potentiodynamic anodic polarisation is to determine the active/passive characteristics of a given metal by increasing its potential at a constant rate and measuring the resulting current.

Often, potentiodynamic scans are run on a series of samples giving the possibility to compare quickly the general behaviour of the specimen studied. It is then possible to judge which material will be the most suitable for the tested conditions by choosing the one with the best tendency to passivate or with the larger passive region.

3.5.1.4. Cyclic polarisation

The cyclic polarisation analysis technique is an extension of the potentiodynamic scan presented in 3.5.1.3. In the case of the cyclic polarisation, the potential scan is reversed when a set potential is reached. The current recorded is then plotted as a function of the applied potential permitting a display of the anodic and cathodic response related to the successive oxidation and reduction reactions of the metal studied.

If the value of the reverse potential is high enough, it is then possible to determine the pitting potential of the specimen studied as explained in part 3.3.3

3.5.2. Scanning electrode techniques

Conventional scanning techniques are now being used to study the mechanisms and kinetics of local metallic corrosion in aqueous environment (13-16). The three scanning electrode techniques presented here are based on the same principle of scanning at a small distance above a surface using a microtip electrode and measuring the electrical potential, the potential gradient or the current.

The data recorded during the experiment is then used to compile an area map or some other spatially resolved representation (surface current density, surface reactivity or surface topography...). The fact that these techniques are able to spatially resolve and quantify localised differences on a surface makes them particularly suitable for localised corrosion studies.

3.5.2.1. Scanning reference electrode technique

The scanning reference electrode technique (SRET) has been designed to measure the variations in potential of the solution above a corroding surface. This is achieved using two reference electrodes between which the potential difference is measured. With a resolution which is dependant on the electrode-sample distance and a minimum distance of 100 μm , the SRET offers a maximum spacial resolution of 346 μm (17).

In SRET, two different types of apparatus can be used: the rotating cylinder and the planar SRET. In the rotating technique, the corroding sample is presented in the form of a cylinder which creates, when rotated highly convected conditions.

3.5.2.2. Scanning vibrating electrode technique

The scanning vibrating electrode technique (SVET) is a derivative of SRET in which, as the name suggests, the scanning microtip electrode is vibrated relative to the scanned surface. In the SVET the electrode is vibrated mechanically at a constant amplitude and frequency using a simple electromagnetic or piezoelectric driver. It then registers an alternating potential at the vibration frequency which is proportional to the potential gradient in the direction of the vibration.

The SVET has a number of distinct advantages over SRET. Which include the ability to measure components of corrosion current density, it has an improved spatial resolution and sensitivity.

3.5.2.3. Scanning Kelvin Probe (SKP)

The Kelvin probe is a non contact vibrating capacitor device that measures the potential difference between a conductive vibrating tip and a conductive sample through measuring the AC current induced by the probe vibration. It is one of the most sensitive measuring techniques and is a well established means of determining metallic work functions.

Offering a lateral resolution of less than 10 μm without using a reference electrode, the SKP technique has been largely used for atmospheric corrosion (18,19) and corrosion studies beneath a coatings (20,21)

3.5.3. Imaging techniques for corrosion analysis

One of the best ways to evaluate the damage caused by corrosion processes is to visualise the effect that it has on the specimen exposed to the environment. As discussed in part 3.3 localised corrosion processes are the most destructive and the most difficult to observe due to their relative small size. Optical, electron and now atomic force microscopy techniques are frequently used to investigate localised corrosion activity.

3.5.3.1. Electron microscopy techniques

Electron Microscopes were developed due to the limitations of light microscopes which are limited by the physics of light to $\times 500$ or $\times 1000$ magnification. Electron Microscopes function exactly as their optical counterparts except that they use a focused

beam of electrons instead of light to 'image' the specimen and gain information as to its structure and composition.

Used regularly for localised corrosion studies, the electron microscopy techniques permit to study the specimen with a magnification up to $\times 200\,000$.²

3.5.3.2. Atomic Force Microscopy (AFM)

The AFM is essentially an imaging system that acquires topographical maps of a surface. A very sharp tip is located at the free end of a cantilever which bends or deflects as the tip moves on the surface. An optical detector measures this deflection which is ultimately related to the surface morphology.

The great advantage of this technique is the lateral resolution of the image can be as small as the tip radius (1-5 nm), and the vertical resolution can be on the order of the angstroms.

3.6. Comparison between Raman spectroscopy and other conventional techniques for corrosion studies.

As it has been shown in part 3.5, many techniques are available for corrosion studies but unfortunately, they all exhibit some limitations. The aim of this section is to compare the Raman technique with the other analysis methods conventionally used for corrosion studies.

First, the type of information given by Raman spectroscopy differs dramatically from other corrosion studies techniques since it's the only method that gives clear chemical information and allows the corrosion products that are developing during the oxidation processes to be identified.

Second, while a cylindrical working electrode is needed for rotating SRET and a flat and level surface has to be used for SVET, any type of sample can be studied by Raman spectroscopy and no specific sample preparation is needed. Like the SKP, Raman spectroscopy can be used to run experiments on dry samples, or under a controlled

² See <http://hypertextbook.com/facts/2000/IlyaSherman.shtml> for more information on electron microscopy.

atmosphere. It also allows the study of real time corrosion processes during in-situ experiments where the sample is analysed during its immersion in solution.

Also, unlike the conventional intrusive techniques (Tafel plot and other polarisation techniques) Raman spectroscopy permits the study of localised corrosion processes with a spatial resolution up to 2 μm . Even if this value is much below the type of resolution obtained using imaging techniques like scanning electron microscopy the sample does not have to be under high vacuum which can be deleterious and change the nature of the sample studied.

Finally, even if a continuous improvement of the analysis technique for corrosion studies can be seen (e.g. three dimensional scanning vibrating electrode technique, micro cells dedicated to localised corrosion studies or environmental scanning electron microscopy allowing the succession of wet/dry corrosion conditions) Raman spectroscopy is a perfect complementary tool for corrosion studies.

3.7. Application of Raman to Corrosion Studies

Laser Raman spectroscopy has become an important tool for the study of electrochemical systems and processes because of the molecular specific information that it provides on the structure of the solid/solution interface in-situ. The determination of the structure and composition of corrosion films on metals constitutes one of the most important practical applications of laser Raman spectro-electrochemistry.

3.7.1. Product identification

Numerous metals (22-27) and metal alloys (28-30) have been studied by laser Raman spectroscopy under a variety of solution environments. Iron and iron based metals have been most extensively studied for their corrosion characteristics because of their industrial importance.

3.7.1.1. Iron oxides and oxyhydroxides

Different phases of the same compound possess quite distinct Raman spectra. Although polymorphs have identical chemical compositions, they have unique crystal structures and hence display different bonding and symmetry, producing very different Raman spectra.

Oxide Name		Band positions (cm ⁻¹)	Reference
α -FeOOH	Goethite	298, 397, 414, 474, 550	(31)
		392	(32)
		307, 393	(33)
		299, 387, 554	(34)
		299, 397, 479, 550	(35)
β -FeOOH	Akaganeite	415, 715	(35)
γ -FeOOH	Lepidocrocite	252, 380	(31)
		257, 393	(33)
		250, 376	(34)
		252, 380, 526, 650, 1307	(35)
Fe ₃ O ₄	Magnetite	616, 663	(31)
		535, 665	(32)
		550, 670	(34)
		662	(35)
α -Fe ₂ O ₃	Hematite	227, 245, 293, 298, 414, 501, 612	(31)
		228, 248, 296, 413, 500, 612, 1324	(36)
		223, 293, 406	(33)
		293, 299, 412, 613	(34)
		220, 238, 288, 408, 498, 608	(35)
Fe(OH) ₂		560	(31)
		544	(37)
Fe(OH) ₃		303, 387, 698	(34)
Cr ₂ O ₃	Eskolaite	300, 350, 540	(22)
		352, 531, 557, 619	(33)
		303, 351, 397, 530, 551, 609	(38)
CrO ₃		213, 233, 336, 376, 399, 495, 562, 975	(38)

Table 3.1. Summary of the band positions for different iron and chromium oxides according to different workers.

Among all iron compounds, the most studied are hematite and magnetite. Hematite belongs to the D_{3d}^6 crystal space group and seven phonons are expected in the Raman spectrum (36), namely two A_{1g} modes (225 and 498 cm⁻¹) and 5 E_g modes (247, 293, 299, 412 and 613 cm⁻¹). De Faria *et al.* (36) assigned the intense feature at 1320 cm⁻¹ to a two-magnon scattering which arises from the interaction of two magnons created on

anti-parallel close spin sites. This result does not confirm the experiment and calculation of McCarty (39) and Massey *et al* (40). Their high pressure measurements over a wide temperature range, and with isotopic oxygen substitution, allows for example identification of the 1320 cm^{-1} band being due to a two-phonon scattering. They also predicted a two-magnon mode at $\approx 1540\text{ cm}^{-1}$ and measured also a weak, broad feature near this energy whose temperature dependence and lack of shift with ^{18}O substitution are consistent with the two-magnon scattering.

Magnetite has a spinel structure O_h^7 giving rise to five Raman active modes: three T_{2g} , one E_g and one A_{1g} . Since magnetite is a poor Raman scatterer, most of the time only two bands are visible at 545 and 670 cm^{-1} . They have been respectively assigned to the T_{2g} and A_{1g} modes (36).

Ferric oxyhydroxide exists in several forms α -, β -, γ -, δ - and ϵ -FeOOH. The β -, δ - and ϵ -phases are, however, rarely encountered. The α - and γ -phases, on the other hand are much more common, existing in nature as goethite and lepidocrocite and can be identified by their main Raman bands respectively at 388 and 250 cm^{-1} .

Since most authors present Raman spectra or peak table of the references they used, a large number of references are available in the literature. The table above presents a summary of band position for the main iron oxides.

3.7.1.2. Green rust

Iron (II-III) hydroxysalts commonly named green rust (GRs), belong to a class of divalent-trivalent ionic minerals which are characterised by a crystal structure that consists of the stacking of $\text{Fe}(\text{OH})_2$ -like layers (carrying a positive charge due to the presence of $\text{Fe}^{(\text{III})}$) and interlayers constituted of anions and water molecules (41). GRs were often reported as corrosion products of iron, low carbon and stainless steel.

Boucherit *et al.* (28), during corrosion of iron under pitting conditions ($+600\text{ mV}$ vs. saturated calomel electrode), observed two bands at 420 and 505 cm^{-1} . They could not relate them to any Raman studies of iron compounds. Recently, Legrand *et al.* (42,43) studied a new carbonate green rust obtained electrochemically and Refait *et al.* (41) analysed the formation of hydroxysulphate green rust during marine corrosion of steel. Even if the GRs are different, the two research groups agreed that two strong bands around 430 and 508 cm^{-1} unambiguously identify the compound resulting from the

oxidation or iron as a GR where the two peaks may be respectively attributed to Fe^{2+} -(OH) and Fe^{3+} -(OH) stretchings.

3.7.1.3. Mixture identification

Figure 3.5 illustrates the identification process, comparing the unknown spectrum (top spectrum) with two other reference spectra: hematite (Fe_2O_3) and lepidocrocite ($\gamma\text{-FeOOH}$). The unknown compounds found at the surface of a corroded sample contain a number of peaks that match with both of the reference spectra. It is therefore possible to say, in this particular example, that the corrosion product present on the sample surface is a mixture of hematite and lepidocrocite.

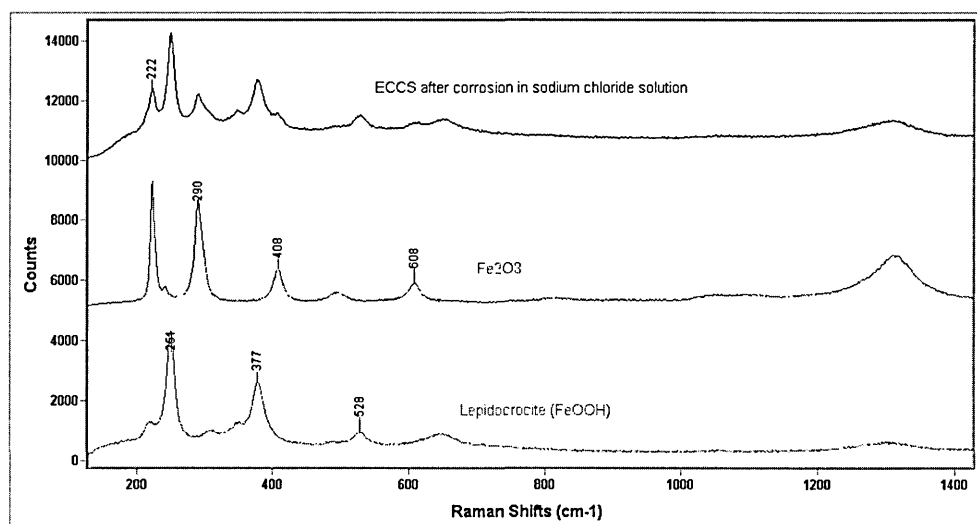


Figure 3.5. Quantitative information: identification of different corrosion products present on an electro chromium coated steel (ECCS) sample surface after corrosion in Sodium Chloride solution using Raman spectra

The challenge concerning that of mixed-product analysis by Raman spectroscopy is developed in more detail in section 4.1.2

3.7.2. Quantitative information and mapping

Band intensities depend on the amount of scattered light detected by the spectrometer. The greater the concentration of a given species present at a sample surface, the higher is the intensity of scattered characteristic light.

Using this relationship, it is possible to follow the evolution, with time, of a corroding system by Raman spectroscopy thereby obtaining information about the quantity of a certain species during the experiment. A second application, illustrated in Figure 3.6, is the possibility to map the sample surface and to determine the

concentration of the compounds across a mapped area. In the example given, it is clearly visible that the oxide on the sample surface is present in greater concentration in the middle ($\approx 30\mu\text{m}$) of the corroded area than on the edges.

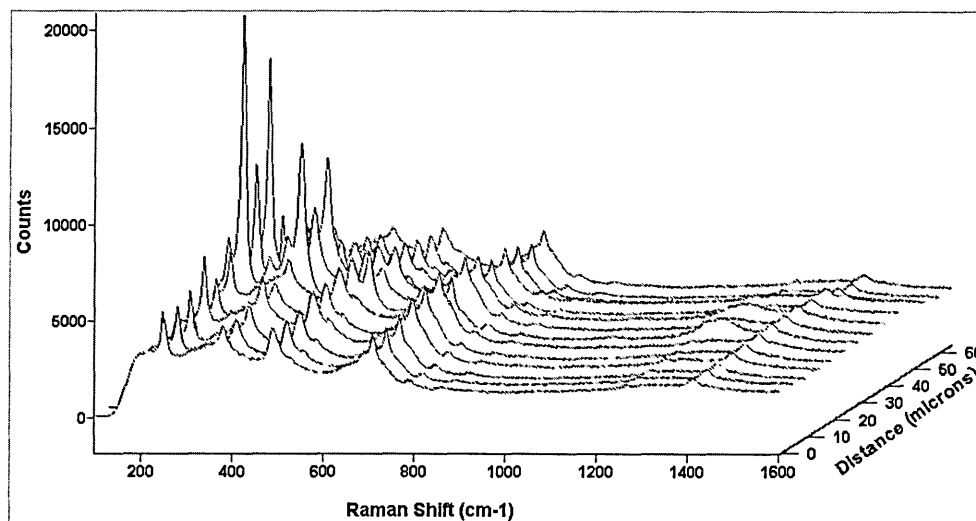


Figure 3.6. Mapping across a corroded area of ECCS steel: evolution of band intensities

Finally, Singh Raman, Gleeson and Young (44) used laser Raman spectroscopy for rapid characterisation of oxide scale layers developed on steel during the hot rolling stage of steel strip production. Chemical characterisation of millscales is relevant to the understanding of steel strip surface quality and its further processing. Singh Raman *et al.* identified the phase constitution of typical thick scales ($500\ \mu\text{m}$) formed on pure iron and mild steel as a superposition of FeO, magnetite mixed with wüstite and of magnetite covered by a thin layer ($5\ \mu\text{m}$) of Fe_2O_3 . Raman spectroscopy can be used to provide phase identification within micrometre thick scales containing different iron oxides.

3.7.3. Raman and Corrosion conditions

Aqueous metal corrosion at elevated temperature (22,45-47) is of great importance in systems such as fossil fuel power plants, nuclear power plant and hydrothermal oxidation reactions. Melendres and Simpson (48) studied, by surface enhanced Raman spectroscopy (SERS) corrosion of iron in aqueous environments at different temperatures and potentials. At 0.6 V Raman spectra showed an increase in intensity of the Raman peaks at $544\ \text{cm}^{-1}$ and $688\ \text{cm}^{-1}$ as the temperature increased. This is consistent with an increase of $\text{Fe}(\text{OH})_2$ and Fe_3O_4 in the corrosion film at higher temperatures. Furthermore, the decrease in intensity of the $552\ \text{cm}^{-1}$ band at 0 V from 25 to 95°C suggests that FeOOH is less prevalent at elevated temperature.

S.J. Tjong (49) investigated the nature of the oxides formed on iron chromium alloys at elevated temperature. He showed that the oxidation of iron at 350°C proceeds at an early stage of high oxidation rate followed by a second stage of low oxidation rate. During the first stage, Fe₃O₄ forms, grows and thickens over a surface of iron substrate. Fe₂O₃ later begins to nucleate and grow over this magnetite layer. As the growth process of the Fe₂O₃ layer is completed, the oxidation of iron proceeds at a lower oxidation rate. For Fe-9Cr alloy exposed to air at 400°C, the Raman spectrum indicates that the majority of the peaks are attributed to α-Fe₂O₃ but complementary Auger elemental depth profile shows that the oxide consists of a multi-layered structure. At 600°C, the Raman bands due to hematite become very weak and a broad band from a spinel oxide (FeO.Cr₂O₃) is observed. As the oxidation temperature is increased to 850°C, the Raman bands due to hematite disappear and only the bands attributed to Cr₂O₃ and spinel oxide are observed in the spectrum. The kinetics of the oxidation temperatures up to 500°C favour the formation of the iron oxide layer. At oxidation temperatures higher than 900°C, however, they favour the formation of Cr₂O₃ as the thermodynamically stable phase.

3.7.4. Utilisation of SERS for corrosion studies

The surface enhanced Raman spectroscopy (SERS) technique has been largely used in corrosion studies to overcome the lack of sensitivity from certain types of sample, such as iron or other metallic specimens. In order to enhance the signal, a large range of methods for roughening the surface can be adopted, e.g. electroplating, evaporation, chemical reduction or etching but the most efficient method is the application of controlled oxidation-reduction cycle.

Mengoli *et al.* (50) described two different strategies for preparing iron and steel electrodes. The first one was based on the deposition of iron onto SERS active substrate while the second was based on the deposition of silver on smooth iron substrates. Aramaki *et al.* used the technique described by Mengoli to study the absorption behaviour of pyridine (51) and other organic compounds (52) on iron but the deposition of iron onto a silver substrate makes the technique far from being representative of the corrosion processes happening on real samples.

Later, Baek *et al.* (53) studied the effect of dissolved oxygen on the corrosion film on low carbon steel in 0.01 M NaCl solution. To enhance the signal, as Simpson and

Melendres *et al.* (48), they chose to electro-deposit silver on the steel substrate by passing 130 mC/cm² of cathodic charge at a potential of -0.6 V in 0.001 M HNO₃ + 0.001 M AgNO₃. While Simpson *et al.* used the SERS technique to study the dependence of iron in aqueous solution, Baek *et al.* showed that different concentrations of dissolved oxygen caused different trivalent iron oxide products to develop. Oblonsky *et al.* (25) studied the passive film formed on transition metals and alloys in borate buffer solution and once again, they used the same technique as described above to create silver islands on the samples studied. Several other papers (26,52,54-58) have been published where the SERS technique was used to study corrosion processes and, even if in all the experiments described the authors managed to obtain more or less well resolved Raman spectra, the application of a noble metal on the metallic substrate can not be neglected since it creates a galvanic cell at the surface of the sample and influence the localised corrosion processes making the technique less than suitable for corrosion studies.

3.8. References

- (1) Threthewey KR, Chamberlain J. Corrosion for students of science and engineering. 3rd ed. Singapore: Longman Scientific & Technical; 1992.
- (2) Heitz E, Henkhaus R, Rahmel A. Corrosion Science an experimental approach. 1st ed. : Ellis Horwood Limited; 1992.
- (3) Fontana MG. Corrosion Engineering. 3rd ed. : International student edition; 1986.
- (4) West JM. Basic corrosion and oxidation. 1st ed. : Ellis Horwood Limited; 1980.
- (5) Mattsson E. Basic corrosion technology for scientists and engineers. 1st ed. England: Ellis Horwood Limited; 1989.
- (6) Scully JC. The fundamentals of Corrosion. 3rd ed. : Pergamon Press; 1990.
- (7) Jones DA. Principles and prevention of corrosion. 2nd ed. U.S.A: Prentice-Hall; 1996.
- (8) Pourbaix M. Atlas of equilibria in aqueous solution. : Pergamon; 1966.
- (9) Guy AG, Rhines FN. Pourbaix diagrams, a firm basis for understanding corrosion.
- (10) Beverskog B, Puigdomenech I. Revised Pourbaix diagrams for Chromium at 25-300 deg C. Corrosion science 1997; 39 (1): pp. 43-57.
- (11) Beverskog B, Puigdomenech I. Revised Pourbaix diagrams for iron at 25-300 deg C. Corrosion Science 1996; 38 (12): pp. 2121-2135.
- (12) EG&G Princeton applied research. Electrochemistry and corrosion: overview and techniques. Application note CORR-4.
- (13) Isaacs HS. The localised breakdown and repair of passive surfaces during pitting. Corrosion Science 1989; 29 (2-3): pp. 313-323.

- (14) Akid R, Mills DJ. A comparison between conventional macroscopic and novel microscopic scanning electrochemical methods to evaluate galvanic corrosion. *Corrosion Science* 2001 7; 43 (7): pp. 1203-1216.
- (15) Isaacs HS, Vyas B. Scanning reference electrode techniques in localised corrosion. *Electrochemical corrosion testing* 1981: pp. 3-33.
- (16) Bard AJ, Faulkner LR. *Electrochemical methods: Fundamentals and applications*. : John Wiley & Sons; 2000.
- (17) McMurray HN, Worsley DA. Scanning electrochemical techniques for the study of localised metallic corrosion. *Research in chemical kinetics* 1997; 4: pp. 149-202.
- (18) Nazarov A, Thierry D. Rate-determining reactions of atmospheric corrosion. *Electrochimica Acta* 2004 7/30; 49 (17-18): pp. 2717-2724.
- (19) Williams G, McMurray HN. The mechanism of group (I) chloride initiated filiform corrosion on iron. *Electrochemistry Communications* 2003 10; 5 (10): pp. 871-877.
- (20) Juzeliunas E, Leinartas K, Furberth W, Juttner K. Study of initial stages of Al-Mg alloy corrosion in water, chloride and Cu(II) environment by a scanning Kelvin probe. *Corrosion Science* 2003 9; 45(9): pp. 1939-1950.
- (21) Grundmeier G, Schmidt W, Stratmann M. Corrosion protection by organic coatings: electrochemical mechanism and novel methods of investigation. *Electrochimica Acta* 2000 5/3; 45 (15-16): pp. 2515-2533.
- (22) Fabis P, Heidersbach RH, Brown CW, Rockett T. Oxide scale formation on iron-chromium alloys in elevated temperature air environments. *Corrosion* 1981; 37 (12): pp. 700-711.
- (23) Gardiner DJ, Littleton CJ. Identification of oxide and sulphide corrosion products using Raman Microscopy. *High Temperature alloys* 1987: pp. 155-164.
- (24) Ferreira MGS, Silva TME, Catarino A, Pankuch M, Melendres CA. Electrochemical and Laser Raman-Spectroscopy Studies of Stainless-Steel in 0.15 M NaCl Solution. *Journal of the Electrochemical Society* 1992 NOV; 139 (11): pp. 3146-3151.
- (25) Oblonsky LJ, Devine TM. A Surface-Enhanced Raman-Spectroscopic Study of the Passive Films Formed in Borate Buffer on Iron, Nickel, Chromium and Stainless-Steel. *Corrosion Science* 1995 JAN; 37 (1): pp. 17-41.
- (26) Maslar JE, Hurst WS, Bowers WJ, Hendricks JH, Aquino MI, Levin I. In situ Raman spectroscopic investigation of chromium surfaces under hydrothermal conditions. *Applied Surface Science* 2001 8/1; 180 (1-2): pp. 102-118.
- (27) Reid ES, Cooney RP, Hendra PJ, Fleischmann M. A Raman spectroscopic study of corrosion of lead electrodes in aqueous chloride media. *Journal of Electroanalytical chemistry* 1977; 80: pp. 405-408.
- (28) Boucherit N, Delichere P, Joiret S, Hugot-Le Goff A. Passivity of iron and iron alloys studied by voltammetry and Raman Spectroscopy. *Material science forum* 1989; 44&45: pp. 51-62.
- (29) Boucherit N, Hugot-Le Goff A, Joiret S. Raman studies of corrosion films grown on Fe and Fe-6Mo in pitting conditions. *Corrosion Science* 1991; 32 (5-6): pp. 497-507.

- (30) Rensch D, Veal B, Natesan K, Grimsditch M. Transient oxidation in Fe-Cr-Ni alloys: A Raman-scattering study. *Oxidation of Metals* 1996 DEC; 46 (5-6): pp. 365-381.
- (31) Thibeau RJ, Brown CW, Heidersbach RH. Raman spectra of possible corrosion products of iron. *Applied Spectroscopy* 1978; 32 (6): pp. 532-535.
- (32) Keiser JT, Brown CW, Heidersbach RH. Use of Raman-Spectroscopy in Iron Corrosion Studies. *American Laboratory* 1982;14 (4): pp. 17-24.
- (33) England WA, Bennett MJ, Greenhalgh DA, Jenny SN, Knights CF. The characterization by Raman spectroscopy of oxide scales formed on a 20Cr-25Ni-Nb stabilized stainless steel. *Corrosion Science* 1986; 26 (7): pp. 537-545.
- (34) Williams KPJ, Smith BJE, Hayward IO. *New Horizons in Raman microscopy and Raman imaging*. : International Labmate.
- (35) Nauer G, Strecha P, Brindakonopik N, Liptay G. Spectroscopic and Thermoanalytical Characterization of Standard Substances for the Identification of Reaction-Products on Iron Electrodes. *Journal of Thermal Analysis* 1985; 30 (4): pp. 813-830.
- (36) De Faria DLA, Venancio Silva S, de Oliveira MT. Raman Microspectroscopy of some iron oxides and oxyhydroxides. *Journal of Raman spectroscopy* 1997; pp. 28: 873-878.
- (37) Ferreira MGS, Melendres CA. *Electrochemical and optical technique for the study and monitoring of metallic corrosion*. : Kluwer Academic Publishers; 1991. pp. 355-388.
- (38) Vuurman MA, Stufkens DJ, Oskam A, Moulijn JA, Kapteijn F. Raman-Spectra of Chromium-Oxide Species in $\text{CrO}_3/\text{Al}_2\text{O}_3$ Catalysts. *Journal of Molecular Catalysis* 1990 MAY 1; 60 (1): pp. 83-98.
- (39) McCarty KF. Inelastic light scattering in $\alpha\text{-Fe}_2\text{O}_3$: Phonon vs. magnon scattering. *Solid State Communications* 1988 11; 68 (8): pp. 799-802.
- (40) Massey MJ, Baier U, Merlin R, Weber WH. Effects of pressure and isotopic substitution on the Raman spectrum of $\alpha\text{-Fe}_2\text{O}_3$; Identification of the two-magnon scattering. *The American Physical Society* 1990; 41 (11): pp. 7822-7827.
- (41) Refait P, Memet J-, Bon C, Sabot R, Génin JMR. Formation of the Fe(II)-Fe(III) hydroxysulphate green rust during marine corrosion of steel. *Corrosion Science* 2003 4; 45 (4): pp. 833-845.
- (42) Legrand L, Abdelmoula M, Gehin A, Chausse A, Génin JMR. Electrochemical formation of a new Fe(II) - Fe(III) hydroxy-carbonate green rust: characterisation and morphology. *Electrochimica Acta* 2001 3/30; 46 (12): pp. 1815-1822.
- (43) Legrand L, Sagon G, Lecomte S, Chausse A, Messina R. A Raman and infrared study of a new carbonate green rust obtained by electrochemical way. *Corrosion Science* 2001 SEP; 43 (9): pp. 1739-1749.
- (44) Raman RKS, Gleeson B, Young DJ. Laser Raman spectroscopy: a technique for rapid characterisation of oxide scale layers. *Materials Science and Technology* 1998 MAY; 14 (5): pp. 373-376.
- (45) Fabis P, Brown CW, Rockett T, Heidersbach RH. An Infrared and Raman-Spectroscopy Study of the Corrosion Products on Carbon-Steel and Weathering Steel. *Oxidation of Metals* 1981; 16 (5-6): pp. 399-407.

- (46) Maslar JE, Hurst WS, Bowers WJ, Hendricks JH, Aquino MI. In situ Raman spectroscopic investigation of aqueous iron corrosion at elevated temperatures and pressures. *Journal of the Electrochemical Society* 2000 JUL; 147 (7): pp. 2532-2542.
- (47) Ohtsuka T, Kudo K, Sato N. Raman spectroscopy of thin corrosion films on iron at 100°C to 150°C in air. *Corrosion* 1986 AUG; 42 (8): pp. 476-481.
- (48) Simpson LJ, Melendres CA. Temperature dependence of the surface enhanced Raman spectroelectrochemistry of iron in aqueous solutions. *Electrochimica Acta* 1996 6; 41 (10): pp. 1727-1730.
- (49) Tjong SC. Laser Raman spectroscopic studies of the surface oxides formed on iron chromium alloys at elevated temperatures. *Materials Research Bulletin* 1983 2;18(2): pp. 157-165.
- (50) Mengoli G, Musiani MM, Fleischmann M, Mao B, Tian ZQ. Enhanced Raman-Scattering from Iron Electrodes. *Electrochimica Acta* 1987 AUG; 32 (8): pp. 1239-1245.
- (51) Aramaki K, Uehara J. The surface enhanced Raman scattering spectra of pyridine adsorbed on an iron surface. *Journal of Electrochemical society* 1990; 137 (1): pp. 185-187.
- (52) Aramaki K, Uehara J. A SERS study on adsorption of some organic compounds on iron. *Journal of electrochemical society* 1989; 136 (5): pp. 1299-1303.
- (53) Baek W, Kang T, Sohn H-, Kho YT. In situ surface enhanced Raman spectroscopic study on the effect of dissolved oxygen on the corrosion film on low carbon steel in 0.01 M NaCl solution. *Electrochimica Acta* 2001 4/30; 46 (15): pp. 2321-2325.
- (54) Melendres CA, Pankuch M, Li YS, Knight RL. Surface enhanced Raman spectroelectrochemical studies of the corrosion films on iron and chromium in aqueous solution environments. *Electrochimica Acta* 1992 12; 37 (15): pp. 2747-2754.
- (55) Gui J, Devine TM. The influence of sulphate-ions on the surface-enhanced Raman spectra of passive films formed on iron. *Corrosion Science* 1994 MAR;36 (3): pp. 441-462.
- (56) Reichert W,M., Andrade J,D. Surface Raman spectroscopy. Surface and Interfacial aspects of biomedical polymers: Joseph D. ANDRADE; 1985. pp. 421-442.
- (57) Rubim JC, Dunnwald J. Enhanced Raman scattering from passive film on silver-coated iron electrodes. *Journal of electroanalytical chemistry* 1989; 258: pp. 327-344.
- (58) Gui J, Devine TM. Obtaining surface-enhanced Raman spectra from the passive film on iron. *Journal of the electrochemical society* 1991; 138 (5): pp. 1376-1384.

Chapter 4. *Experimental approaches and Technical challenges*

4.1. Technical challenges

The advantages of Raman spectroscopy for in-situ corrosion analysis have previously been presented. However, the effect of experimental parameters can have a dramatic consequence on the sample, transforming Raman investigation into a real challenge.

In the following sections, the effect that the laser source may have on the sample studied will be illustrated through two basic experiments. The problems encountered during sample interpretation, such as compound identification and quantification, will then be introduced through the utilisation of quantitative analysis techniques. Finally the difficulties met during the realisation of in-situ experiments will be presented.

4.1.1. Sample degradation

4.1.1.1. Introduction

The danger of thermal degradation of the sample has been pointed out by many authors. In 1978, Thibeau, Brown and Heidersbach (1) reported a study based on the identification of possible products of iron, recording spectra from polycrystalline samples of iron oxides and oxyhydroxides. They found that the Raman spectra obtained from wüstite (FeO) and magnetite (Fe₃O₄) were similar even if the X-ray diffraction patterns confirmed that the two samples were different. Their first assumption was to explain the similarity between the two spectra by the nature of the Fe-O bonds which cause Raman bands of Fe₃O₄ to be nearly identical to those of FeO. After further consideration, they believed that a more likely explanation was that FeO, unstable at temperature below 570 °C, was transformed by the laser. Recently, de Faria *et al.* (2) used a defocused laser, with a low power (0.7 mW), to decrease the possibility of decomposition. They shown that wüstite and magnetite were different since the 300 and 535 cm⁻¹ bands were not present in the FeO spectrum and the 670 cm⁻¹ peak from magnetite shifted to 652 cm⁻¹ and appeared significantly broadened because of the contributions from non-equivalent sites in the wüstite structure. Nevertheless, they

showed, using a higher power laser, that wüstite was decomposed to magnetite which was then further transformed to hematite ($\alpha\text{-Fe}_2\text{O}_3$).

In order to evaluate the effect of the laser power on our sample, two different experiments have been devised. While the first experiment consisted in studying the evolution of the Raman spectrum of a magnetite sample as a function of the intensity of the laser used, the second experiment was based on the determination of the sample 'molecular' temperature of a hematite powder by comparing the intensity of the Stokes and anti-Stokes bands.

4.1.1.2. Transformation of magnetite under laser excitation

a. Experimental

To illustrate the deleterious effect that the laser source may have on the sample studied, a 98 % iron (II,III) oxide powder from Aldrich Chemical Corporation Ltd has been exposed to different laser powers. For this experiment, a 25 mW He/Ne (632 nm) laser has been used. Using the attenuation wheel enclosed in the Raman spectrometer, the power of the excitation light could be adjusted from 100 % to, 1, 10, 25 or 50 % of the maximum power delivered by the laser source. For each laser power available, a Raman spectrum was recorded. In order to facilitate the comparison between each spectrum, the same objective ($\times 50$ magnification) and spectrometer settings (5 \times 60 seconds accumulation time) have been used for all spectra. Finally, to complete the result obtained by Raman spectroscopy, the magnetite powder was studied under a microscope before and after the exposure to the laser source.

b. Results

The Raman spectra obtained after focussing the laser on the magnetite powder using a laser power of 10, 25 and 50 % of the maximum power are shown in Figure 4.1. At 10 % of the laser power, the spectrum presents a strong band at 670 cm^{-1} which can be attributed to the A_{1g} vibrational mode of magnetite. After increasing the laser power up to 25 % of its maximum, important changes in the Raman spectra can be observed. Several new broad bands, in the lower wave number region (between 200 and 600 cm^{-1}) and one band in the 1320 cm^{-1} region become visible. Additionally, the signal to noise (S/N) ratio is about twice as high in the spectrum recorded using 25 % laser power than in the one recorded at 10 % laser power showing that the new compound is a much better light scatter than the original magnetite. When 50 % of the laser power is used,

the S/N ratio is again doubled. The 670 cm^{-1} band from magnetite is still visible, but now overlaps with a band located at 607 cm^{-1} . Finally, as well as a broad band at 1320 cm^{-1} , three more intense bands, characteristic from hematite ($\alpha\text{-Fe}_2\text{O}_3$) can be observed in the spectra at 225 , 290 and 408 cm^{-1} .

Comparing the Raman spectrum of maghemite ($\gamma\text{-Fe}_2\text{O}_3$) recorded by de Faria *et al.* (2) and the one obtained here using 25 % laser power, shows that the spectrum acquired using 25 % laser power could be identified as a mixture of magnetite and maghemite. At 50 % laser power, the bands reveal the presence of both hematite and magnetite.

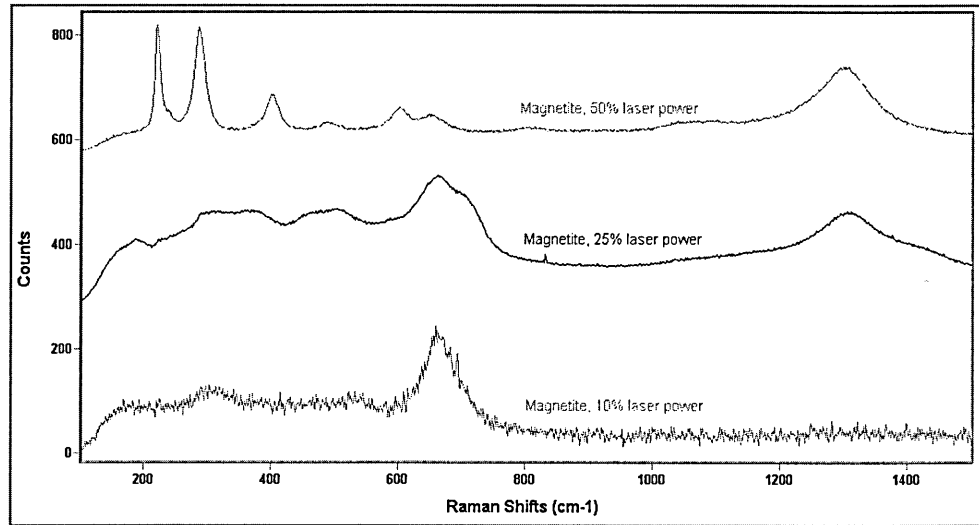


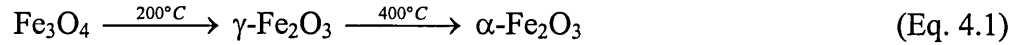
Figure 4.1 Raman spectra of magnetite acquired using a laser power of 10, 25 and 50 % of the maximum laser power.

In addition, observation using an optical microscope revealed that the sample, originally black, presented a reddish spot at the same position as where the laser spot has been focussed. The reddish colour was identical to the colour of the hematite reference powder supplied by Aldrich Chemical Corporation.

c. Discussion

De Faria *et al.* tried to correlate the sample degradation due to the high intensity laser source with the increase of the temperature within the sample. In order to achieve this, they decided to run two comparative experiments. The first one was based on acquiring Raman spectra of a magnetite crystal before and after heating it up in a flame while the second one was based on the utilisation of a temperature stage to raise the temperature of the magnetite sample up to $300\text{ }^\circ\text{C}$.

Firstly, the authors proved that the degradation of magnetite observed using a high intensity laser was due to an increase of the temperature. Secondly, they showed that the change of Fe_3O_4 to $\gamma\text{-Fe}_2\text{O}_3$ occurred at a temperature between 200 and 300 °C. In a paper published in 1964, Goto (3) showed that magnetite undergoes a phase transition with a temperature increase (equation 4.1). Moreover, Nauer *et al.* used a derivative thermal analysis technique to demonstrate that lepidocrocite dehydration occurs at 260 °C according to equation 4.2.



Even if the temperature that causes the dehydration of lepidocrocite (260 °C) is much lower than the one at which degradation of magnetite to hematite occurs (400 °C), such a transformation has not been observed using the maximum laser power on lepidocrocite powder. It appears that the sensitivity to laser power depends on the characteristics of the different oxide analysed (e.g. surface morphology, colour, etc...). The fact that magnetite is subject to a much more important increase in temperature can be simply due to its black colour, absorbing more radiation from the red laser than the red powder of lepidocrocite which should reflect most of the exciting light.

4.1.1.3. Temperature calculations (Stokes / Anti Stokes ratio)

The experiments described above highlighted the fact that even if the laser had a deleterious heating effect on the sample, the temperature increase was not really quantified. In the current work, a different approach has been used to try to calculate the temperature changes due to exposure to the laser source. The aim of the experiment was to use the Boltzmann distribution law (see section 2.3.2.2) to calculate the microscopic temperature of the sample. By rearranging equation 2.7, the temperature can be expressed as a function of the amount of energy between two considered levels and their intensities as shown by equation 4.3.

$$T = \frac{-\Delta E}{k \ln(I_{AS} / I_S)} \quad (\text{Eq. 4.3})$$

where ΔE is energy of the transition, k the Boltzmann constant and I_{AS} and I_A , the intensities of the energy level, which are directly related to the intensities of the anti-Stokes and Stokes bands.

a. Experimental

Since magnetite was subject to degradation, a 99.99 % pure hematite powder from Aldrich chemical Ltd was used. Raman spectra were recorded from hematite in air and immersed in deionised water, from both anti-Stokes and Stokes regions, using a 5 mW He/Ne laser and at different laser powers (1, 10, 25, 50 and 100 %). A $\times 20$ long working distance objective was used in order to avoid contact between the objective lens and the solution.

b. Results and discussion

The anti-Stokes and Stokes Raman spectra of hematite in air and in water, at full laser power, are presented in Figure 4.2 and Figure 4.3. By comparing the spectra displayed in both figures, it can first be seen that the Raman bands are three to four times weaker in water than in air. This intensity drop is due to the absorption of the scattered light by the water, reducing the probability of the light to be collected by the microscope objective and then by the CCD detector.

Second, it can be noticed that the most intense peak is not the same in the anti-Stokes and Stokes region for either hematite in air or in solution. In the anti-Stokes spectrum, the most intense feature is the A_{1g} vibrational mode at -225 cm^{-1} while for the Stokes spectrum it is the E_g mode at 291 cm^{-1} . Then, by comparing the intensities of the Stokes bands obtain from hematite in air and in water, it can be seen that the intensity ratio of the 225 and 291 cm^{-1} bands is different in air and in water showing that a reduction of the number of counts is not the only phenomenon that occurs when the sample is immersed in water. In the anti-Stokes spectrum, the same phenomenon can be observed where the ratio between the band at -225 and -291 cm^{-1} is about 3:2 in air and of about 1:1 in water.

Finally, the very high band intensities observed in the Stokes spectra suggest that Raman scattering is not the only phenomenon that is occurring when hematite is exposed to a laser source. This could be explained by either a contribution of fluorescence or of Resonance Raman. Since the increase in the background characteristic of fluorescence is not observed here, Resonance Raman is probably the only phenomenon at the origin of the high spectra intensities and band ratio changes.

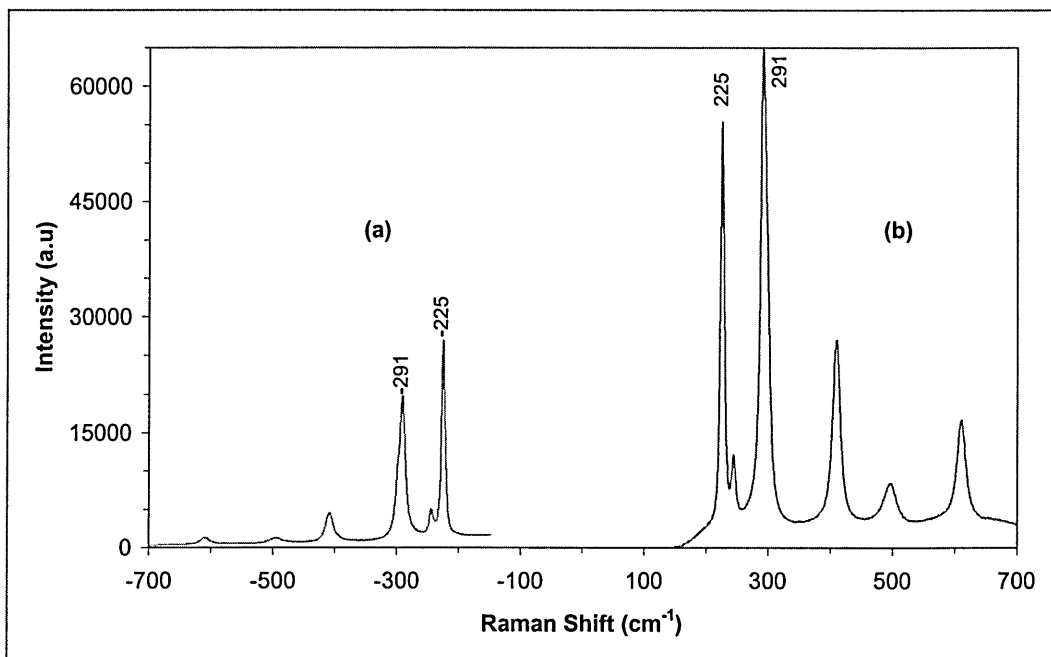


Figure 4.2 Anti-Stokes (a) and Stokes (b) bands of hematite in air. Spectra acquired using a 5 mW He/Ne laser (100% laser power).

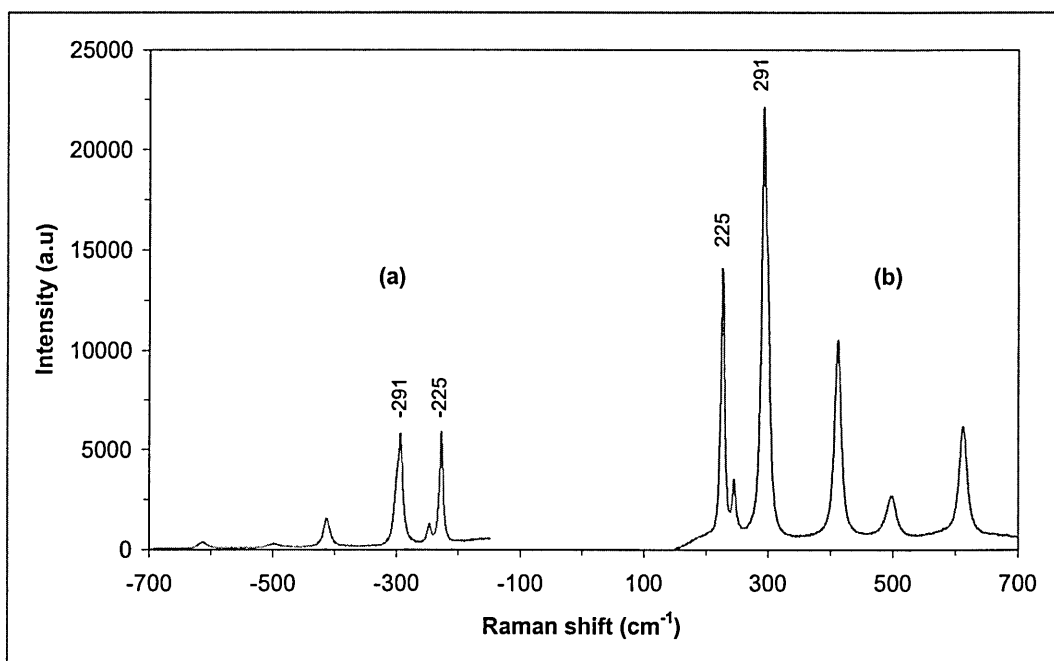


Figure 4.3 Anti-Stokes (a) and Stokes (b) bands of hematite in water. Spectra acquired using a 5 mW He/Ne laser (100% laser power).

Unfortunately, the fact that hematite is subject to the resonance Raman effect make it unsuitable for temperature calculation by the Boltzmann distribution since the consideration of two different bands will give two different temperatures for the same sample. For example, in the case of the sample in solution, if we consider the $\pm 291 \text{ cm}^{-1}$ bands, the resulting temperature is 24°C . If we consider the $\pm 225 \text{ cm}^{-1}$ bands, the calculated temperature reaches a value of 119°C .

4.1.2. Compound identification and quantification

In the current work, an attempt to evaluate the quantity of each oxide present within an oxide mixture has been made using quantitative analysis. One of the keys to quantitative analysis is the assumption that the amounts of the constituents of interest in the samples are directly related to the data from a measurement technique. The ultimate goal is to create a calibration scheme which, when applied to data of unknown samples measured in the same manner, will accurately predict the quantities of the constituents of interest. In order to calculate the necessary set of equations, a set of standard samples have to be made. Once the model equations have been established, they can be used to identify and quantify the amount of each compound in an unknown sample.

4.1.2.1. Calibration set preparation

In order to evaluate the method, a model system has been designed using only three different reagent grade powders of iron oxides: lepidocrocite, hematite and magnetite. Lepidocrocite was purchased from Alfa Aesar; magnetite and hematite from Aldrich Chemical Company Ltd.

	γ -FeOOH	Fe ₃ O ₄	Fe ₂ O ₃
1	100 %	0 %	0 %
2	0 %	100 %	0 %
3	0 %	0 %	100 %
4	50 %	50 %	0 %
5	0 %	50 %	50 %
6	50 %	0 %	50 %
7	50 %	25 %	25 %
8	25 %	50 %	25 %
9	25 %	25 %	50 %
10	60 %	20 %	20 %
11	20 %	60 %	20 %
12	20 %	20 %	60 %
13	40 %	30 %	30 %
14	30 %	40 %	30 %
15	30 %	30 %	40 %
16	33 %	33 %	33 %

Table 4.1 Composition of the 16 standards used for the calibration model.

In order to avoid magnetite degradation, a $\times 20$ long working distance objective has been used to focus the 5 mW He/Ne laser set to 25 % of its maximum power. The three powders have been weighed and mixed in 16 different standards as shown in Table 4.1.

To achieve good homogeneity in the composition of the standards, each mixture has been ground using a mortar and pestle for a set time of 2 minutes before observation by Raman spectroscopy.

4.1.2.2. Results and discussion

The Raman spectra of the three pure powders, displayed in Figure 4.4, show the characteristic bands for each oxide. The two main peaks for γ -FeOOH (fig. 4.4.a) are at 250 and 377 cm^{-1} . These peaks are about 10 times more intense than the main magnetite (fig. 4.4.b) broad band centred at 670 cm^{-1} but are about 6 times less intense than the two sharp peaks of hematite (fig. 4.4.c) located at 225 and 291 cm^{-1} . The difference in intensity between the spectra suggests that a very small amount of hematite might be detected by Raman, but that a large quantity of magnetite will be needed for detection.

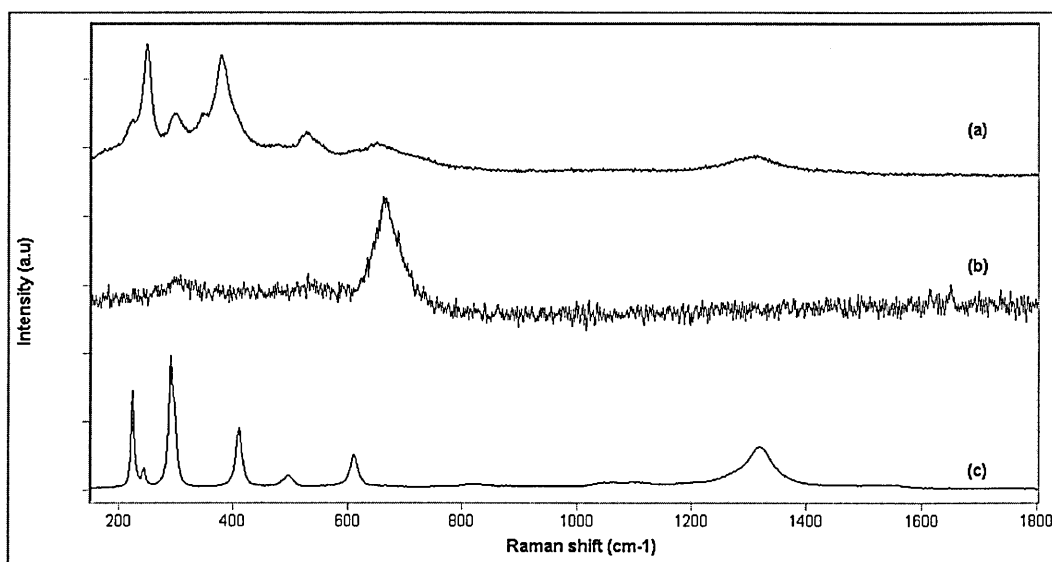


Figure 4.4 Raman spectra of pure powders of lepidocrocite (a), magnetite(b) and hematite (c)

When a Raman spectrum of the same amount of magnetite, hematite and lepidocrocite is recorded (Figure 4.5), all the main bands from each oxide can be observed but the relative bands intensities do not match with the expected intensities shown in the reference spectra (Figure 4.4).

Additionally, the main feature visible is the magnetite band while the four main bands of both lepidocrocite and hematite are badly resolved and show a low signal to noise ratio. The difficulty in detecting hematite and lepidocrocite might be due to the

presence of large magnetite particles within a non homogeneous sample, even after the two minutes grinding process.

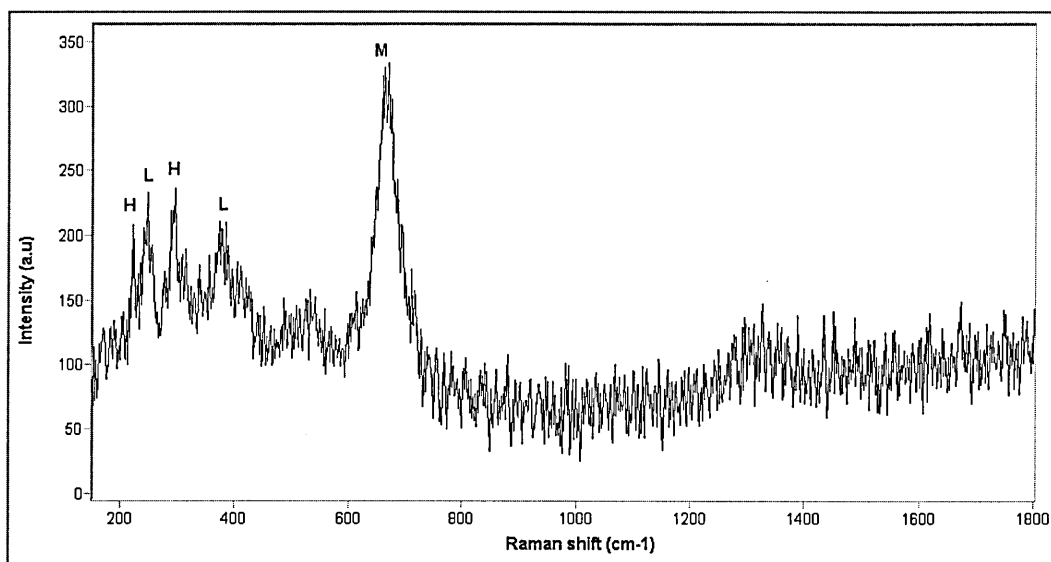


Figure 4.5 Mixture containing 33 % in weight of magnetite (M), hematite (H) and lepidocrocite (L)

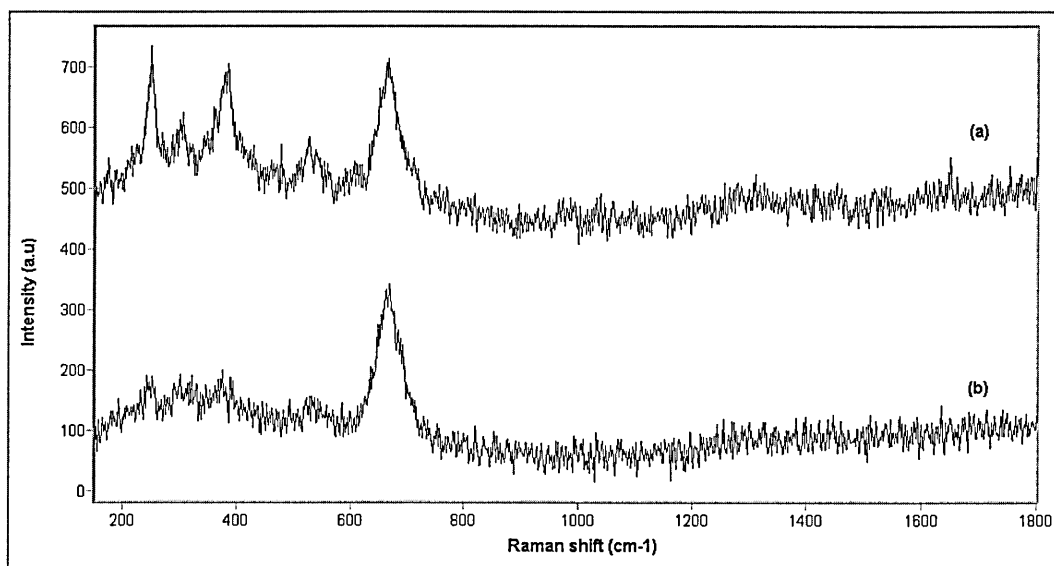


Figure 4.6 Mixture containing 50 % lepidocrocite and 50 % magnetite. Same sample studied but with spectra taken from two different positions (a) and (b).

In order to check the homogeneity of the mixed sample, two Raman spectra of a mixture made of 50 % magnetite and 50 % lepidocrocite have been recorded from a single sample, at two different positions (Figure 4.6). In both spectra, the contribution of magnetite are equivalent showing the main 670 cm^{-1} with almost the same intensity as the pure sample spectra.

For lepidocrocite, even if the bands at 250 and 377 cm^{-1} are clearly identified and are as intense as the magnetite band in spectrum (a), it's very difficult to detect the lepidocrocite bands in spectrum (b). The difference between spectra (a) and (b) highlight the difficulty of mixing effectively the reagent grade powders. While lepidocrocite is a thin dry powder, magnetite is 'sticky', making the mixing process difficult.

In 1978, Thibeau et al (1) recorded Raman spectra from different pure iron oxides in order to create a spectra database. After recording spectra from FeO, Fe_3O_4 , $\alpha\text{-Fe}_2\text{O}_3$ and α - and $\gamma\text{-FeOOH}$, they recorded a spectrum of a mixture of 90 % magnetite and 10 % hematite by weight. They observed that, despite the concentration difference, the bands due to ferric oxide, $\alpha\text{-Fe}_2\text{O}_3$, were as strong as those of Fe_3O_4 . They also concluded that, because of to the wide variation in spectral intensities between the two different compounds, it was not possible to determine exactly a single minimum concentration necessary to observe the spectrum of a minor component in a mixture. According to their results, as little as 5 % of $\alpha\text{-Fe}_2\text{O}_3$ could be identified in Fe_3O_4 . But, in a mixture with Fe_3O_4 as the minor component, at least 30 % Fe_3O_4 was required before it could be detected in $\alpha\text{-Fe}_2\text{O}_3$.

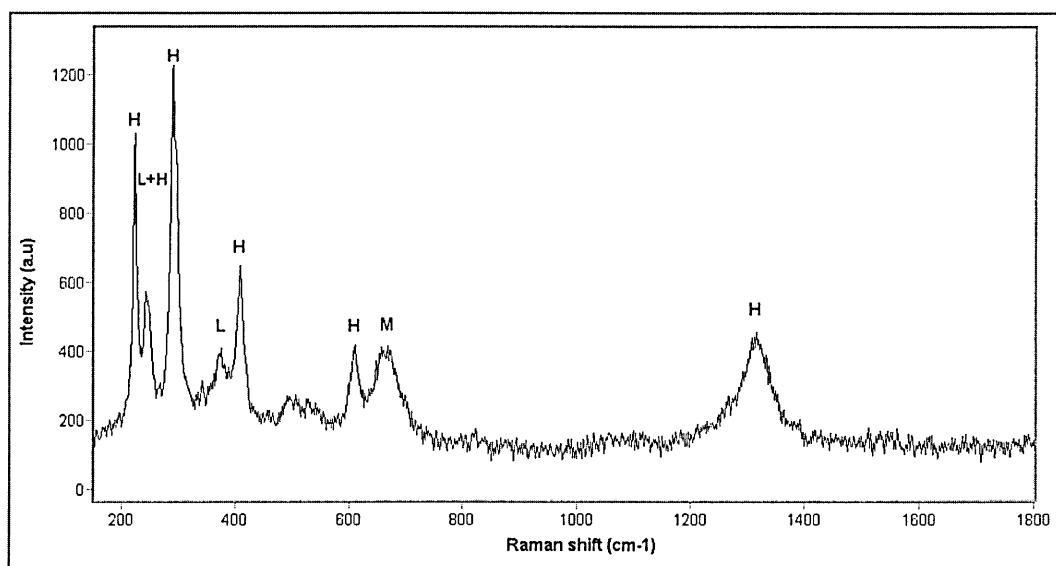


Figure 4.7 Mixture of 60 % lepidocrocite (L), 20 % magnetite (M) and 20 % hematite (H)

In Figure 4.7, the Raman spectrum of a mixture of 60 % lepidocrocite, 20 % magnetite and 20 % of hematite is presented. Even when $\gamma\text{-FeOOH}$ is the main compound of the mixture, the 250 and 377 cm^{-1} bands do not appear to be as intense as expected. The first one, overlapping with the 242 cm^{-1} band of $\alpha\text{-Fe}_2\text{O}_3$, is not resolved

and the second one, much weaker than the 408 cm^{-1} band of hematite, is present on the left hand shoulder of the hematite peak. Moreover, even if only 20 % of magnetite is present in the mixture, the 670 cm^{-1} band is clearly visible, with a Raman scattering as strong as in a pure spectrum. This result does not confirm Thibeau *et al.* experiment but the KBr-iron oxides pellets they used may give a much more homogeneous oxides mixture.

4.1.2.3. Conclusions

The experiment described above revealed the difficulty of mixing together the reagent iron oxides powder to create of a set of standard spectra for quantitative analysis. Even if the mixing procedure might be improved by using KBr-iron pellets, as it as been done by Thibeau *et al.* (1), the reference preparation process will make the quantitative technique inappropriate for in-situ corrosion analysis because the sample under investigation will have to be analysed in exactly the same conditions as the one used for the creation of the standard. Moreover, since a large number of oxides can be formed on a simple substrate, depending on the experimental conditions (e.g.: pH, temperature, oxygen concentration, nature of the solution etc...) a large number of calibration standards would need to be made. These would be valid only with a limited type of experiment, making the analysis process long and laborious.

Furthermore, it has been highlighted in section 4.1.1.3, iron oxides are subject to resonance enhancement. It might be possible that the fact that the 670 cm^{-1} band from magnetite appears so strongly in all the mixtures is due to a selective resonant enhancement due to the utilisation of the red laser. Such a problem has not been highlighted by Thibeau *et al.* and it can partially be explained by the utilisation of a 488 and a 514.5 nm lasers. Therefore, the unpredictable behaviour of one of the compounds used for the creation of the calibration spectra would discredit the analysis method.

Finally, since the quantitative analysis technique can not be applied to in-situ corrosion analysis, it is impossible to determine accurately the absolute amount of each compound present in a Raman spectrum collected. The only way to obtain quantitative information is to study two different spectra from the same system and compare the shape, intensity and position of the band to check how they have changed with experimental parameters (potential applied, time etc...).

4.1.3. In-situ experiment

The main interest of using Raman spectroscopy for corrosion studies relies on first, the type of chemical information that it offers and second, on the possibility of running real time in-situ experiments. When a sample is immersed in solution, the excitation laser has to be focused onto the sample surface, through the solution, using a long working distance objective. It is necessary to use a long working distance objective to avoid contact between the stainless steel objective and the solution. This will protect the objective from the corrosive environment and avoid the alteration of the corrosion behaviour of the sample studied by creating a galvanic cell. However, the use of a long working distance objective and the presence of the solution above the sample combine to reduce drastically the amount of scattered light. This results in a considerable reduction of the signal to noise ratio and of the spectral quality.

As presented in section 3.7.4, numerous authors, have improved their spectral quality either by using surface enhanced Raman spectroscopy (SERS), or by taking the sample out of the solution. Depositing silver particles for SERS or exposing the sample to air might have a detrimental effect on the sample by creating a galvanic cell or by changing the oxide developed during the corrosion processes. This may make the results irrelevant to the real system studied. It is obvious that if we wish to obtain results without perturbing the system, we must avoid the use of SERS, and keep the sample in solution.

The most common ways of improving the Raman signal to noise ratio are to increase either the acquisition time or the laser power. While an intense laser source might damage the sample (section 4.1.1) an increase of the Raman acquisition time (between two successive spectra) may make the collection process incompatible with the kinetic study of the corrosion processes. It is necessary to have a relatively quick acquisition process to avoid missing some crucial phases of the development of the corrosion products.

The key to in-situ corrosion studies by Raman spectroscopy is then based on our ability to design an experimental cell allowing the minimum amount of solution between the sample surface and the laser source, and to find the best compromise between laser power and accumulation time. A well planned selection of experimental parameters will allow us obtain good quality spectra within a reasonable amount of

time, without altering the sample and losing the possibility to study the kinetic of the corrosion processes.

4.1.4. Effect of the electrochemical factors

4.1.4.1. Chloride contamination

Two different reference electrodes have been used to measure the potential of the working electrode during all the in situ experiments. The first one, employed for the experiment on iron in sodium chloride solution was a saturated calomel electrode (SCE) with a potential of +244 mV versus standard hydrogen electrode (SHE). The second electrode used was a double junction Ag/AgCl electrode with a potential of +222 mV versus the SHE. The double junction electrode has been utilised in all the experiments realised in chloride free solutions. A double junction electrode was needed to avoid chloride contamination of the solution. Such a precaution was necessary since Gui and Devine (4) noticed that the film grown in borate solution was different if chloride ions were added to the solution. To avoid the contamination of the solution they used a double junction reference electrode instead of a conventional saturated calomel electrode. In order to confirm that they did not have any chloride contamination, they repeated one of the experiments using a sulphate reference electrode and concluded that the double junction electrode was appropriate for the experiment. To check if our SCE was compatible with chloride free experiment, the electrode was dipped in a silver nitrate solution. After few seconds of immersion, a white precipitate of silver chloride became visible, highlighting the fact that the solution was contaminated by the chloride ions. A similar test was run using the double junction Ag/AgCl electrode and no precipitate was visible in the solution. We conclude that a double junction electrode should be used for an experiment where chloride contamination needs to be avoided.

4.1.4.2. Effect of the scan rate on potentiodynamic studies

To study the different systems presented in the current work, some potentiodynamic studies have been run. Since such experiments had to be performed using a potentiostat driven by the appropriate software, a range of parameters such as the scanning range, the minimum and maximum current and more importantly the scan rate had to be set. In most of the papers published, a conventional scan rate of $5 \text{ mV}\cdot\text{s}^{-1}$ was used, without real justification.

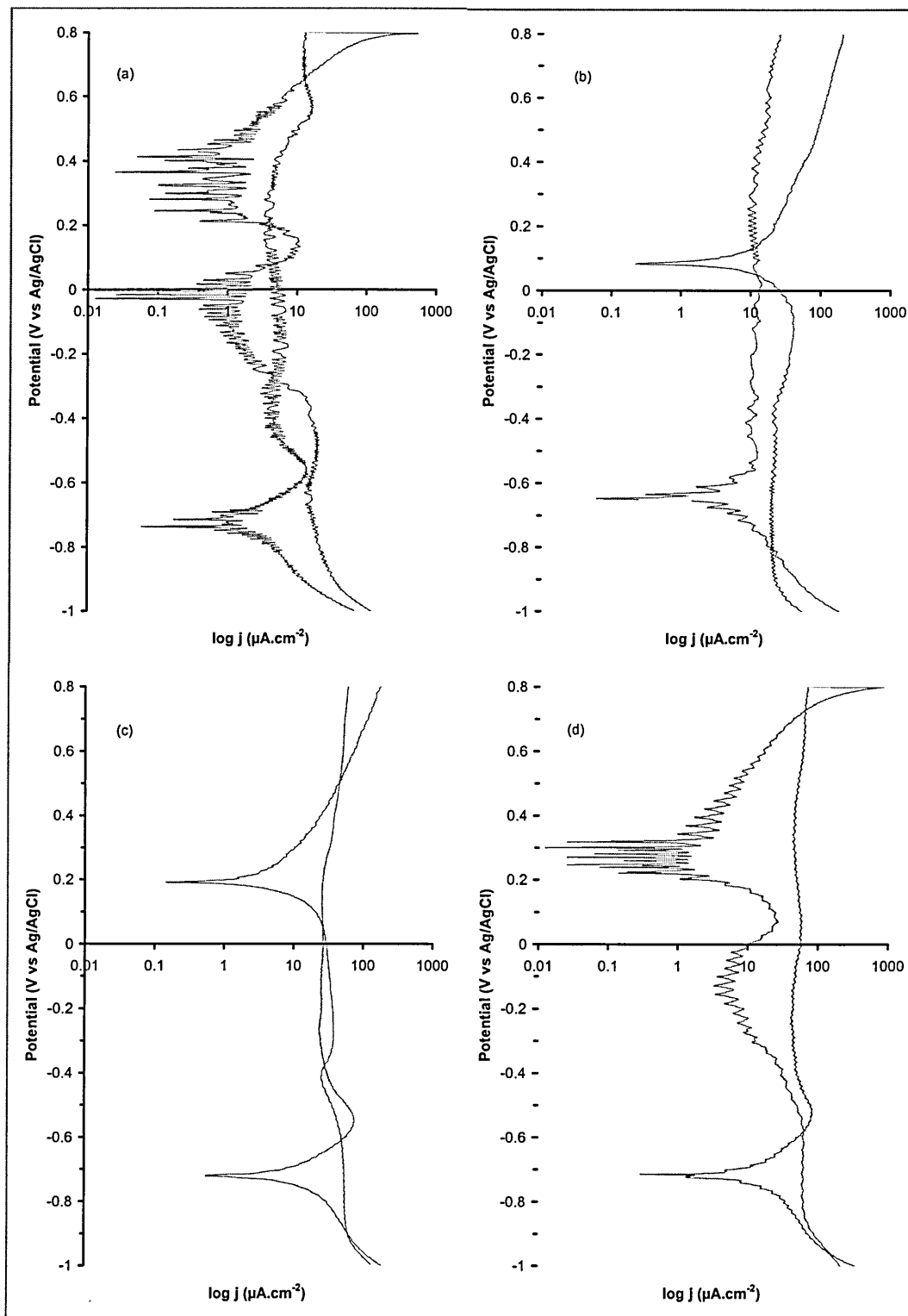


Figure 4.8 Effect of the scan rate on the cyclic polarisation curve of pure iron in borate buffer solution. (a) 1 mV.s^{-1} , (b) 2.5 mV.s^{-1} , (c) 5 mV.s^{-1} and (d) 10 mV.s^{-1}

In Figure 4.8, four cyclic polarisation curves; recorded from a pure 10 mm diameter iron disc immersed in a pH 7.7 borate buffer solution, using different scan rates of respectively 1, 2.5, 5 and 10 mV.s^{-1} are presented. In order to allow the study of the effect of the scan rate, all curves have been recorded under identical conditions using

freshly cleaned and polished iron working electrode. The potential was scanned in both anodic and cathodic directions for all samples between -1.0 and +0.8 V versus a double junction Ag/AgCl reference electrode. The current recorded during the potentiodynamic experiment is expressed in current density j (μ).

The first comment that can be made (after a general observation of the four different curves) is that they all reflect roughly the same electrical behaviour, showing in all cases the open circuit potentials (where the current value drop toward $0 \mu\text{Acm}^{-2}$) in both forward and reverse scan. It is then interesting to note that the main difference between the curves remains in the quality of the data recorded. When a scan rate of 1 mV.s^{-1} is used, a very noisy current is recorded during the scan of the potential resulting in a very large potential range in which the reverse free corrosion potential could be present (between +0.20 and +0.45 V). Increasing the scan rate to 2.5 mV.s^{-1} permits to reduce drastically this phenomenon giving two well defined forward and reverse open circuit potential at respectively -0.65 and +0.1 V. By increasing again the scan rate to 5 mV.s^{-1} , a clear improvement in the quality of the potentiodynamic curve can be seen resulting in a very smooth curve. The final plot presented in the graph has been recorded using a scan rate of 10 mV.s^{-1} . Strangely, the smoothing effect due to the increase of the scan rate disappeared making it difficult to identify of the open circuit potentials. Furthermore, it is interesting to note that the noise in the current recorded at 2.5 mV.s^{-1} is very different than the one recorded using a scan rate of 10 mV.s^{-1} . While using a low scan rate produces a 'random noise', the current measured at a scan rate of 10 mV.s^{-1} seems to present a high frequency periodic trend.

As it has been shown above, the choice of the scan rate for potentiodynamic studies has a non negligible effect on the data recorded. While increasing the scan rate to reduce the noise (due to the fact that the sample is left free between two potential changes), a too high scan rate cannot be used since it will produce a periodic artefact. This is because the sample studied cannot follow the evolution of the potential imposed by the potentiostat. As it has been used by others workers, a 5 mV.s^{-1} scan rate appears to be the most suitable choice to run cyclic polarisation studies. Hence, all potentiodynamic studies presented in the current work have been made using a scan rate of 5 mV.s^{-1} .

4.1.5. Nature and size of the working electrode

As a preliminary experiment, a piece of electro chromium coated steel (ECCS) was used to evaluate the feasibility of the analysis of corrosion processes by Raman spectroscopy. Due to its duplex layer of hydrated chromium oxide and metallic chromium, the sample was very resistant to corrosion, even once it has been exposed to the aggressive 3.5 % sodium chloride solution. In order to increase the corrosion activity of the sample, the ECCS was prepared by scratching its surface. This intentional defect created a weakness and increased the chances that anodic activity could occur. Furthermore the presence of a defect also defined the area of the sample to be analysed.

4.1.5.1. Experimental

Two types of experimental tests have been run. First, the ECCS has been left at open circuit potential for 12 hours in 3.5 % sodium chloride solution and second. Once corroded, it has been rinsed in deionised water and dried in air prior to further Raman analysis of the corrosion product grown during the experiment.

During most of the in situ analysis, the laser was set to its maximum power (100 %) because the thermal degradation of the sample was not expected due to the presence of the solution above the sample surface. In the case of the ex situ experiment, the value of the acquisition time used during the analysis depended on the resolution of each spectrum. When the value of the signal/noise ratio was not high enough, a complementary spectrum was acquired with a longer acquisition time.

Once the sample has been corroded and analysed in-situ, the sodium chloride solution has been removed and the sample gently rinsed with deionised water and dried at room temperature. This process permitted the elimination of the high background from the solution visible during in-situ investigation. Also, it allowed checking which products were really present at the sample surface by revealing the weakest Raman bands.

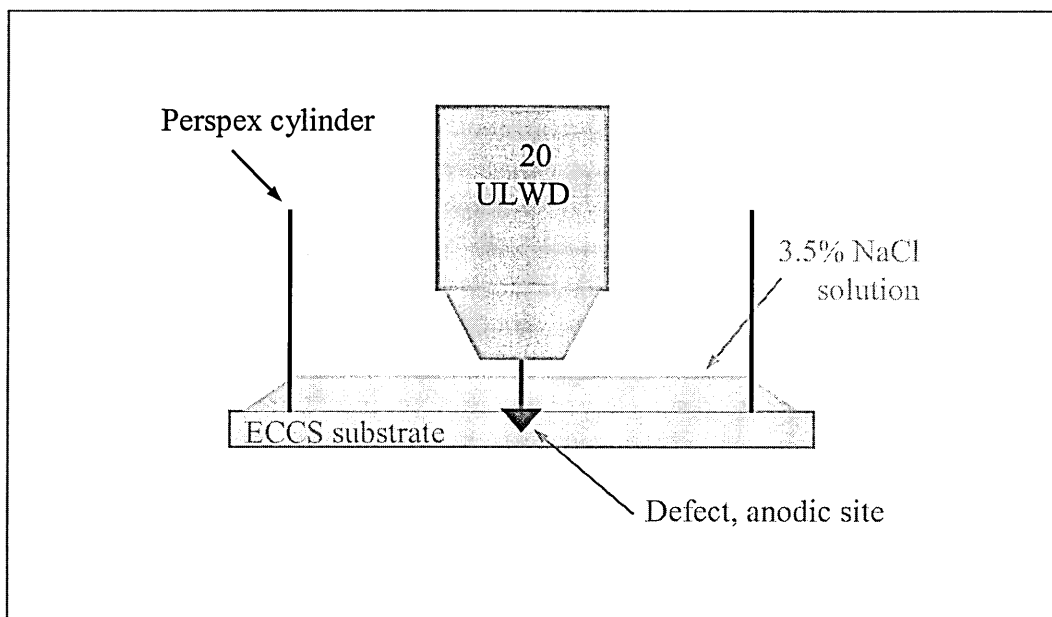


Figure 4.9 Schematic representation of ECCS and its experimental set up.

To establish that the sample surface analysed during the previous in situ investigation was representative of the full area exposed, a survey of the surface was completed by acquiring spectra from different corroded sites. The selection of the different spot analysed was based on the sample colour which could be due to the presence of different corrosion products or different concentration. A schematic representation of the experimental set up used to run the described experiments is presented in Figure 4.9. To validate the results obtained by the Raman analysis, each experiment was run five times using a fresh sample and solution.

4.1.5.2. In situ analysis

The changes observed between the Raman spectra recorded during the first experiment allowed information to be gained on the evolution of corrosion products forming on the surface of the sample with time. At the start of the investigation, only a high background and a broad band at 180 cm^{-1} (from hydrogen bonding of the water molecule) were visible on the first Raman spectrum. Then, subsequent spectra, recorded during the corrosion process revealed a regular development of two sharp and intense bands at respectively 250 cm^{-1} and 377 cm^{-1} (Figure 4.10). Using the reference spectra presented in Figure 4.4 these two bands have been attributed to lepidocrocite: the γ - crystalline form of the oxyhydroxide FeOOH .

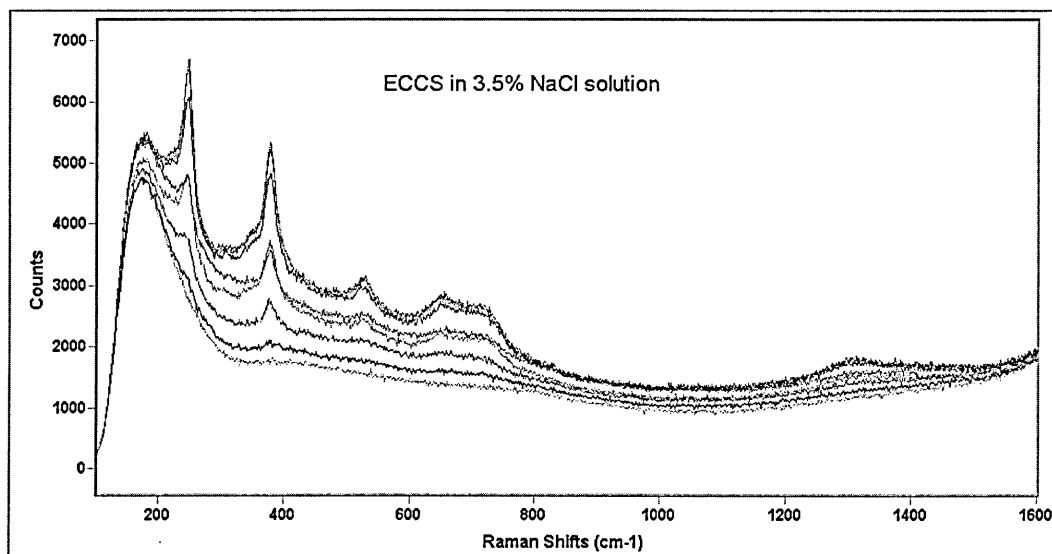


Figure 4.10 Evolution with time of ECCS Raman spectra during corrosion experiment (run 1). The bottom spectrum is the first acquired at the start of the experiment and the top one has been recorded after 6h in solution.

In order to follow the evolution of the corrosion product on the sample surface, the 377 cm^{-1} band was integrated. This mathematical process permitted the peak area between two arbitrarily selected boundaries to be analysed. Once this calculation had been completed, it was possible to plot the evolution of the peak intensity with respect to time as shown in (Figure 4.11).

The curve obtained from the first analysis shows two distinctive areas. During the first 3 hours of the experiment, the band intensity shows little change. Lepidocrocite ($\gamma\text{-FeOOH}$) then started to be visible and the associated calculated peak area increased linearly with time. This result implies that the corrosion of ECCS (Figure 4.11, 1st exp.) was preceded by an incubation period during which some reactions, not visible by Raman, could occur.

Attempts to repeat this experiment did not succeed. In some cases, with the same time spent in solution, no corrosion products were visible by Raman spectroscopy while they were clearly visible by eye. This lack of Raman activity could then be attributed to the possibility that the laser source was, in this specific case, focused on a cathodic site. While corrosion does occur on the anode sites, only reduction reactions take place and no oxides or oxyhydroxide would grow. Moreover, in cases where corrosion had been detected by Raman spectroscopy, the evolution of lepidocrocite concentration detected in the area analysed did not show a similar results to those shown in Figure 4.11. For example, the final values of the integrated area were nearly three times lower than the

one calculated from the data shown. Furthermore, the incubation period recorded in the first experiment was never reproduced.

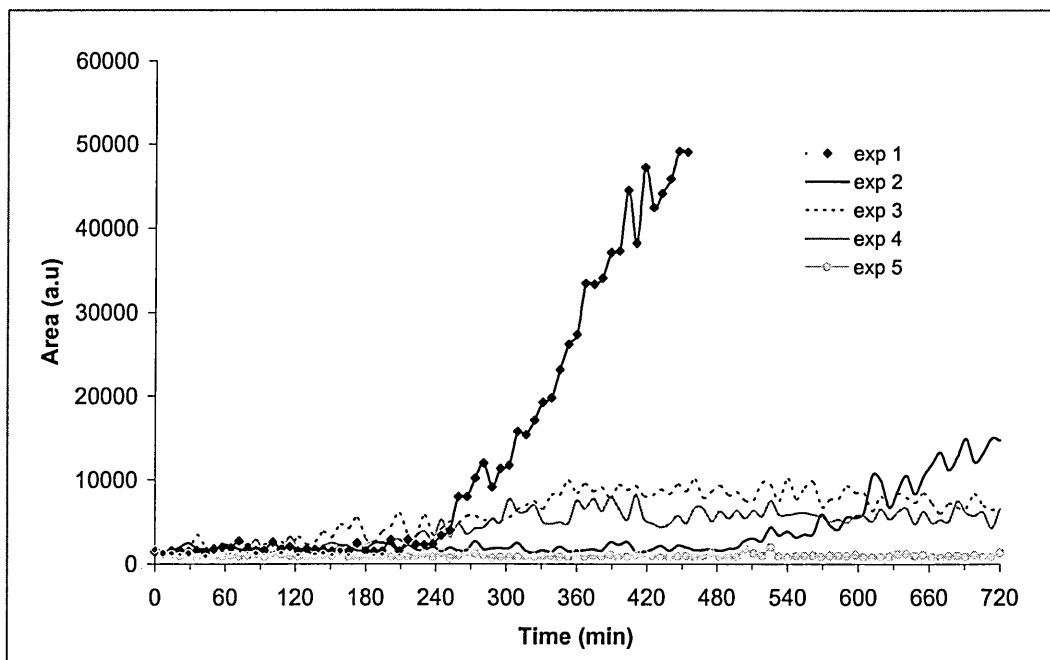


Figure 4.12 Plot of the relative area obtain from the integration of the 377 cm^{-1} band with respect to time.

Finally, the last spectrum of each experiment, acquired after 12 hours in solution, did not always present the same set of peaks. In some cases, two bands at 430 cm^{-1} and 495 cm^{-1} were clearly visible. These two bands, observed and interpreted in more detail in chapter 5 and 6, have been often attributed to an oxide, commonly called ‘green rust’.

4.1.5.3. Ex situ analysis

The aim of the ex situ experiments was to detect whether a particular passive layer had been grown during the oxidation of the exposed area. In Figure 4.12 three spectra acquired from three different corroded regions of a sample are presented.

In spectrum presented in fig.4.12.a, five resolved bands and one visible on the left shoulder of the 400 cm^{-1} broad peak can be seen. While the 220 , 290 , 400 and 1315 cm^{-1} bands have been attributed to hematite, the two less intense bands at 250 and 377 cm^{-1} have been identified as vibrational bands of lepidocrocite ($\gamma\text{-FeOOH}$). It is then possible to conclude without any real ambiguity that the corrosion product detected at this particular position of the sample could be identified as a mixture composed of lepidocrocite and mainly hematite ($\alpha\text{-Fe}_2\text{O}_3$).

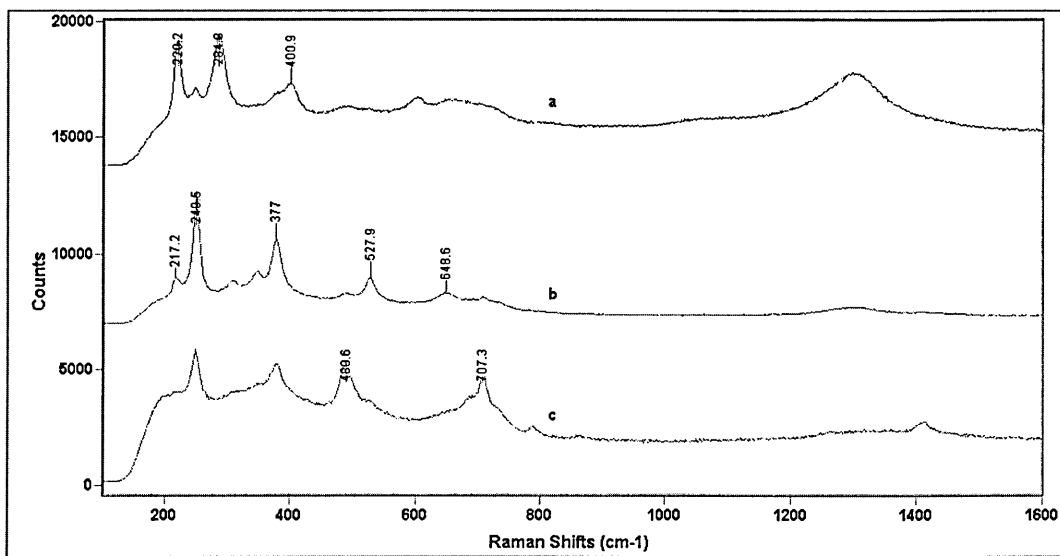


Figure 4.12 Raman spectra from different sites of an ECCS sample exposed in NaCl for approximately 12 hours and then rinsed with deionised water and dried at room temperature.

The second spectrum presented (fig.4.12.b) looks very similar to the reference spectrum of lepidocrocite presented in Figure 4.4. Since no additional bands can be detected it is clear that, in the area analysed, γ -FeOOH is the only oxide grown, at open circuit potential. Finally, in spectrum shown in fig.4.12.c, the main peaks from lepidocrocite (250 and 377 cm^{-1} bands) can be identified but two intense and broad bands around 490 cm^{-1} and 705 cm^{-1} can be observed. These two bands, unidentified so far, could be due to the presence of an iron oxide or even a chromium oxide but do not correspond to any band listed in table 3.1.

4.1.5.4. System assessment

The results presented above allow us to show that, for both in situ and ex situ analysis the use of Raman spectroscopy was not always compatible with localised corrosion studies. Since the results obtained from the in situ analysis were not reproducible and, since the dry sample analysis showed the presence of several different oxides, it was possible to conclude that the different parameters had to be controlled before we could reliably analyse and understand the behaviour of complex systems. A suitable assessment of the system was therefore necessary.

a. Nature of the defect

The way in which the defect had been created on the sample surface was not easily controlled. The area of the substrate exposed to the media was not easily reproducible and it was difficult to determine if the laser was focused onto the steel substrate or on

one of the chromium layers. Then, both reasons could partially explain the lack of reproducibility between similar experiments conducted at the free corrosion potential.

b. Ex situ analysis

The preparation processes preceding the ex situ analysis probably influenced the system. For example, by rinsing the ECCS to avoid the production of salt crystals at the sample surface, the floating rust particles may have been lost and not analysed. Moreover, a top oxide layer could easily have been removed by the water used during the cleaning process. Furthermore, before analysing the dry surface, the samples were left for few hours exposed to air at room temperature. By this time the corrosion products analysed (which may have contained considerable amounts of water) were likely to have been affected by drying. Thus, the corrosion oxides observed during the ex situ experiment might not be representative of the corrosion products that evolve at the ECCS surface during corrosion in sodium chloride solution.

c. Sample composition

Since several metals were present on the sample (steel substrate, hydrated chromium and metallic chromium), a large number of oxides could grow during the experiment. This made the interpretation of the corrosion processes difficult, and presented an additional challenge to more fundamental limitations of the technique itself.

d. Size of the electrode

Due to the large size of the electrode and to the fact that only a spot of $3 \mu\text{m}^2$ was examined by the Raman technique, it was impossible to know if the area on which the laser was focussed will act as an anode or a cathode before the start of the experiment.

Then, to overcome the different problems met during the preliminary experiments on ECCS, two model systems based on pure iron have been used to evaluate the utilisation of the Raman technique for corrosion studies. The first one was designed from a pure $25 \mu\text{m}$ iron wire. The choice of such dimension for the electrode was made to reduce the ratio Area exposed / Area analysed in order to survey an area much more representative of the whole surface. The second model, based on a twin electrode system, has been designed to force the analysed area to react either as an anode or a cathode by applying a potential difference between the two wires. The results obtained from the analysis of both model systems are presented in chapter 5.

4.2. Experimental

To evaluate the feasibility of an in-situ study, by Raman spectroscopy, the corrosion processes that can take place at a sample surface, three different systems were used. The two first systems were exposed to 3.5 % NaCl solution, the third one was exposed to three different buffer solutions: a borate, a carbonate and a phosphate solution.

4.2.1. Iron in 3.5% NaCl solution

4.2.1.1. Simple iron wire system (25 μm)

To make sure that the results obtained by Raman were representative of the surface exposed to the environment, a 25 μm diameter iron wire, supplied by Goodfellow was used in cross section. To facilitate the electrical connection and the sample preparation, the iron wire was connected to an electrical wire using high conductivity silver paint supplied by Agar Scientific Ltd. Then, to protect the sample and avoid exposure to atmosphere between the experiments, the wire was mounted in an epoxy resin (supplied by Buehler®).

Prior to each experiment, the iron electrode was polished with 1200 grade emery paper, washed in copious amounts of distilled water and then polished using first a 6 μm and a 1 μm diamond paste (Buehler®) to give the iron disc a mirror like finish. Once polished, the electrode was degreased using industrial methylated spirit and ultrasonically cleaned in distilled water.

In order to allow the control of the potential of the iron sample, a Radiometer Copenhagen PGP201 Potentiostat / Galvanostat was utilised. All potentials were measured against a saturated calomel electrode (SCE) and a 50 μm diameter gold wire was used as a counter electrode. During the first set of experimental tests, the iron wire was left at open circuit potential and the electrode potential was recorded, versus the SCE, via the potentiostat. Once this first series of tests were completed, the iron wire had been polarised at -300 mV for 6 hours and the current flowing between the counter and the working electrodes recorded. Prior to the start of the polarisation, the sample was prepolarised at -1.0 V for 30 minutes in order to clean the sample surface from any oxide film that could have been developed during the sample preparation processes.

The Raman system used is one described in section 2.3 and equipped with a 25 mW He/Ne laser, producing a power of 2-3 mW at the sample surface. The amount of 3.5 %

solution required was determined by the thickness of the layer of solution above the sample (2-3 mm). To avoid contact between the solution and the objective, a long working distance objective ($\times 20$) was utilised. A schematic representation of the system is presented in Figure 4.13.

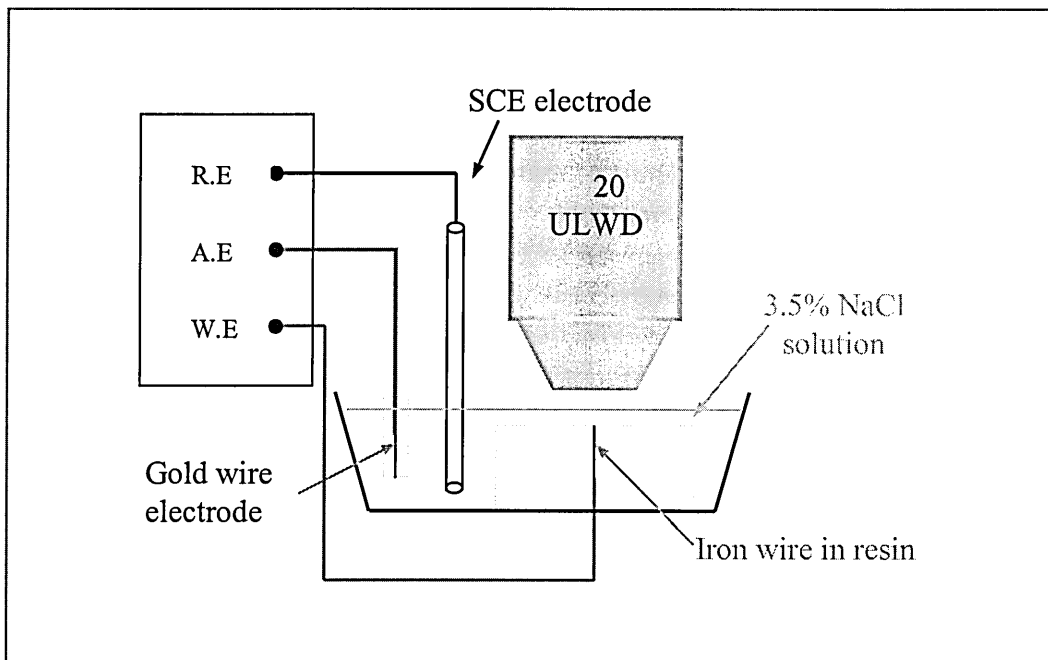


Figure 4.13 Schematic representation of Iron wire polarisation and its experimental setup. The three electrodes are connected to the potentiostat. The SCE electrode is the reference electrode (RE), the Gold wire is the auxiliary electrode (AE) and the iron wire is the working electrode (WE). The NaCl solution level is adjusted in order to assure the electrical contact between the electrodes without having too much solution above the sample (2-3 mm)

4.2.1.2. Twin iron wire model system

To compare the evolution of a cathodic and an anodic site during the corrosion processes, two 400 μm diameter iron wires were mounted in epoxy resin, as presented in section 4.2.1.1. The distance between the two wires was about 1 mm. This distance was large enough to avoid any eventual contact between the electrodes but small enough to ensure efficient ion exchange between the two electrodes. A similar polishing sequence was used to prepare the surface of the electrodes.

To create artificially an anodic and a cathodic site, the two wires were connected to a power supply delivering a constant potential difference of 1 V. To control the potential difference applied between the wires, two resistor precision boxes were connected as shown in Figure 4.14 and set to obtain the desired potential difference between the wires. The value of potential applied was checked by a voltmeter (V_2). A series of

experiments were run over a six-hour period. Between each experiment, the potential difference was increased by 10 mV. The first experiment was realised using a 20 mV potential difference and the last one with a 100 mV potential difference.

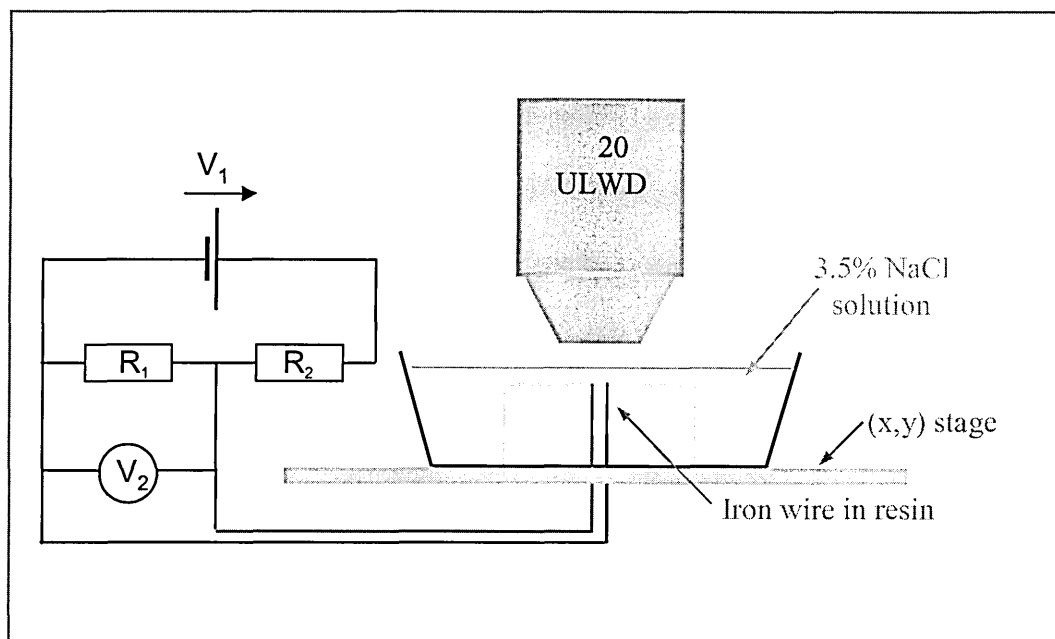


Figure 4.14 Schematic representation of the experimental setting used for the twin iron model system.

To allow the analysis of both wires by Raman spectroscopy, the system was mounted on a 2 dimensional mapping stage allowing the acquisition of Raman spectra from two different positions: one from the anode, one from the cathode. Once again, a $\times 20$ magnification objective was used to focus the laser through a layer of 2-3 mm of solution.

4.2.2. Iron in buffer solution

4.2.2.1. Sample

A 10 mm diameter pure iron disc, supplied by Goodfellow Cambridge Limited, was attached to an electrical wire and mounted in epoxy resin in order to isolate the electrical connection from the solution. The same polishing sequence as the one described in section 4.2.1.1 was used for the surface preparation. The iron electrode was then immersed in one of the three buffer solutions described below and cathodically cleaned by applying a potential of -1.0 V (vs. the Ag/AgCl reference electrode) for 30 minutes.

The potential applied was controlled using the potentiostat previously described. The choice of the double junction Ag/AgCl reference electrode was justified to avoid the possibility of chloride contamination, as mentioned in section 4.1.4.1. Finally, the auxiliary electrode was a platinum electrode.

4.2.2.2. Solutions

Three different solutions were used for the experiments presented in chapter 6. The pH 7.7 borate buffer solution was made from 0.3 M H_3BO_3 and 0.0375 M $\text{Na}_2\text{B}_4\text{O}_7 \cdot 10\text{H}_2\text{O}$. The boric acid was supplied by Fisher scientific and the sodium tetraborate decahydrate was supplied by Sigma Aldrich.

The pH 7.5 carbonate buffer solution was made from a 0.05 M carbonate / 0.05 M bicarbonate buffer solution which were both supplied by Sigma Aldrich.

Finally, the phosphate buffer solution was made from 0.1 M KH_2PO_4 (Sigma Aldrich) and 0.1 M NaOH hydroxide pellets from Riedel-de Haën.

4.2.2.3. Cyclic polarisation

To obtain electrochemical data on the behaviour of pure iron in the different buffer solution, a number of cyclic polarisation curves were recorded. In all the cases, the same experimental settings were used. The starting and reverse potential were respectively -1.0 V and +0.8 V. The scan rate selected, according to the results presented in section 4.1.4.2, was $5 \text{ mV} \cdot \text{s}^{-1}$ and 10 successive cycles were run.

4.3. References

- (1) Thibeau RJ, Brown CW, Heidersbach RH. Raman spectra of possible corrosion products of iron. *Applied Spectroscopy* 1978; 32 (6): pp. 532-535.
- (2) De Faria DLA, Venancio Silva S, de Oliveira MT. Raman Microspectroscopy of some iron oxides and oxyhydroxides. *Journal of Raman spectroscopy* 1997; 28: pp. 873-878.
- (3) Goto Y. *Japanese journal of applied physics* 1964; 3: p. 741.
- (4) Gui J, Devine TM. In situ vibrational spectra of the passive film on iron in buffered borate solution. *Corrosion Science* 1991; 32 (10): pp. 1105-1124.

Chapter 5. Iron model systems in Sodium Chloride solution

As shown in the previous chapter, the lack of homogeneity and the difficulty to obtain reproducible results from the electro chromium coated steel brought, to light the necessity to develop different systems. To give an evaluation of the use of Raman spectroscopy for in situ corrosion studies, two different systems, based on pure iron, were designed. While the first system, relied on a 25 μm diameter pure iron wire, the second, called the “twin iron model system”, was made from two 400 μm diameter wires mounted one next to the other.

For the simple model system, two different experiments were conducted. First, the iron wire was left at open circuit potential in sodium chloride solution. Second it was polarised for 2 hours at -300 mV. In both types of experiment, a set of Raman spectra was recorded in order to follow the evolution of the wire surface with time. Finally, to give complementary information, the potential between a reference electrode and the iron wire was recorded with time, during the experiment.

For the twin iron model system, several potential differences were applied between both iron wires, forcing one of the electrodes to react as a cathode and the other one as an anode. Once immersed in solution, and the potential difference applied between the electrodes, Raman spectra were recorded alternately from each site over 10 hours. Then, to complete the information obtained from the ‘in situ’ analysis, some optical pictures were taken during the experiments, and further Raman investigations were conducted from the dry electrodes.

Since the solution involved in the current chapter contains a large quantity of chloride ions, the application and measurement of potentials was referred to a Saturated Calomel Electrode (SCE). Thus, all the potentials given in the following paragraphs, unless stated differently, are expressed versus the SCE.

5.1. Simple iron wire model system

5.1.1. Open circuit potential analysis

5.1.1.1. Raman investigation

Once polished to 1 μm , a pure iron wire was immersed in 3.5% NaCl solution for 5 hours. During the whole experiment a Raman spectrum was recorded every 3 min to follow the evolution of the oxidation product with time. For clarity, only few of the spectra are displayed in Figure 5.1.

On the first spectrum, recorded after 30 minutes, a large amount of fluorescence is visible but despite the high background, a broad feature, centred at about 670 cm^{-1} , can be seen. In most cases, this band, when observed on its own, is often attributed to the A_{1g} vibrational mode of magnetite (Fe_3O_4) (1-5). The spectrum recorded 30 minutes later shows that the amount of fluorescence has been largely reduced and, even if the large band at 670 cm^{-1} is less intense and appears to shift toward 650 cm^{-1} , it does not remain the only feature present. Two bands, located at respectively 250 and 386 cm^{-1} are now well resolved. The diminution of the fluorescence observed along the experiment can be due to either, the fact that it has been burnt out due to the long exposure time under the laser or, to the fact that the fluorescing substrate was being covered by the oxide layer. While the 250 cm^{-1} band is attributed to $\gamma\text{-FeOOH}$, the presence of the band at 386 cm^{-1} could either be due to $\alpha\text{-}$ (characterised by a band 388 cm^{-1}) (6), $\gamma\text{-}$ (377 cm^{-1}), or even a mixture of both crystalline forms of FeOOH. Furthermore, since the 300 cm^{-1} band, representative of the $\alpha\text{-}$ form is not visible, the presence of the 250 cm^{-1} band confirms that the oxide is made of only lepidocrocite ($\gamma\text{-FeOOH}$).

Moreover, it is essential to note that in the presence of lepidocrocite, the band at 650 cm^{-1} can not be attributed to magnetite, for two reasons. First, the band position is too far away from the original A_{1g} mode from magnetite; and second, the 650 cm^{-1} frequency correspond to one of the vibrational modes of lepidocrocite.

After 90 minutes at open circuit potential, two more bands become visible in addition to the three from lepidocrocite. The first one is located on the left hand shoulder of the 377 cm^{-1} band, and the second one is centred around 530 cm^{-1} . Until 150 minutes at OCP, no further bands are seen in the Raman spectrum, but a clear improvement of the

signal to noise ratio can be observed. After 180 minutes at OCP, a final band, located at 316 cm^{-1} , becomes visible. No further evolution of the nature of the spectra can be observed during the remaining time of the experiment.

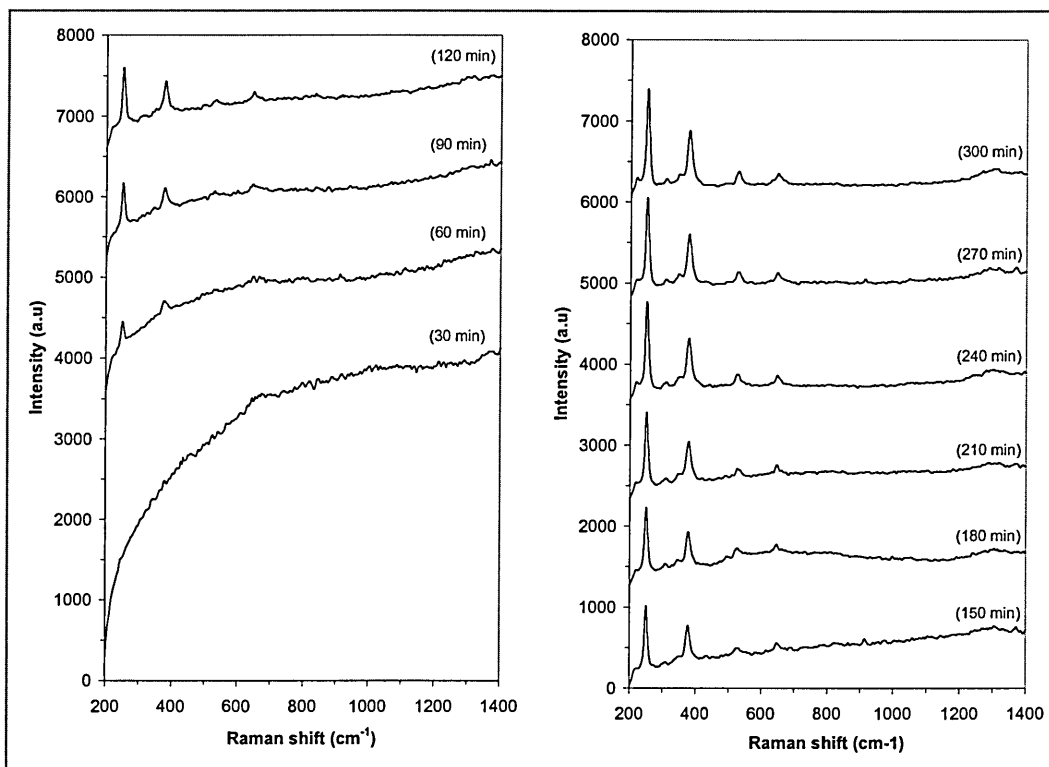


Figure 5.1. Evolution with time of the Raman spectrum of a 25 m iron disc in 3.5 % NaCl solution at open circuit potential.

Comparing the spectra recorded at the end of the experiment with the reference spectrum recorded from a pure lepidocrocite powder (see figure 4.4), permits us to identify all the bands as lepidocrocite vibrational modes. It is then possible to conclude that, despite the presence of the 670 cm^{-1} band from magnetite, the oxide developing at the surface of a pure iron sample immersed in 3.5 % NaCl solution contains only lepidocrocite. The presence of magnetite observed at the start of the experiment can not be explained here, and it is not possible to distinguish, due to the large fluorescence, whether magnetite is grown first on the sample surface (to then be oxidised to FeOOH), or whether the film formed on the iron wire is made of a bi-layer structure.

5.1.1.2. Comparison between Raman and OCP data.

All along the analysis, the open circuit potential has been recorded to explore whether the variation of the potential could be related to the evolution of the oxide present on the iron surface. In order to allow the comparison between two independent data sets (potential and Raman activity), the 250 and 384 cm^{-1} bands described in

5.1.1.1 have been integrated. The result of such integration, obtained between two set of fixed boundaries, permitted us to plot the evolution of the amount of oxide, against time. The area of the 250 and 384 cm^{-1} bands could then be plotted on the same graph as the OCP, as presented in Figure 5.2.

a. Raman bands area

The first observation that can be made from Figure 5.2 is that both curves (a) and (b) show exactly the same trend. Both areas are constant during the first 90 minutes of the experiment and then increase linearly between 90 and 300 minutes. Since both peaks show a similar behaviour, the first interpretation that can be made is that they probably arise from the same oxide. Since the 250 cm^{-1} band had been attributed to $\gamma\text{-FeOOH}$, and no band could be observed at 300 cm^{-1} , it is then possible to conclude that the 384 cm^{-1} band is due to the presence of $\gamma\text{-FeOOH}$ (and not to $\alpha\text{-FeOOH}$). This confirms the presence of a single oxide, as stated previously from the results on the Raman spectra.

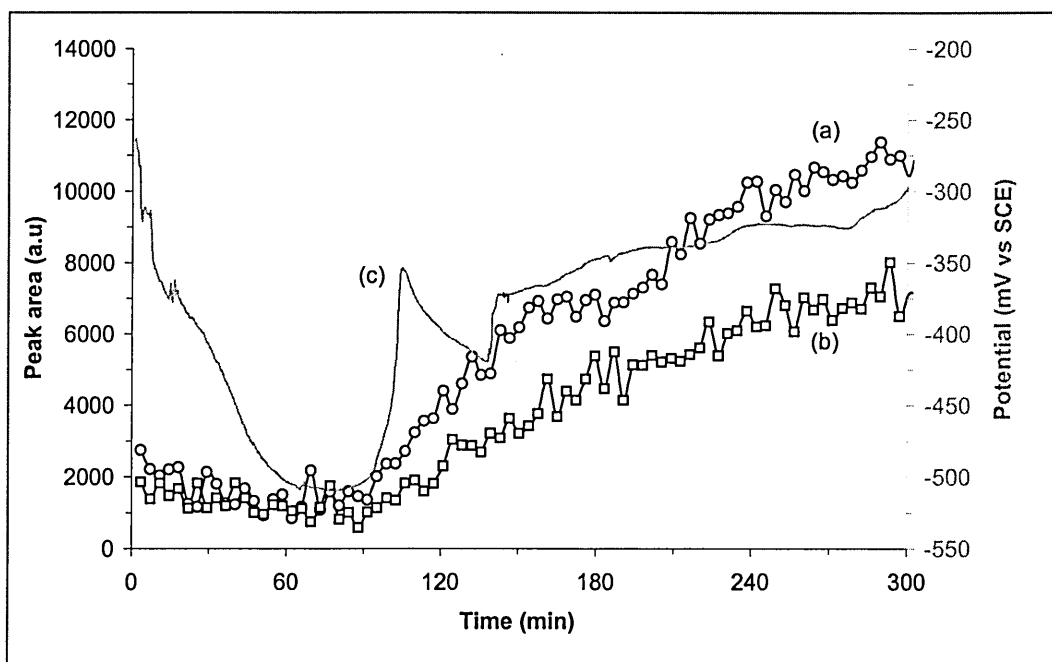


Figure 5.2. Comparison between the evolution of the area of the (a) 250 and the (b) 386 cm^{-1} integrated bands with the (c) open circuit potential measured during the exposure of a pure iron wire in 3.5 % NaCl solution. While the curves (a) and (b) are related to the left hand side axis, curve (c) is related to the right hand side axis.

b. Open circuit potential data

Similarly, the evolution of the free corrosion potential can be divided in two sections. During the first 90 minutes, a large drop of the OCP was observed. Then the potential rose again sharply within a period of 10 minutes to reach -325 mV. During the remaining time of the experiment, the potential did not change so drastically and rose slowly toward -300 mV. We also note that between 90 and 150 minutes, the OCP dropped again to -400 mV, but such behaviour did not correlate with any spectral changes visible by Raman spectroscopy. It is then impossible to relate this potential change to any eventual oxidation process.

c. Data interpretation

As implied by the Nernst equation (eq. 3.2), the first potential drop can be interpreted as due to a change in the ionic concentrations of the species present in solution. During the first 90 minutes of the experiment, the evolution of the 250 and the 377 cm^{-1} peak areas did not match with the potential changes. It can then be supposed that the potential shift is due to a chemical reaction preceding the development of lepidocrocite. This could explain the presence of magnetite in the early stage of the experiment. Interestingly, Ferreira *et al.* (7) polarised a pure iron electrode in 0.15 M NaCl solution at -600 mV (vs. SCE) and recorded an in situ surface enhanced Raman spectrum. On their spectrum, only the 550 and 670 cm^{-1} band from Fe_3O_4 could be seen, suggesting that at such potential, oxidation of iron to Fe_3O_4 was the only reaction that was occurring. It is worthwhile to note that their potential used for the polarisation was close to the one toward the free corrosion potential evolved during the first 90 minutes of the experiment. (Figure 5.2)

The evolution of the potential observed after 90 minutes of experiment corresponds to the increase of the intensities of the γ - FeOOH bands. This potential change confirms the evolution of the nature of the film which is induced by a change in the solution concentration of ions, thereby also affecting the electrode potential.

5.1.2. Polarisation

As shown above, after five hours at open circuit potential, the electrode potential was relatively stable tending toward -300 mV. To complete the results presented in section 5.1.1, a pure iron wire was polarised at -300 mV for 100 minutes. To reduce any passive film that could have been developed on the sample during its preparation, the

polarisation was preceded by a 10 minutes pre-polarisation at -1.0 V. The Raman spectra recorded during the polarisation are presented Figure 5.3.

Within 10 minutes of polarisation at -300 mV, two bands located at respectively 430 cm^{-1} and 503 cm^{-1} can be observed. Such bands characteristic of iron (II-III) hydroxysalts, commonly named 'green rust's, have been observed in a large number of different environments by several research groups (8-13).

According to the literature, different types of such 'green rusts' can be formed, and the presence of anions such as CO_3^{2-} , HCO_3^- , SO_4^{2-} have an effect on the oxide. Since none of these anions should be present in the sodium chloride solution, only the presence of an hydroxychloride 'green rust' can explain the presence of the two vibrational bands.

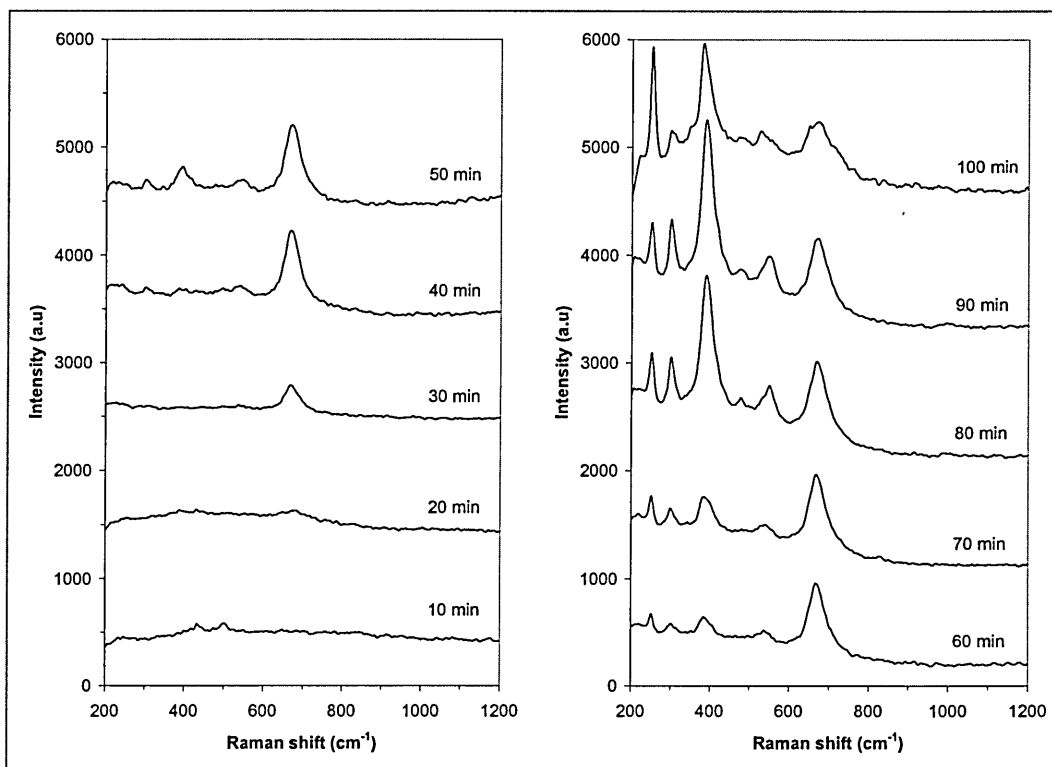


Figure 5.3. Evolution with time of the Raman spectra of the surface of a pure iron wire polarised at -300 mV (vs. SCE).

After 20 min of polarisation, none of the bands of 'green rust' could be seen anymore, but a weak and broad band became visible around 670 cm^{-1} . Ten minutes later, the intensity of the 670 cm^{-1} band increased and a broad and well resolved band could be observed. Using the literature, it has been identified as the A_{1g} mode of magnetite (14,15). On the subsequent spectrum (40 min), the magnetite band appeared

with twice the intensity, suggesting a development of the magnetite layer on the sample surface (since the Raman response is directly linked to the amount of compound observed (section 2.3.2.)). Additionally, a set of bands started to become visible at 305, 396 and 540 cm^{-1} . The band at 540 cm^{-1} is identified as a vibrational mode of magnetite (1) and the two other bands, which do not correspond to any vibrational mode of Fe_3O_4 , have to be the consequence of the presence of a different oxide. As explained in section 5.1.1.1, these two bands may be due to the presence of goethite (α - FeOOH).

After 50 min of polarisation, the intensity of the 540 and 670 cm^{-1} bands from magnetite did not show any change, but the intensities of the goethite bands increased. After 60 minutes of polarisation, while, once again, no changes could be seen on the magnetite bands, a sharp band started to become visible at 250 cm^{-1} and the 396 cm^{-1} bands started to shift towards 390 cm^{-1} . The band shift towards the lower wave number can be explained by the presence of a different oxide with a band overlapping with the 396 cm^{-1} band from α - FeOOH . After 70 minutes, no changes could be observed in the Fe_3O_4 bands but the 250, 305 and 391 cm^{-1} bands increase in intensity suggesting the presence of both α and γ - FeOOH at the iron surface.

After 80 minutes a radical change in the general form of the Raman spectrum was noticed. First, the 550 cm^{-1} band became much broader and its intensity increased. Such band evolution permitted to reveal the presence of a 530 cm^{-1} band (from lepidocrocite) which overlapped with the 540 cm^{-1} magnetite band. Moreover, while the 250 and the 391 cm^{-1} bands were as intense after 70 minutes of polarisation, the 391 cm^{-1} band appeared to be almost three times more intense. This suggested a change in the balance between the amount of the two iron α - and γ - FeOOH oxides present in the oxide layer. Finally, this oxide proportion change was confirmed by the increase of the 302 cm^{-1} band from α - FeOOH .

After a further 10 minutes of polarisation, an additional increase of the goethite bands could be seen, as well as a diminution of the 670 cm^{-1} band from magnetite. Finally, the last spectrum, recorded after 100 minutes, showed that the corrosion product had changed again but this time with the dominance of lepidocrocite over magnetite.

5.1.3. Corrosion processes

The experiment described above allowed us to follow the evolution with time of the nature of the film growing on an iron surface, during polarisation at -300 mV. Due to the technique itself and, even if four different oxides have been identified, it was not possible to establish whether the film grown was made of several layers or, to the successive oxidation stages from one oxide to another. Despite this uncertainty, a possible model of structure of the passive film grown at -300 mV, which is consistent with the results described above, is proposed (Figure 5.4).

The oxidation occurring during the first 10 minutes of the experiments could be identified without too much difficulty, since only the two bands from 'green rust' were visible. Then, after the disappearance of the 'green rust' bands, and the development of the magnetite bands, two types of suppositions could be made. First, the 'green rust' could have been oxidised to magnetite or second, a magnetite layer could have been grown above the 'green rust' layer. These two possibilities are shown by the two possible paths on the oxide formation representation (Figure 5.4). Between 30 and 50 minutes, magnetite and goethite were the two oxides detected by the Raman investigation. A possible interpretation of such observation could be the development of a discontinuous layer of goethite above the magnetite grown previously. Then, between 50 and 90 minutes, magnetite, lepidocrocite and goethite could be observed in the spectra. But the intensity of goethite band increased with time, suggesting a development of the goethite layer. A possible interpretation of such observation could be a further development of goethite onto the magnetite layer as well as an 'ageing' process during which α -FeOOH is transformed to γ -FeOOH. Finally, during the last ten minutes of the experiment, a further transformation of goethite toward lepidocrocite occurred. The presence of a discontinuous layer of lepidocrocite, as shown in the last stage of the passive film formation, was confirmed by the observation of the 670 cm^{-1} magnetite band, overlapping with the lepidocrocite bands.

Even if such representation corresponds to what has been observed by Raman during the polarisation at -300 mV, no real information on the oxidation processes and kinetics can really be obtained. Further work needs to be undertaken in order to complete such analysis. Some guidelines for this work are presented in chapter 7.

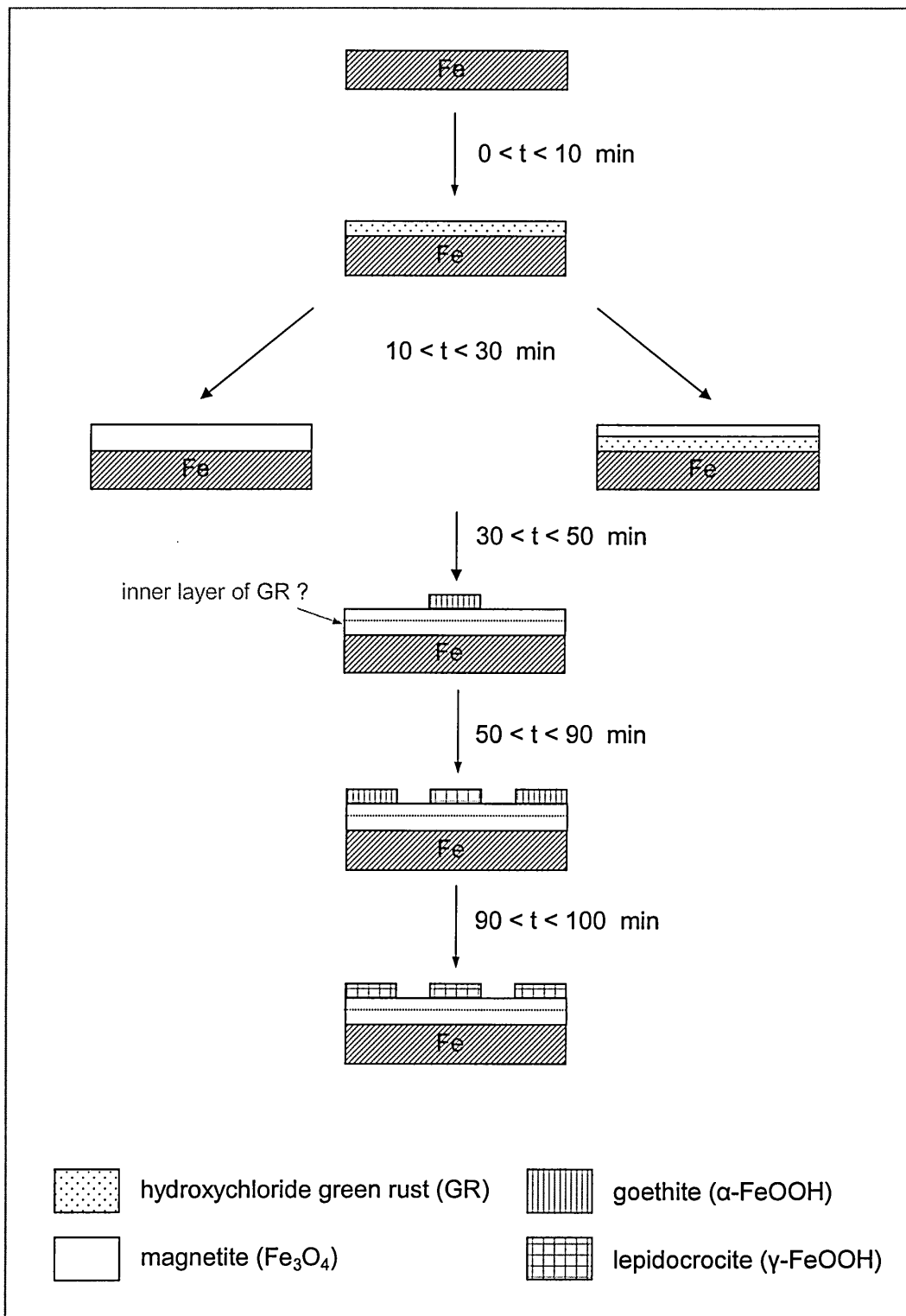


Figure 5.4. Model representation of the passive film formation on iron in 3.5 % NaCl solution during polarisation at -300 mV (vs. SCE).

5.2. Twin iron wire model system

Forcing one of the wires to act as either a cathode or an anode, by simply applying a potential difference between the electrodes, gave us the opportunity to follow simultaneously, optically and by Raman spectroscopy, the evolution of both reaction

surfaces with time. To observe the phenomenon, nine potential differences, from 20 to 100 mV (with a 10 mV increment), were applied between the two wires immersed in 3.5 % NaCl solution. To complete the results obtained from the experiment in solution, a study of the anodic site was also made, once it had been rinsed and dried in air.

5.2.1. Evolution of the electrodes surfaces with time

5.2.1.1. Raman analysis

What ever the potential difference applied between the anode and the cathode, a similar evolution of both surfaces occurred during all experiments. Therefore only the experiment performed using a potential of 50 mV is presented here in details. The Raman spectra collected, with time, from the anodic and cathodic sites are presented in Figure 5.5.

a. Evolution of the anodic site

The first spectrum recorded from the anode, after 15 minutes of application of a 50 mV potential difference, showed two bands at 430 and 503 cm^{-1} . As mentioned already several times (sections 3.7.1.2 and 5.1.2) in the current work and in the literature (8,9,11,12), these bands have been attributed to the Fe^{2+} -OH and Fe^{3+} -OH vibrational modes of 'green rust'. After 1h40, the two bands were still visible in the spectrum but were not as well resolved as on the previous one. Moreover, they were no longer the only features present, since the strong and broad band from the A_{1g} mode of magnetite was clearly present, in addition to two weak bands at 250 and 377 cm^{-1} . After 3h20, the same bands were visible on the spectrum but the 503 cm^{-1} from 'green rust' overlapped with a band centred around 530 cm^{-1} . Additionally, it was noticed that, while the intensity of the magnetite band decreased between the two spectra, the intensity of the 250, 377 and 530 cm^{-1} bands increased, suggesting a further development of a layer of γ -FeOOH.

After five hours, all the bands from lepidocrocite became visible (as shown by the reference spectra presented in section 4.1.2.2) but, despite the presence of a band at 430 cm^{-1} , the 503 cm^{-1} band attributed to the Fe^{3+} -OH vibrational mode from 'green rust' could no longer be observed.

After 7h30, the intensity of all the lepidocrocite bands increased again and the 670 cm^{-1} band, attributed originally to magnetite, shifted toward 660 cm^{-1} . This shift

may be explained by the fact that the band observed in this spectral region was due to the contribution of two different vibrational modes; one from lepidocrocite at 650 cm^{-1} , and one from magnetite at 670 cm^{-1} .

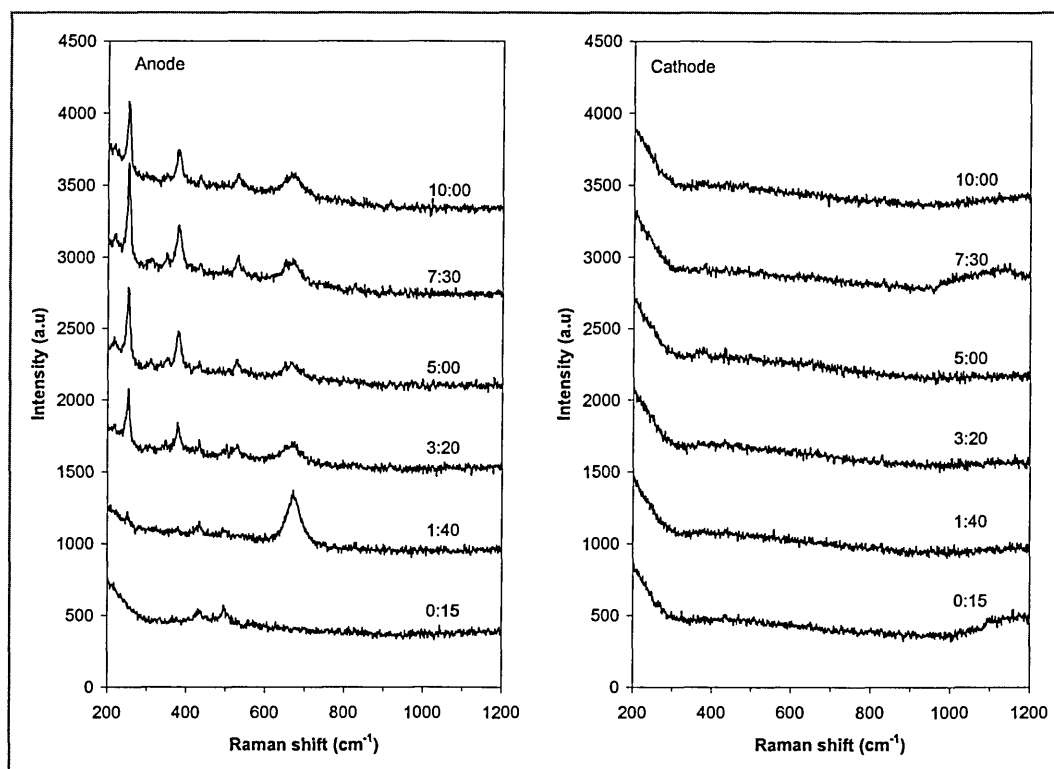


Figure 5.5. Evolution with time (hr : min) of the Raman spectra collected from the anode (left hand side) and the cathode (right hand side) when a 50 mV potential difference is applied.

Such interpretation was confirmed by the spectra recorded after 10 hours of potential difference application, where a difference in the ratio between the 650 and 670 cm^{-1} bands, and the other lepidocrocite bands, was observed.

b. Evolution of the cathodic site

Except for a few minor changes, the spectra recorded from the cathode did not change during the ten hours of potential difference application. No Raman bands could be seen in the region where the usual oxide bands are present ($200\text{-}800\text{ cm}^{-1}$). Nevertheless, one noticeable artefact, located at 430 cm^{-1} and observed on most of the spectra recorded during the whole experiment was puzzling. This artefact was also observed on the spectra collected from the anode but, due to the fact that it has exactly the same position as the $\text{Fe}^{2+}\text{-OH}$ vibrational mode from 'green rust', its interpretation became difficult. Finally, the origin of the band has been identified as a 'spurious' peak due to 'parasitic' light. Firstly, despite the nature and quantity of the oxides detected by

Raman, its intensity stayed constant from one spectrum to the other. Secondly, a similar band was observed in spectra recorded on entirely different system (such as a pure silicon).

Moreover, on the spectrum recorded after 5 hours, a broad feature around 380 cm^{-1} could be observed as well as a band at 250 cm^{-1} , suggesting the presence of $\gamma\text{-FeOOH}$. The first interpretation could be that even if the wire was polarised cathodically, some site may have finally started to corrode. Surprisingly, these two bands were not detected anymore 2h30 later, eliminating the possibility to see long term oxidation on the cathode. However, the fact that the lepidocrocite bands could not be observed anymore, may be explained by the fact that the oxidation was highly localised on the electrode. The reason why it had not been detected again could be due to a ‘backlash’ on the mapping stage used to move the sample under the laser source.

5.2.1.2. Optical analysis

To complement the information given by Raman spectroscopy, six optical pictures of both the anode and the cathode were taken regularly during the experiment. Such pictures are presented in Figure 5.6. On each picture, the intersection between the two lines represents the position from which the Raman spectra have been recorded.

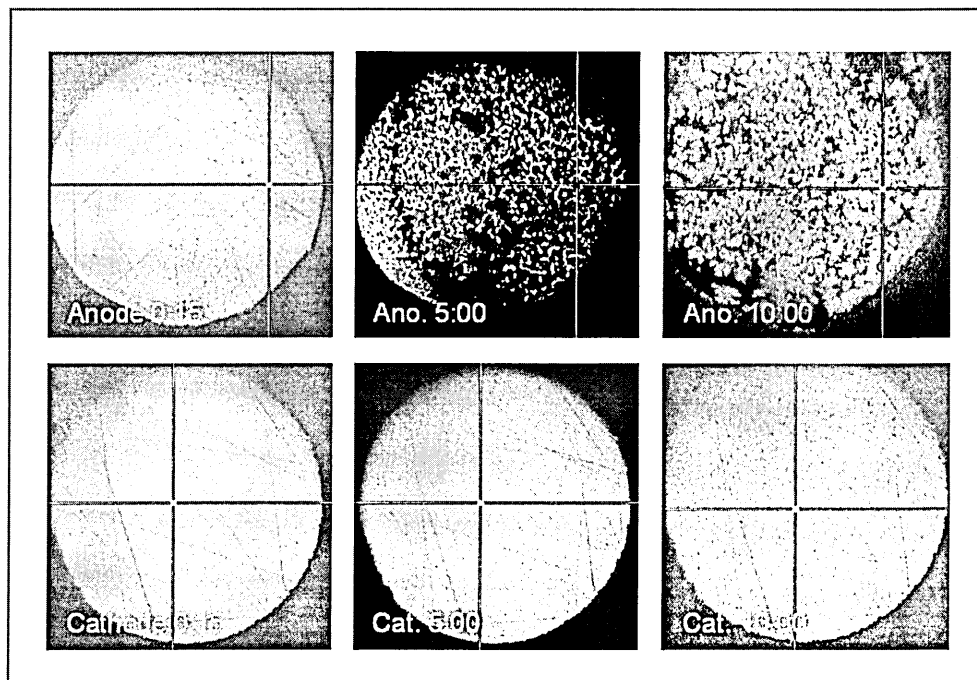


Figure 5.6. Optical pictures taken from the anode and cathode after 15 min., 5h and 10 hours of application of 50 mV potential difference between the electrodes.

After 15 minutes of polarisation, a slight oxidation started to be visible on the anode. The picture shows that the spatial distribution of the oxide was not homogenous, over the whole surface of the electrode, and that the left hand side of the electrode was still 'clean'. Five hours later, the majority of the anode had been corroded, showing some isolated islands of brownish oxide on the electrode surface. Once again, a difference in the coverage of the electrode could be noticed, revealing much more corrosion product on the right side of the picture than on the left one. After ten hours of polarisation, the whole anode surface was heavily corroded and a two layer structure was clearly visible on the electrode. The black inner film has been identified as magnetite (Fe_3O_4) and the reddish outside layer as lepidocrocite ($\gamma\text{-FeOOH}$).

As expected, no real oxidation occurred on the cathode and the wire stayed clear during the first five hours of the experiment. Nevertheless, some oxide started to become visible on the top left quarter of the electrode.

The non-homogeneity of the film grown on the anodic site can be explained by the relative position between the two wires. Since the two wires were mounted one next to the other, different areas of the anode were at different distances from the cathode. With the anode mounted on the left hand side of the cathode, the left hand side of the anode was further away from the cathode, resulting in a reduced anodic activity at this position. Similarly, due to its proximity to the anode, the left hand side of the cathode started to corrode at the end of the experiment since it was the closest to the anode.

5.2.2. Effect of the potential applied

As stated previously, the nature of the oxide and the processes observed were similar what ever was the potential difference applied between the two wires. However, the potential difference applied had a non negligible effect on the kinetics of the oxidation process. To evaluate the effect of the potential, some analysis of the Raman spectra recorded during the experiments has to be realised.

5.2.2.1. The overlapping band system

In Figure 5.7, two reference spectra of magnetite and lepidocrocite, recorded from pure reagent powders, are presented and compared to one of the typical spectra of the compound grown on the anode during the oxidation process.

As it can be seen, the oxide is clearly constituted from both magnetite and lepidocrocite. This is revealed by the presence of the magnetite band at 670 cm^{-1} and the presence of the 250 , 377 and 530 cm^{-1} bands from lepidocrocite. It is also clear that the 650 cm^{-1} band of $\gamma\text{-FeOOH}$ overlaps with the magnetite band, and then cannot be resolved, making it difficult to track the amount of each oxide during the experiment. One possibility to evaluate the amount of each oxide will be to use the principal component analysis (PCA) technique. However as pointed out previously, the technique was not really suitable for such system due to the resonance enhancement effect observed on some of the reagent oxides and the difficulties in the realisation of references for the calibration (see section 4.1.2).

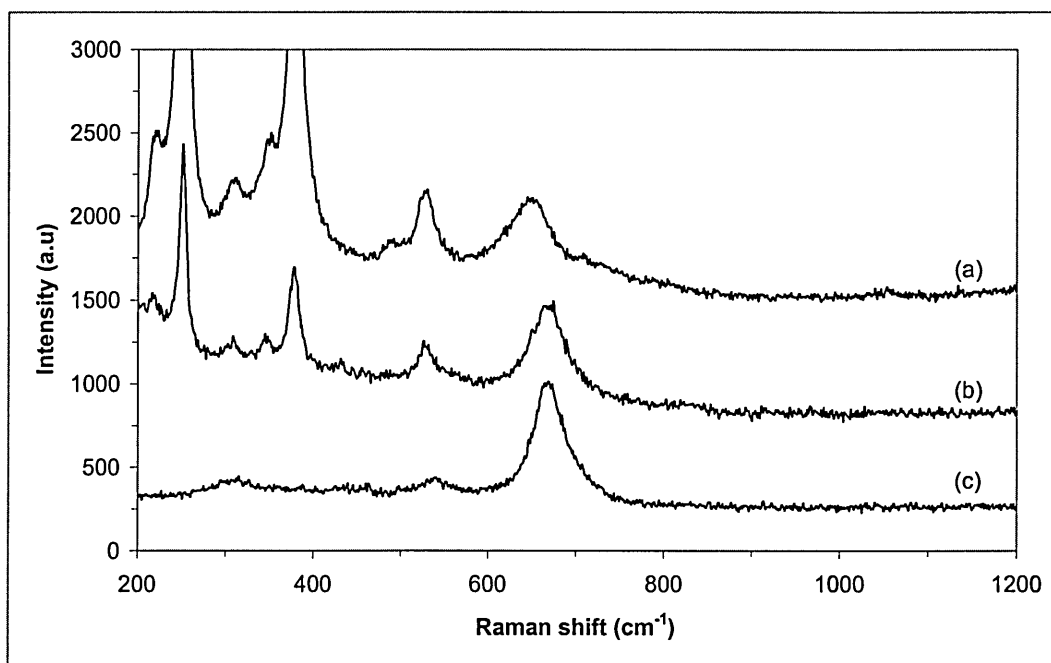


Figure 5.7. Identification of the bands present on a (b) typical iron oxide spectra by comparison with the reference spectra of (a) lepidocrocite and (c) magnetite.

A different approach had to be used, and it was decided that only the $450\text{-}800\text{ cm}^{-1}$ would be studied to evaluate the amount of magnetite and lepidocrocite. The choice of such region can be explained by the presence of a pure band of lepidocrocite located at 528 cm^{-1} , and a band whose centre could be located between 650 and 670 cm^{-1} which could be due to lepidocrocite, magnetite or even both compounds. To make possible the comparison of the different spectra whose content depend on the potential applied and the time during which it has been applied, the whole band system had to be fitted.

5.2.2.2. Fitting process

To achieve a valid band fitting process, applicable to all cases that were encountered during the analysis, several issues about the technique itself had to be addressed. The main questions were about the number of bands to use and the choice of parameters that had to be fixed to achieve viable fitting. If the decision concerning the band at 530 cm^{-1} was fairly easy due the presence of only one band in the region, the approach treatment of the two overlapping bands in the $650\text{-}670\text{ cm}^{-1}$ was more ambiguous.

Therefore, two different options were considered. The first one consisted of fitting the $450\text{-}800\text{ cm}^{-1}$ region using only two bands: one for the 530 cm^{-1} lepidocrocite and one for the two overlapping bands from magnetite and lepidocrocite. The second option consisted of using, once again one band for the 530 cm^{-1} lepidocrocite, plus two separated bands for respectively the 650 cm^{-1} band from lepidocrocite and the 670 cm^{-1} band from magnetite.

In order to illustrate the difference between the two processes, one of the spectra has been tested according to both fitting processes. The choice of the spectrum was made because on the basis that the 670 cm^{-1} magnetite band, overlapping with the 650 cm^{-1} lepidocrocite one could be detected simply by eye. The two types of fitting processes are presented in Figure 5.8.

While the original trace, the fitted peaks and the base line for respectively the two or three peaks fitting process are shown on traces (a) and (b), traces (c) and (d) only show the resulting fitted traces. According to the 'visual' results obtained from the fitting trace, it seems evident that the three band fitting process is the most efficient since, in the case of the two band fitting process, the presence of the magnetite band has been completely hidden by that of lepidocrocite. Nevertheless, a deeper analysis of the band details needed to be performed in order to choose the best fitting technique.

As introduced in part 2.4.2.2, four different parameters can be obtained from the band fitting process (band position, maximum intensity, width at half maximum and area). The values obtained for the oxide studied and the two reference spectra of magnetite and lepidocrocite are presented in Table 5.1.

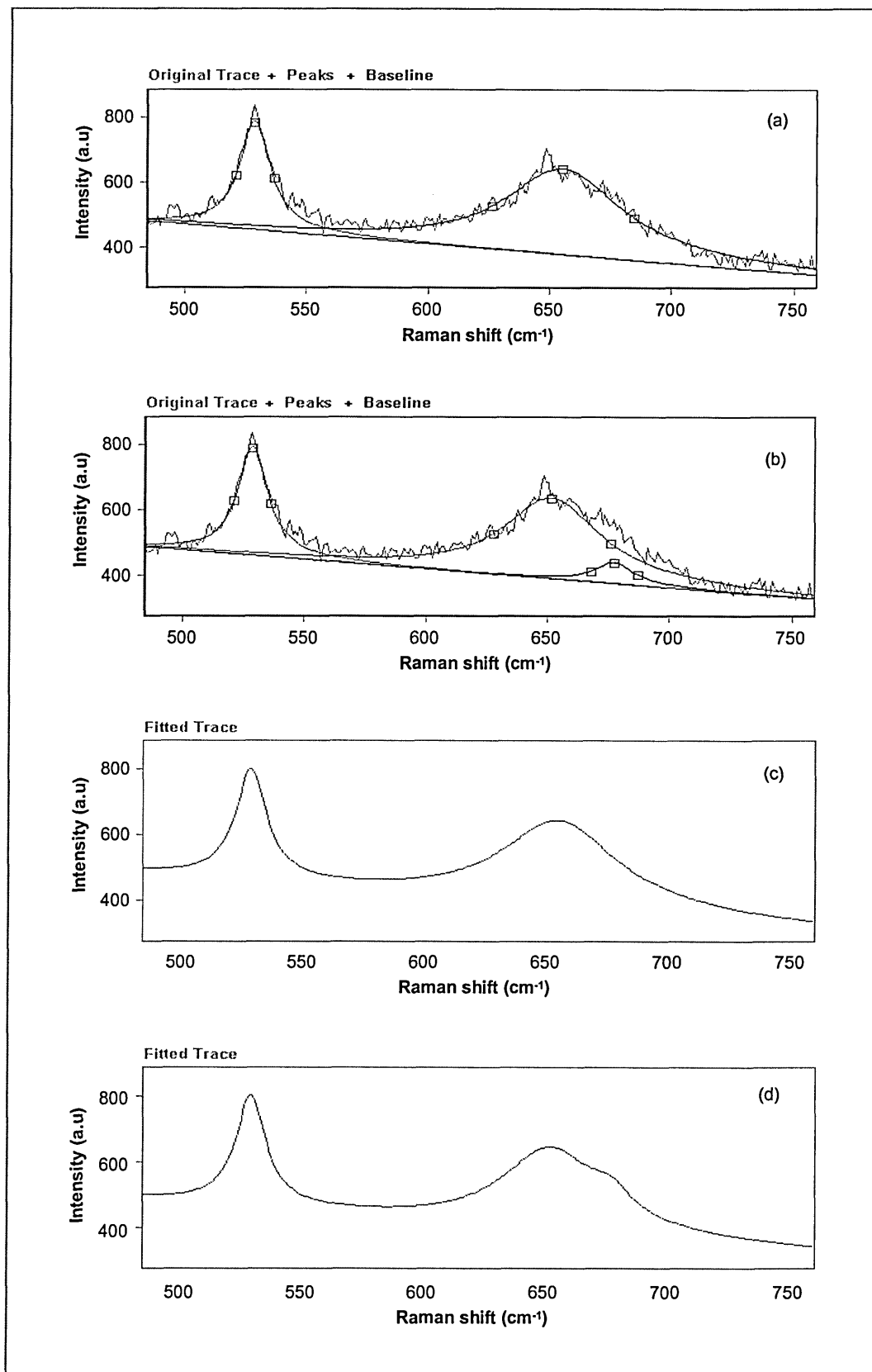


Figure 5.8. Comparison between two and three peak integration processes. (a) original trace with the 2 bands used for the fitting, (b) original trace with the 3 bands used for the fitting and their respective fitted traces (c) and (d).

From either the two or three peaks fitting processes, the resulting 'fitted' band for the 528 cm⁻¹ peak gave similar results, with exactly the same band position, and a similar

intensity, width and area. This showed that the number of peaks to use to achieve the fitting did not affect parameters for the 528 cm⁻¹ band. Moreover, by comparing the data obtained from the 2 and 3 peak fitting processes with data from the lepidocrocite and magnetite reference spectra, it can be seen that the ratio area/height of the 528 cm⁻¹ band from the oxide ($r_{A/H}=22.9$) is very similar to the area/height ratio of the 528 band from pure lepidocrocite ($r_{A/H}=25.8$) and very different from the magnetite one ($r_{A/H}=36.7$), suggesting a very different band shape. This calculation also showed that the presence of the weak magnetite band at 540 cm⁻¹ present in the pure magnetite spectrum did not affect the fitting of the 528 cm⁻¹ band. It can therefore be considered as a pure lepidocrocite band. In order to secure the quality of the fitting, one of the parameters imposed for the fitting process was that the centre of the fitted band had to be located at 528±1 cm⁻¹.

As shown by Figure 5.8, the ‘two peak fitting process’ considers the 650-670 cm⁻¹ doublet as a single band but, according to the characteristics given in the table 5.1, the resulting band is made from a contribution of both oxides, with a centre located 5.5 cm⁻¹ above the position of the lepidocrocite band, and 14.4 cm⁻¹ below the position of the magnetite band, the position of the resulting band directly depended on the contribution of each oxide. Therefore, even if an approximation on the constitution of the band has to be made, the result stays valid and relatively easy to implement.

	Position (cm ⁻¹)	Height (a.u)	Width (cm ⁻¹)	Area (a.u)
Magnetite (Ref)	540.9	64.2	34.4	2354.2
	669.7	619.0	49.0	32323.5
Lepidocrocite (Ref)	528.1	358.0	24.2	9236.8
	647.7	364.2.0	58.3	2261.2
Two peak fitting process	528.7	334.6	15.6	7654.1
	655.3	263.6	58.3	20774.3
Three peak fitting process	528.7	332.9	15.2	7438.6
	651.8	249.2	48.4	16552.9
	677.4	63.45	19.34	1862.3

Table 5.1. Summary and comparison of the bands characteristics depending on the fitting process.

Considering the 'three peak fitting' process applied to the relatively easy case presented here, where both magnetite and lepidocrocite bands could be easily separated, the shape of the resulting band looks very satisfying. However, the band positions obtained after the fitting differed non-negligibly from the reference spectra. For example, both bands located at 651.8 and 677.4 differ respectively by +4.1 and +7.7 cm^{-1} . Moreover, using a complex fitting method for the all data set acquired at different potential increase the chances of error in the fitted bands. Therefore, when the three peak fitting process had been applied to all the spectra recorded during the different experiment a large number of erroneous results were obtained. This unsuccessful calculation was due to the difficulty met by the software to identify two separated peaks in the 650-670 cm^{-1} region.

Therefore, in order to limit the errors and to have a wider range of application, the 'two peak fitting process' has been used to allow the analysis of the data acquired during the whole experiment

5.2.2.3. Results interpretation

Once all the experiments were run at each applied potential, and the Raman spectra recorded, the 450-800 cm^{-1} region were analysed using the 'two peak fitting process'. In order to present the large amount of data easily, the ratio between the intensity of the 650-670 cm^{-1} band over the 530 cm^{-1} band from lepidocrocite has been calculated and plotted on a 3D graph as shown in Figure 5.9. The higher the calculated ratio, the more important is the quantity of magnetite present within the oxide mixture.

As it may be understood from the 3D plot, the corrosion process happening at the surface of the anode starts with the development of a layer of magnetite above the iron surface. Later, the presence of lepidocrocite is found within the oxide layer and the ratio of magnetite to lepidocrocite decreases with time. According to the plotted results, it can be noticed that the value of the applied potential has a direct effect on the kinetics of the oxidation. For potential above 50 mV, the ratio stays high for more than five hours, suggesting a large presence of magnetite on the sample surface. This phenomenon can easily be explained by the high potential accompanied by the drive of a large current, making the iron dissolution easier and therefore also the production of magnetite. This iron dissolution is then slowed down, once a sufficient oxide barrier has been developed on the sample surface, stopping the Fe^{n+} ion transfer from the metal to the oxide system.

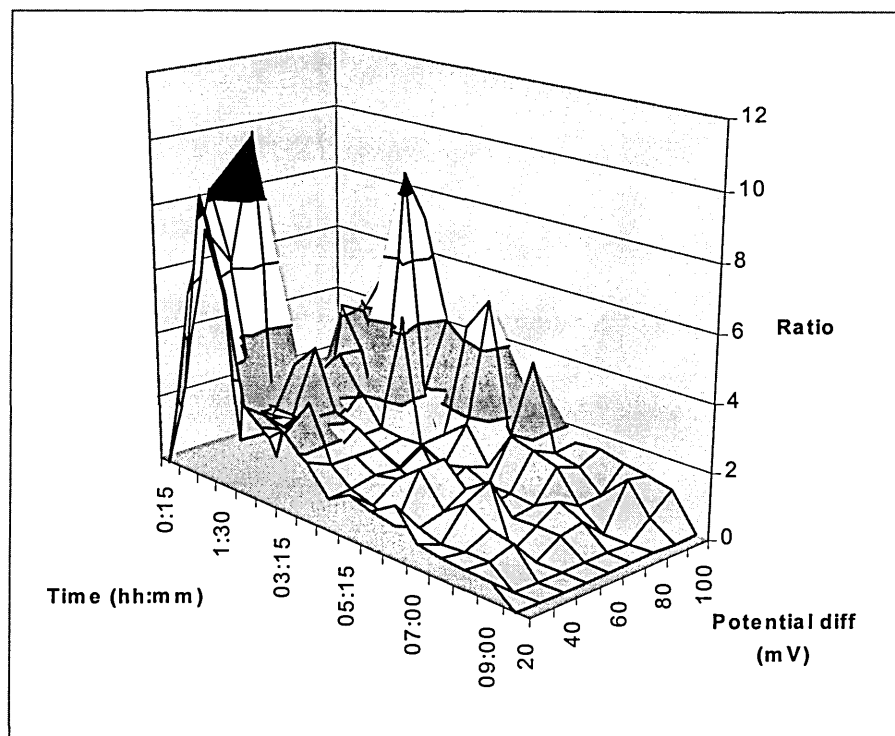


Figure 5.9. Evolution of the amount of magnetite over lepidocrocite at the anode surface in function of the potential difference applied.

5.2.3. Dry sample analysis

Once removed from the solution, the sample was rinsed and left in air for two hours, prior to a complementary Raman analysis. This experiment permitted us to acquire spectra from different position on the surface of the electrode. This allowed a check on the homogeneity of the corrosion layer developed during the oxidation process. An optical picture of the dry sample, showing the four different sites analysed by Raman is presented in Figure 5.10. The four different sites have been selected depending on the colour of the oxide, and their associated spectra are presented in Figure 5.11

On the spectrum recorded from the first position (a), where a black oxide product developed on the surface, two bands at 430 and 503 cm^{-1} are seen. As mentioned previously in this chapter, these two bands have been attributed to 'green rust'. Surprisingly, they have been observed in situ only at the start of the different experiments, suggesting that their presence was directly due to the first oxidation stage of the iron, and more particularly, to the iron dissolution to give Fe^{2+} and Fe^{3+} ions. It is even more surprising to see this oxide in such quantity, as shown by the large amount of black corrosion product present on the anode after its exposure to air. However; the presence of such quantity of 'green rust' on the sample could be due to the fact that the sample had been rinsed in order to avoid creating any salt crystals on the sample surface

during the drying process. An outer oxide layer could have been easily removed by the deionised water used to rinse the electrode, exposing the 'green rust' layer to air.

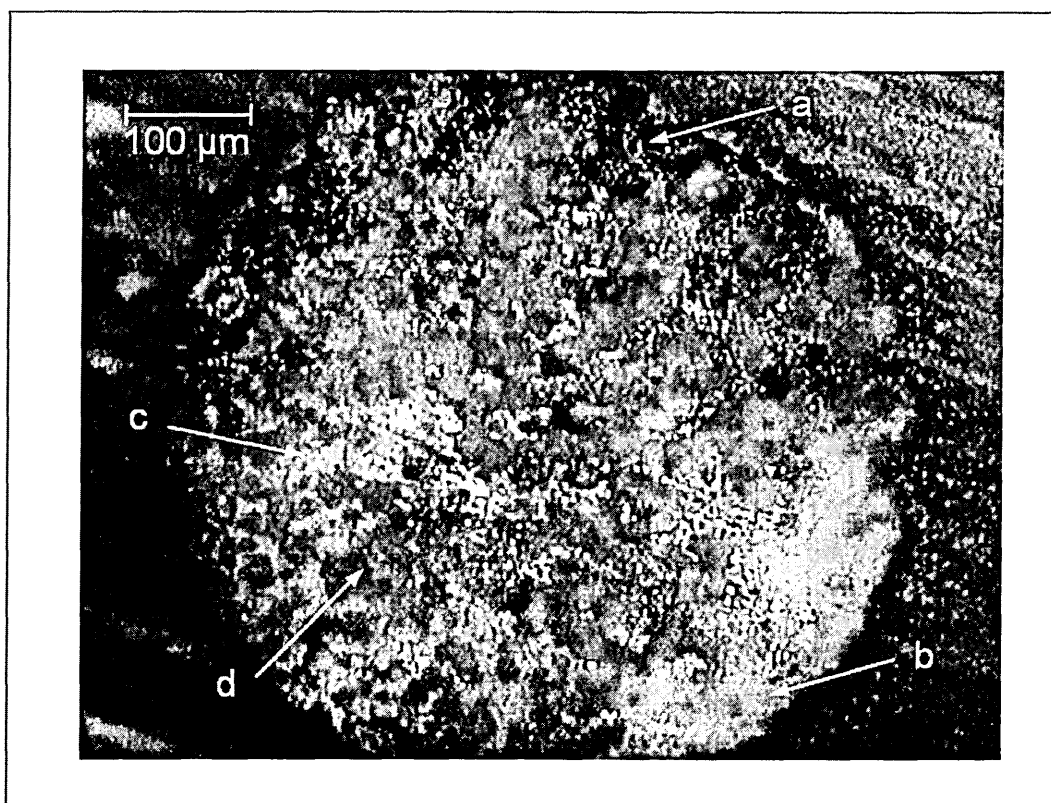


Figure 5.10. Optical picture of the dry anode after 10 hours in 3.5 % NaCl solution with an applied potential difference of 100 mV.

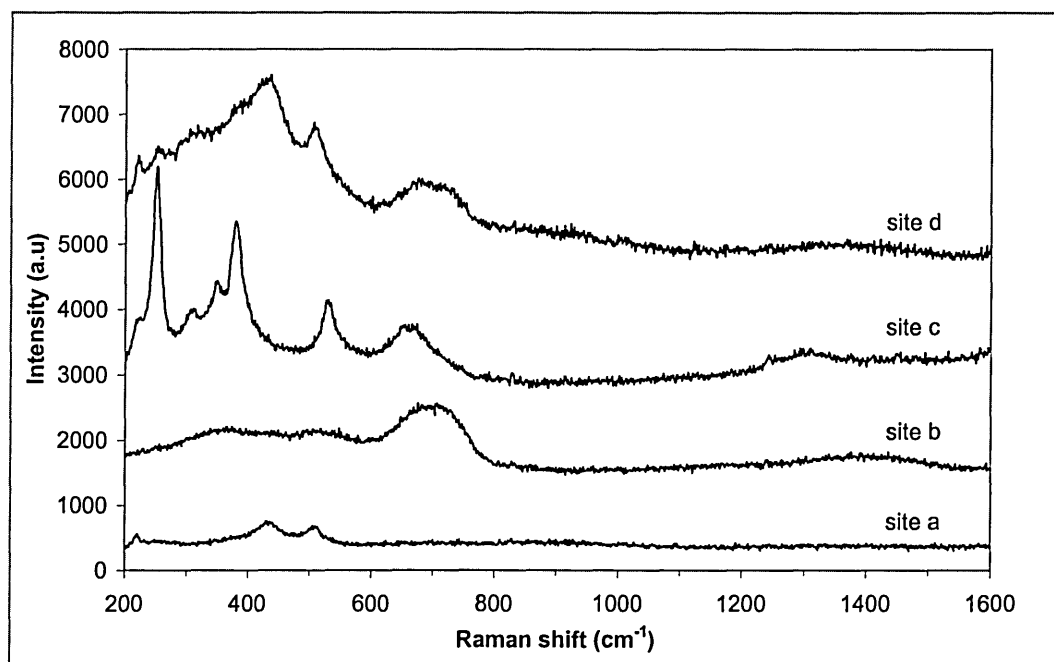


Figure 5.11. Raman spectra collected from a dry anode, after 10h immersion in 3.5 % NaCl solution with a potential difference Anode / Cathode of 100 mV. The four sites corresponds to the positions a, b, c and d shown in Figure 5.10.

On the spectrum recorded from site b, only a broad feature centred around 700 cm^{-1} is visible. According to Dünwald and Otto (16), such band is indicative of the presence of $\text{Fe}(\text{OH})_3$ and/or amorphous FeOOH . Surprisingly, even if the spectrum collected here matches well with the spectra given by Dünwald and Otto, the explanation they gave for the presence of $\text{Fe}(\text{OH})_3$ does not match with our observation. While we observed different crystalline forms of FeOOH in situ, we never observed the presence of $\text{Fe}(\text{OH})_3$ until the sample has been removed from the solution and exposed to air. This is in contradiction with the explanation of the production of the crystalline forms of FeOOH given by Dünwald and Otto who state that the oxidation starts with an initial formation of $\text{Fe}(\text{OH})_3$, which is then transformed to FeOOH , transformation due to the gradual loss of water. Moreover, according to the optical picture, the oxide layer from which the $\text{Fe}(\text{OH})_3$ has been observed appear to be located the furthest away from the iron substrate. This suggests an evolution of FeOOH toward $\text{Fe}(\text{OH})_3$ during the drying process.

From site c, a 'pure' spectrum of lepidocrocite, with a very good resolution was recorded, showing all the characteristic bands as observed from the reference powder. This time, the presence of $\gamma\text{-FeOOH}$ was predictable, since it has been observed in all experiments in sodium chloride solution, and was characteristic of the later corrosion process happening on all oxidised surfaces.

Finally the spectrum from site d, recorded from the dark brown oxide show, the spectrum shows the same band of $\text{Fe}(\text{OH})_3$, as well as two band at 425 and 501 cm^{-1} . Even if these two bands have their position relatively close to the $\text{Fe}^{2+}\text{-OH}$ and $\text{Fe}^{3+}\text{-OH}$ stretching modes of 'green rust', they are due to a different oxide and have been identified as vibrational modes of akaganeite ($\beta\text{-FeOOH}$). These bands are presented in more detail in section 6.2.

5.3. Summary and Conclusions

5.3.1. Simple iron model system

The analyses performed on this simple model system permitted us to follow the evolution of the oxidation process occurring in 3.5 % NaCl solution. The results obtained by Raman, during the experiment at free corrosion potential, allowed the identification of lepidocrocite as the main corrosion oxide developing on the electrode. This development happened linearly once an initiation period during which a different

reaction, unidentified here, occurred. This initiation process has been confirmed by the evolution of the free corrosion potential measured along the experiment.

During the polarisation at -300 mV, the nature of the oxide observed was entirely different. The corrosion stages have been identified showing firstly, the development of a magnetite layer on the sample surface, secondly, the growth of a porous goethite layer (α -FeOOH) and thirdly, the transformation of goethite to lepidocrocite (γ -FeOOH) over time. Despite the observation of the different oxides, the oxidation processes could not be analysed in detail using these simple experiments. To obtain more information on the film creation and the interaction between the different oxides, further experimental work is needed.

Finally, the utilisation of a 25 μ m pure iron wire permitted us to obtain reproducible results, highlighting the possibility of using Raman spectroscopy to analyse 'in situ' the development of oxide films. It permitted us as well to prove that Raman spectroscopy was a technique able to follow (with time) the surface changes due to the corrosion reactions.

5.3.2. Twin iron model system

Using the twin iron model system permitted us to isolate the different sites from where the anodic and cathodic reactions occurred. It then allowed us to follow their evolution (with time) by Raman spectroscopy as a function of the applied potential difference. The 'in situ' experiment showed that the oxidation of the anode starts with the iron dissolution, induced by the reaction of the free Fe^{n+} ions with the solution to create some 'green rust'. Quickly, the presence of such oxide is hidden by a layer of magnetite, which is later covered by a porous film of lepidocrocite. Increasing the applied potential difference increases the iron dissolution, resulting in a thicker magnetite layer that takes more time to develop above the surface.

A complementary analysis of the electrode, once removed from the solution showed that the oxide was not as homogenous as expected and four different oxides have been identified on the whole surface. Despite the fact that it has not been observed in solution, $\text{Fe}(\text{OH})_3$ was largely present on the electrode but its presence can be due either to the rinsing process prior to the analysis, or to the evolution of the oxide film once it has been exposed to air.

Once again, the results obtained from the experiment on the twin iron model system showed the capacity of Raman spectroscopy to study 'in situ' corrosion processes. Some limitation due to the system will be presented in more detail in chapter 7.

5.4. References

- (1) Ohtsuka T, Kudo K, Sato N. Raman-Spectroscopy of Thin Corrosion Films on Iron at 100-C to 150-C in Air. *Corrosion* 1986 AUG; 42 (8): pp. 476-481.
- (2) Nauer G, Strecha P, Brindakonopik N, Liptay G. Spectroscopic and thermo-analytical characterization of standard substances for the identification of reaction-products on iron electrodes. *Journal of Thermal Analysis* 1985; 30 (4): pp. 813-830.
- (3) Keiser JT, Brown CW, Heidersbach RH. Use of Raman spectroscopy in iron corrosion studies. *American Laboratory* 1982; 14 (4): pp. 17-24.
- (4) Thibeau RJ, Brown CW, Heidersbach RH. Raman spectra of possible corrosion products of iron. *Applied Spectroscopy* 1978; 32 (6): pp. 532-535.
- (5) Williams KPJ, Smith BJE, Hayward IO. *New Horizons in Raman microscopy and Raman imaging. : International Labmate.*
- (6) Perardi A, Zoppi A, Castellucci E. Micro-Raman spectroscopy for standard and in situ characterisation of painting materials. *Journal of Cultural Heritage* 2000 8/1; 1 (Supplement 1): pp. S269-S272.
- (7) Ferreira MGS, Silva TME, Catarino A, Pankuch M, Melendres CA. Electrochemical and Laser Raman-Spectroscopy Studies of Stainless-Steel in 0.15 M NaCl Solution. *Journal of the Electrochemical Society* 1992 NOV; 139 (11): pp. 3146-3151.
- (8) Refait P, Memet J-, Bon C, Sabot R, Génin JMR. Formation of the Fe(II)-Fe(III) hydroxysulphate green rust during marine corrosion of steel. *Corrosion Science* 2003 4; 45 (4): pp. 833-845.
- (9) Legrand L, Sagon G, Lecomte S, Chausse A, Messina R. A Raman and infrared study of a new carbonate green rust obtained by electrochemical way. *Corrosion Science* 2001 SEP;43 (9): pp. 1739-1749.
- (10) Odziemkowski MS, Schuhmacher TT, Gillham RW, Reardon EJ. Mechanism of oxide film formation on iron in simulating groundwater solutions: Raman spectroscopic studies. *Corrosion Science* 1998; 40 (2-3): pp. 371-389.
- (11) Legrand L, Abdelmoula M, Gehin A, Chausse A, Génin JMR. Electrochemical formation of a new Fe(II)-Fe(III) hydroxy-carbonate green rust: characterisation and morphology. *Electrochimica Acta* 2001 3/30; 46 (12): pp. 1815-1822.
- (12) Boucherit N, Delichere P, Joiret S, Hugot-Le Goff A. Passivity of iron and iron alloys studied by voltammetry and Raman Spectroscopy. *Material science forum* 1989; 44&45: pp. 51-62.
- (13) Drissi SH, Refait P, Abdelmoula M, Génin JMR. The preparation and thermodynamic properties of Fe(II)-Fe(III) hydroxide-carbonate (green rust 1); Pourbaix diagram of iron in carbonate-containing aqueous media. *Corrosion Science* 1995; 37 (12): pp. 2025-2041.

- (14) Tjong SC. Laser Raman spectroscopic studies of the surface oxides formed on iron chromium alloys at elevated temperatures. *Materials Research Bulletin* 1983; 18 (2): pp. 157-165.
- (15) Raman RKS, Gleeson B, Young DJ. Laser Raman spectroscopy: a technique for rapid characterisation of oxide scale layers. *Materials Science and Technology* 1998 MAY; 14 (5): pp. 373-376.
- (16) Dunnwald J, Otto A. An investigation of phase transitions in rust layers using Raman spectroscopy. *Corrosion Science* 1989; 29 (9): pp. 1167-1176.

Chapter 6. Iron disc in Buffer solutions

In order to evaluate the capacity of Raman spectroscopy to follow, in situ, the evolution of the corrosion processes, the behaviour of a pure iron substrate has been studied in three different environments: a borate, a carbonate and a phosphate buffer solution.

The choice of using buffered solution was motivated by the fact that it was necessary to control as many parameters as possible to validate the results. The decision to control principally the pH of the solution was justified; firstly, by the fact that an anodic reaction is balanced by a cathodic reaction, which usually generates a change in the local pH; and secondly, by the necessity to obtain results similar enough to be compared. Finally, since the pH of the environment has an effect on the nature of the corrosion product, as shown by the Pourbaix diagram (figure 3.3), it was necessary to choose three different solutions that could be made within approximately the same pH range.

The three types of solutions listed above met the requirements explained previously and offered three different characteristics. Since the behaviour of iron in borate buffer solution have been largely studied so far, it offered a large amount of data that could be used to validate the results obtained during the study by Raman of iron in such environment. The carbonate solution, often present in water pipes, had a great relevance in terms of 'real life' conditions and matched perfectly with the chosen pH range selected. Finally, the particular case of phosphate solution was selected because of its common use in commercial formulations as a corrosion inhibitor.

All the Raman spectra displayed in the following chapter have been smoothed using a binomial smoothing process as described in section 2.4.2. Unless stated differently, the potentials have been measured and then expressed versus a silver/silver chloride reference electrode.

6.1. Iron in Borate buffer solution

In the last 30 years, numerous studies (1-10) have been reported in order to throw light onto the composition profile of the passive film formed on iron at different

potentials in a borate solution. Several techniques including ellipsometry (6,9), Mössbauer spectroscopy (10), electrochemical scanning tunneling microscopy (7,8), conventional Raman (2) and more frequently, surface enhanced Raman spectroscopy (SERS) (1,3-5) have been used to analyse the behaviour of iron in borate solutions.

The aim of the current study was to evaluate the possibility of analysing the film grown on pure iron in a pH 7.7 borate buffer solution using Raman, without enhancing the signal by depositing silver particles on the sample surface prior the corrosion studies. In order to investigate the nature of the film, two different studies were conducted. While the first study was based on the evolution of the iron surface with time, at open circuit potential (OCP), the second was focussed on the evolution of the film at different potentials. In order to determine which potential to use, a set of cyclic polarisation curves have been recorded.

6.1.1. Open circuit potential

Figure 6.1 shows the evolution of the open circuit potential of iron in pH 7.7 borate buffer solution made from 0.3 M H_3BO_3 and 0.0375 M $Na_2B_4O_7 \cdot 10 H_2O$. Before the recording of the free corrosion potential, the sample was kept at -1000m V (vs. Ag/AgCl) for 30 min in order to reduce any film that may have been developed before the start of the experiment. Once the sample is left at OCP, it can be seen that the potential increases within 15 minutes from -1000 mV to stabilise at -635 mV. Subsequently, no major changes can be seen during the following 6 hours at open circuit potential, suggesting that the film grew in a single stage process at OCP and did not evolve with time.

To complete the results given by the open circuit potential measurement, a Raman spectrum was recorded every 15 minutes. For clarity, only one in every three recorded spectra are presented in Figure 6.2. The first spectrum was recorded during the cathodic polarisation at -1.0 V and shows a sharp band centred at 880 cm^{-1} due to the symmetric stretching mode of borate ions in solution. Additionally, a few weak bands, located at 482, 601 and 745 cm^{-1} can be seen. Although these bands have not been identified thus far, it is clear that they can not originate from any identified iron oxide. That is, they do not match with any of the known iron oxide bands nor correspond to the 405 and 490 cm^{-1} attributed respectively to $Fe(H_2O)_6^{2+}$ and $Fe(H_2O)_6^{3+}$ observed by Oblonsky *et al.* (3) by SERS under similar conditions.

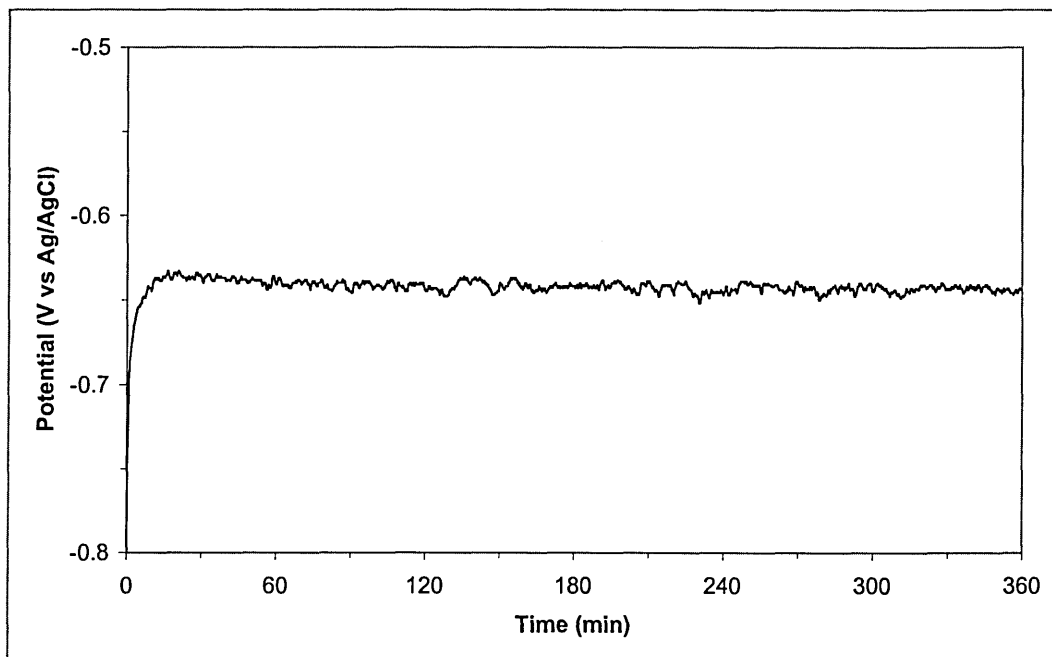


Figure 6.1. Evolution of the open circuit potential of a pure iron disc immersed in borate buffer solution (pH 7.7). Potential measured versus Ag/AgCl electrode.

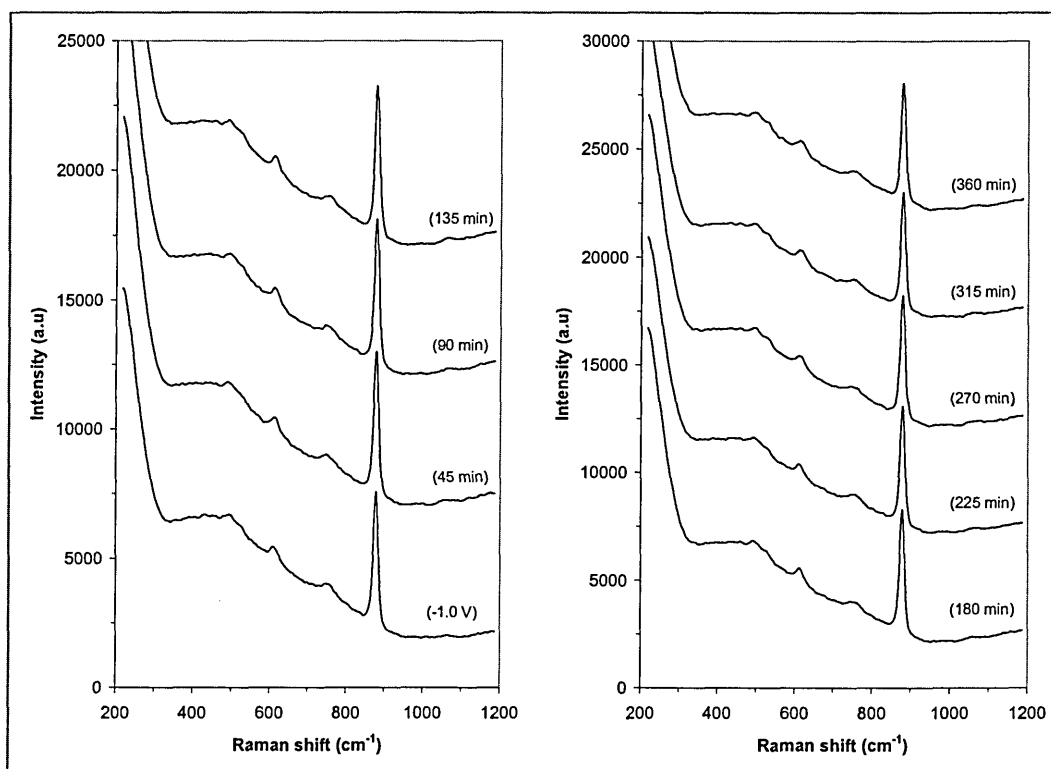


Figure 6.2. Evolution with time of the Raman spectrum of iron in borate buffer solution (pH 7.7) at open circuit potential after 30 minutes at -1.0 V.

The spectra recorded between 45 min and 540 minutes were similar to the one acquired during the pre-polarisation. They did not show any band evolution suggesting

a change in the nature of the film present at the sample surface, even though, a brownish film was clearly visible by eye.

Due to the preparation process and the Raman spectra recorded during the prepolarisation of iron in carbonate (section 6.2) and phosphate (section 6.3) solutions, it is reasonable to conclude that no oxide should be present on the sample after the 30 minutes of cathodic polarisation. Consequently the most probable explanation for the presence of such bands is that they are due to the vibrational modes of the solution itself (see below).

The first interpretation of the lack of visible oxide bands in the spectra could be the lack of Raman activity of the layer grown during oxidation at OCP. A similar spectrum has been observed by Bonin *et al.* (2) who immersed an iron sample for 24 hours in borate buffer solution before injecting CCl_4 into the solution and acquiring an in situ Raman spectrum. The only signal seen was the 880 cm^{-1} Raman band from the borate ions dissolved in the solution. The second possible reason of the absence of Raman bands could be the lack of thickness of the passive film inducing poor scattering and therefore, difficulty in detecting any Raman activity.

6.1.2. Anodic oxidation

6.1.2.1. Cyclic voltammograms

In order to grow a thicker film by polarising the sample and then identifying the potentials to be used to study the stages of the evolution of the passive film, a set of ten successive cyclic voltammograms of iron in borate buffer solution have been recorded. The first, fifth and tenth polarisation curves are shown in Figure 6.3.

For each cycle, the potential has been anodically scanned from -1000 to $+800$ mV before being reversed and cathodically scanned back to the starting potential. All cycles were recorded a rate of $5\text{ mV}\cdot\text{s}^{-1}$. The first cycle is characterised by a first anodic wave located at -550 mV, a wide passive region of 650 mV (between -400 and $+250$ mV) and the initiation of the electrodisolution of the passive film for potentials above $+250$ mV. The cathodic scan shows a large reduction activity (between $+200$ and -200 mV) which is probably due to the reduction of the passive film. When the potential is scanned further toward the starting potential, a second cathodic wave, at -500 mV, is observed.

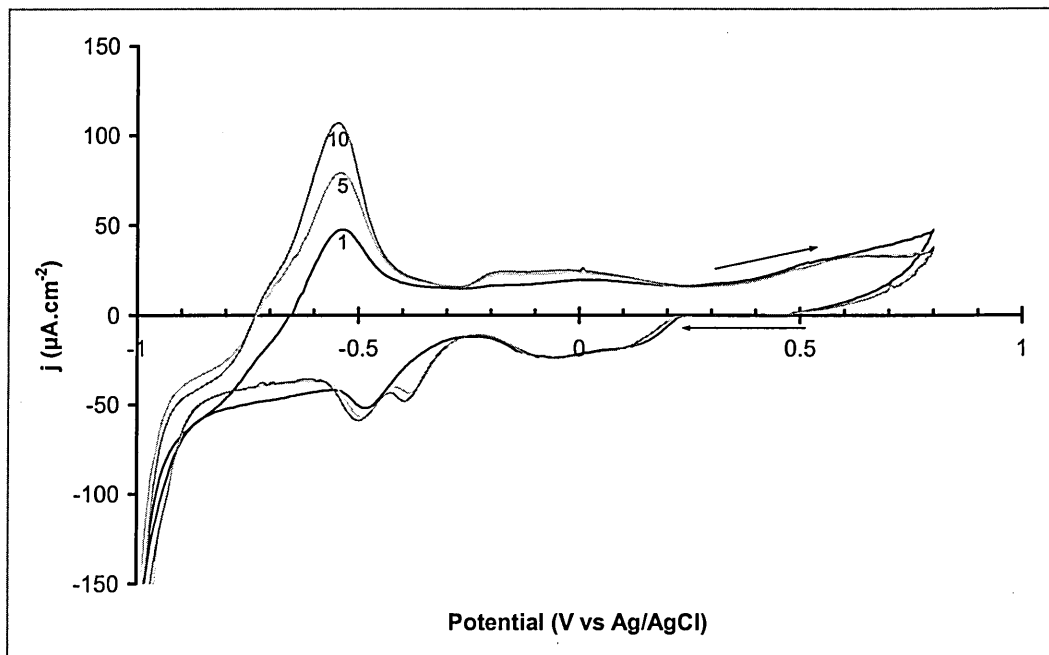


Figure 6.3. Cyclic polarisation of a 10 mm pure iron disc in 7.7 borate buffer solution after 1, 5 and 10 cycles. Potential switched at +0.8 V, scan rate $5 \text{ mV}\cdot\text{s}^{-1}$. The arrows indicate the scanning direction.

Between the first and the fifth cycles, a large increase of the first anodic wave can be observed (from 50 to $75 \text{ }\mu\text{A}\cdot\text{cm}^{-2}$) as well as an increase of the current density within the passive region, suggesting a further oxidation stage in the passivation process. Moreover, an additional cathodic wave can be observed around -400 mV which is then expected to be due to the reduction of the oxide developed between -200 and $+100 \text{ mV}$. On the tenth cycle the same anodic/cathodic features can be seen but with a slight difference in current density. The -550 mV anodic wave now reaches a maximum current density of $120 \text{ }\mu\text{A}\cdot\text{cm}^{-1}$ and the two cathodic ones at respectively -390 and -500 mV are equivalent and reach a value of $-50 \text{ }\mu\text{A}\cdot\text{cm}^{-1}$.

Despite the fact that no Raman bands could be attributed to the oxide film grown on the iron surface during the experiment realised at open circuit potential, a pure iron disc was immersed in borate buffer solution at different potentials. The choice of the potentials was made to match with the anodic and cathodic waves identified in Figure 6.3. Before the start of the experiment, the sample was pre-polarised for 30 min at -1.0 V . During the pre-polarisation, a Raman spectrum, presented in Figure 6.4 (a) was recorded in situ. Once again, the 880 cm^{-1} band from the borate ions in solution was identified as well as the three unidentified bands at respectively 482 , 601 and 745 cm^{-1} .

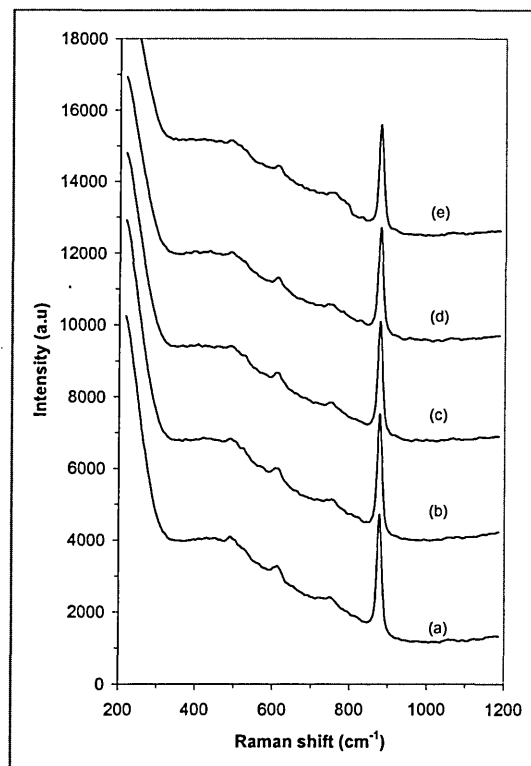


Figure 6.4. Evolution of the Raman spectrum of Iron in borate buffer solution (a) after 30 min at -1.0 V, (b) 15 min at -550 mV, (c) 2 hours at -550 mV, (d) 15 min at -100 mV and (e) 2 hours at -100 mV.

At the end of the pre-polarisation process, the sample was polarised for 2 hours at -550 mV. A first spectrum, recorded after 15 min, and a second one, recorded at the end of the polarisation period, are respectively presented in Figure 6.4 on spectra (b) and (c). No additional bands due to any iron oxides can be observed despite the fact that a strong anodic oxidation process, highlighted by the high current density measured at this potential, is occurring. Spectra (d) and (e) respectively show the Raman spectra recorded after 15 minutes and after 2 hours at -100 mV. Despite the fact that an oxide layer was clearly visible by eye on the whole iron surface, no noticeable change could be seen on the spectra. Since no oxide bands were visible by conventional Raman analysis, the potential associated with the reduction reaction were not applied to the sample. The reduction processes have therefore not been studied by Raman spectroscopy.

Since the thinness of any oxide film could be one of the reasons of the lack of Raman activity and, since the polarisation at fixed potential did not seem appropriate to grow a passive film thick enough, a complementary experiment, based on successive anodic potentiodynamic polarisation was run. Between each polarisation, a Raman spectrum

was recorded but while an oxide layer was clearly visible by eye, no noticeable changes in the Raman spectrum could be identified.

6.1.2.2. Cyclic voltammograms interpretation

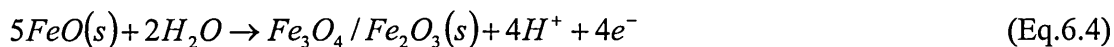
After polarising the iron sample for two hours at different potentials, it was impossible to identify any Raman activity due to film development during the oxidation process of iron in borate buffer solution. In 2001, Díez-Pérez *et al.* (7) studied the first stages of electrochemical growth of the passive film on iron by electrochemical scanning tunneling microscopy. In their study, they recorded the cyclic voltammogram of iron under the same conditions as stated above (pH 7.5, scan rate 300 mV.min⁻¹) and identified the different reactions taking place for anodic and cathodic waves using results from previous studies. The first anodic wave was attributed to two different reactions. It could be first due to the electrodisolution of the metal into the solution (equation 6.1) and second to the reaction of the metal with the hydroxide ions from the solution (equation 6.2) to form Fe(OH)₂.



The fact that no Raman bands could be observed when the sample was polarised at -550 mV could be explained by the competition between the iron dissolution and the passive-film formation on the bare iron surface. This has also been stated by Oblonsky *et al.* (11), in a study on the potential dependence of the formation of the passive film on iron in borate solution by X-ray absorption near edge structure (XANES). They claim that, at low potentials, the film formation was too slow and the dissolution of iron occurred prior to complete passivation of the surface. This phenomenon was also compatible with the results from Nagayama and Cohen (12), who remarked that below a potential of -0.2 V (vs. SCE), ferrous ions were observed in the solution.

According to Díez-Pérez *et al.* the broad feature observed on cycles 5 and 10, between -250 and +200 mV was due to two different reactions presented, as in equations 6.3 and 6.4





The equations presented above are in agreement with Oblonsky *et al.* (11) who suggested that, at potentials above -150 mV, the passive film was made of Fe₃O₄, γ-Fe₂O₃ and that the passivation rate of iron increased with increasing potential. It is interesting to note that the presence of FeO in equation 6.4 could be justified by the fact that wüstite is the dry form of Fe(OH)₂. Unfortunately, the composition of the passive film at potentials above -150 mV did not match with that observed here, during the 2 hours polarisation at -100 mV. None of the characteristic bands of Fe(OH)₂, magnetite nor hematite were observed.

6.1.2.3. Interpretation of the lack of Raman activity

Assuming that magnetite and hematite were the two oxides that developed at potentials above -150 mV, the only explanation of the lack of characteristic Raman bands from Fe₃O₄ and Fe₂O₃ could be due to the low thickness of the passive film, since both oxide spectra were successfully recorded from reference powders (see 3.7.1). Moreover, in several studies of iron in borate solution realised by SERS (13,14) a broad band at 550 cm⁻¹ has been attributed to Fe(OH)₂. As stated previously, it could not be detected by conventional Raman spectroscopy (2). To prove that Fe(OH)₂ was developed in borate solution, Boucherit *et al.* (15) recorded the Raman reference spectrum of Fe(OH)₂ obtained by chemical reaction between 0.003 M NaOH solution de-aerated by argon bubbling and Mohr solution of 0.003 M Fe(SO₄)₂(NH₄)₂. The technique they used to record the Raman spectrum was not conventional since once the precipitate had been grown, it was crushed between two glass plates in which it was stable enough to allow the acquisition of a Raman spectrum. Once the spectrum had been recorded, they compared it with the spectrum obtained by SERS by Rubim and Dünwald (16) on an electrode passivated in a neutral medium. The compound observed was similar.

Even if the experiment realised by Boucherit *et al.* permitted the identification of Fe(OH)₂, and confirmed its presence when iron was exposed to borate solution, they proved that the use of SERS was not necessary to allow the observation of iron hydroxide. The result is still disputable, since the amount of oxide film present on the iron sample immersed in borate solution is much lower than the precipitate itself. It

appears that SERS is the only method that permits the acquisition of a Raman spectrum to follow the corrosion processes on iron in borate buffer solution.

Nevertheless, several drawbacks due to the technique are worthy of mention. First, one of the disadvantages of using silver to enhance Raman scattering is the eventual contamination by graphitic carbon, as observed and interpreted by Cooney *et al.* (17-19). The contamination could be identified on the Raman spectra by the presence of a large number of strong peaks between 800 and 1500 cm^{-1} . Such observation pushed Oblonsky and Devine to raise two different questions (3): What was the origin of the contamination, and what are the effects it has on the passive films?

The question of the origin of the graphitic carbon contamination has been answered by Cooney *et al.* themselves who identify CO_2 as the compound at the origin of the contamination. They managed to reduce the contamination to a minimum only by following carefully a silver specimen and solution preparation procedure, which included polishing the sample in dilute HCl under a strong directed nitrogen stream. They then concluded that, even if similar reactions occur on most metal surfaces, it does not happen with the same high efficiency as in the case of silver.

In view of the fact that such contamination occurs in the presence of silver it is not known whether the carbon contamination is confined to the silver surfaces or whether it also extends to the surface of the iron metal studied during corrosion investigation by SERS. It is then difficult to assert that SERS is suitable for corrosion studies, since it can have an influence on the corrosion behaviour of the material studied.

Another limitation of the use of SERS for in situ corrosion studies is the oxidation of silver at potential above +150 mV, as stated by Gui and Devine (4). In Figure 6.5, the cyclic polarisation curves of silver in borate buffer solution are presented. These curves have been recorded in the same conditions as the ones used for the evaluation of iron in borate as presented in Figure 6.3. Even if, during the first cycle, the dissolution occurs at +450 mV, after several cycles it starts at a lower potential of +300 mV (figure 6.5, cycles 5 and 10). The fact that silver ion may be present in the solution can dramatically change the nature of the environment in which the sample is exposed. Thus may then affect the corrosion behaviour.

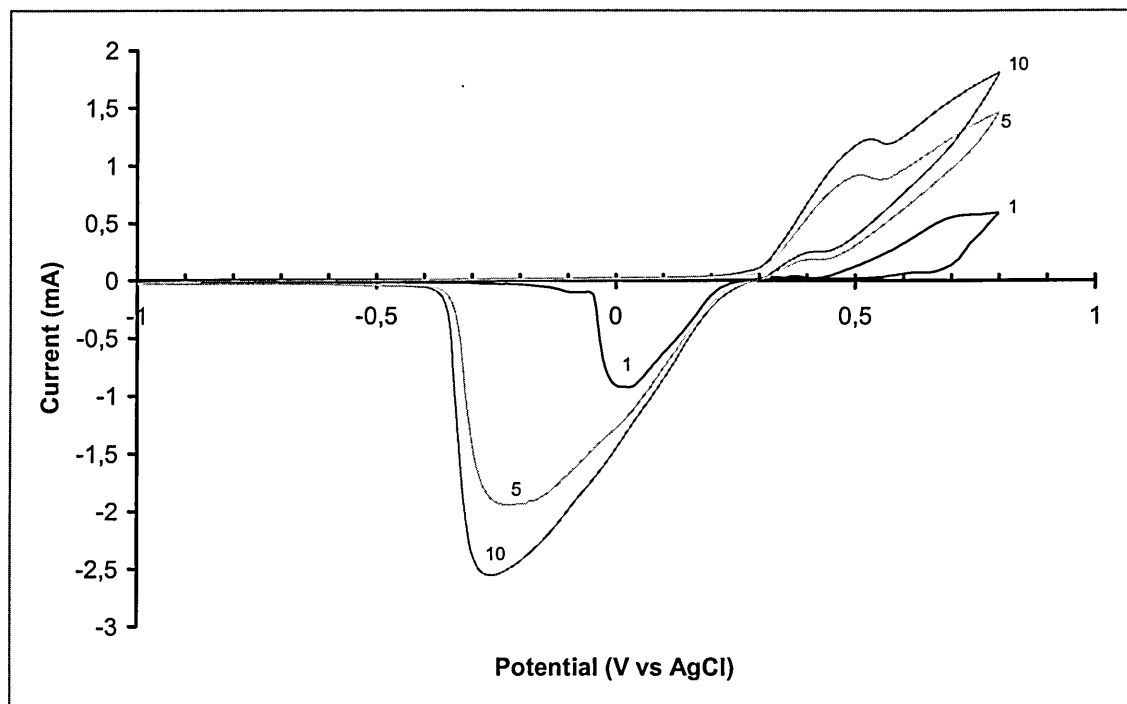


Figure 6.5. Cyclic polarisation curve of a silver electrode in a 7.7 borate buffer solution after 1, 5 and 10 cycles. Potential switched at +0.8 mV, scan rate $5 \text{ mV}\cdot\text{s}^{-1}$.

Finally one of the main limitations of the SERS technique for corrosion studies is the silver deposition. Two different techniques can be used. The first one, used by Thanos (20) consists of developing the passive film on iron in borate buffer solution; then removing the sample from the liquid in order to deposit some silver by immersing it in a silver nitrate mixture, and then putting the sample back in the original borate solution to continue the experimental test. Gui and Devine (4), who disagreed with the method, called it 'quasi-in situ technique' and proposed to deposit the silver islands on the sample before its oxidation. They proceeded by first cathodically polarising the sample at -0.9 V in borate buffer solution to reduce any passive film present at the iron surface. Next, they electrodeposited the silver on the electrode of iron by polarising the electrode at a potential of -0.6 V in a solution of 1 mM AgNO_3 + 1 mM HNO_3 . The deposition process was stopped after the passage of a total cathodic charge density of 35 mC. Once the silver was deposited on the iron substrate, the new system was returned back to the borate solution and cathodically polarised at -0.9 V for 10 min. Even if the corrosion studies of iron were preceded by a cathodic polarisation with the purpose of reducing any passive film present on the iron surfaces, it is obvious that the final system could not be representative of a pure iron sample exposed to a borate solution.

6.2. Iron in carbonate/bicarbonate buffer solution

6.2.1. Open circuit potential

Figure 6.6 shows the evolution of the surface of a pure iron disc in 0.05 M carbonate / 0.05 M bicarbonate buffer solution at open circuit potential. The first spectrum, recorded during the pre-polarisation, shows two bands respectively located at 1007 and 1062 cm^{-1} as well as an intense 'tail' between 200 and 330 cm^{-1} . While the two bands around 1000 cm^{-1} can be attributed to the symmetric stretching modes of the free carbonate ions in solution, HCO_3^- and CO_3^{2-} (21), the intense tail, identified as the wing of the Rayleigh scattering by Guy *et al.* (22) is more likely due to the bulk water since it is not visible when a dry iron sample is studied. (13).

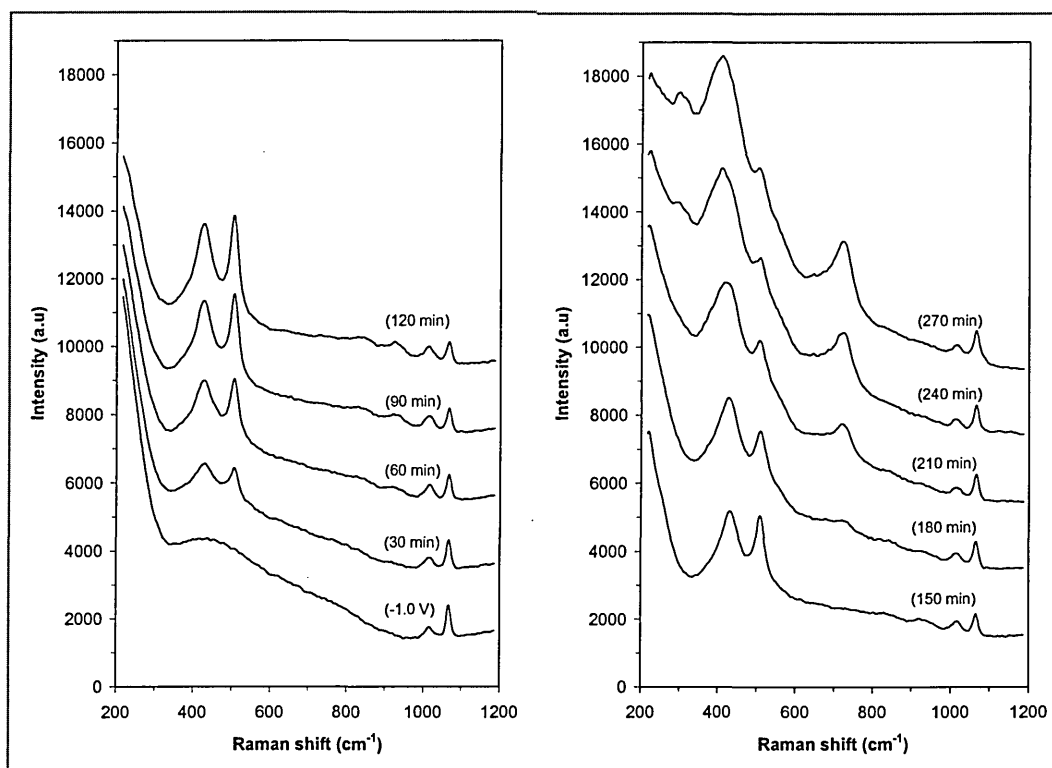


Figure 6.6. Evolution with time of the Raman spectrum of iron in 0.05 M carbonate / 0.05 M bicarbonate buffer solution at open circuit potential after 30 min at -1.0 V.

After 30 min at open circuit potential (OCP), two overlapping bands located at 425 and 503 cm^{-1} are clearly visible. Such bands have been previously observed by several authors who worked on iron in sulphate or carbonate solutions (13,23-26). These two bands have been identified as the two stretching modes of Fe^{2+} -OH and Fe^{3+} -OH from 'green rust'. Subsequently, during the 120 min at OCP, the 425 and

503 cm^{-1} bands become sharper and more intense, suggesting the development of 'green rust' on the sample surface, and an increase of the crystallinity of the corrosion product. Meanwhile, two bands at 835 and 917 cm^{-1} , not reported elsewhere in any 'green rust' spectra, can be seen next to the free carbonate bands.

After 150 min at OCP, the intensities of the two 'green rust' bands start to decrease and, within a period of 30 minutes, the 425 bands appears to shift to the lower wave number while the 503 band decreases drastically in intensity. At the same time, a band located around 715 cm^{-1} becomes visible and the 835 and 917 cm^{-1} unidentified bands are no longer detected. Consequently, the spectrum recorded after 210 minutes at open circuit potential, showed an entirely different corrosion product to the original 'green rust'. The new oxide is characterised by a band at 715 cm^{-1} and a broad band at 415 cm^{-1} with a small peak on its shoulder located at 503 cm^{-1} . Finally, the spectrum recorded after 270 minutes at OCP is similar to the one recorded at 240 min but a broad feature located between 290 and 310 cm^{-1} can be seen.

In 1985, Nauer *et al.* (27) presented the Raman spectra of three of the crystal forms of FeOOH (α -, β - and γ -) and shown that akaganeite (β -FeOOH) was characterised by two bands: a strong one located at 715 cm^{-1} and a weak one at 415 cm^{-1} . In the experiment described above, the intensity ratio between the 415 and 715 cm^{-1} bands is the inverse of the one shown in the literature, suggesting that the broad band at 415 cm^{-1} contains a contribution from several products. According to Nauer *et al.* (27), the spectrum of goethite (α -FeOOH) has two main vibrational bands at 299 and 397 cm^{-1} . The 299 cm^{-1} band is visible in the spectrum recorded after 270 minutes at OCP and then can be attributed to the presence of goethite in the corrosion product. Finally, since the strongest band of γ -FeOOH, located at 250 cm^{-1} cannot be detected, the presence of lepidocrocite in the passive film, as suggested by Nauer can not be confirmed. It can be concluded that the oxidation of a pure iron sample in carbonate buffer solution follows a two step process. It starts with the oxidation of iron into 'green rust' which is then transformed, within a period of 30 min, to a mixture of α - and β -FeOOH.

As well as the evolution of the surface by Raman spectroscopy, the changes in the free corrosion potential have been recorded as shown in Figure 6.7. During the first two hours of the experiment, the free corrosion potential is relatively constant around -750 mV and suddenly increases, within a period of 20 minutes, by an amount of

400 mV to reach a maximum potential of -366 mV. According to the Nernst equation (section 3.2.4) such an important shift in the potential can only be explained by either, a very large change in the ion concentration or, by the presence of an entirely different species of ion near the sample surface due to the presence of a new corrosion product.

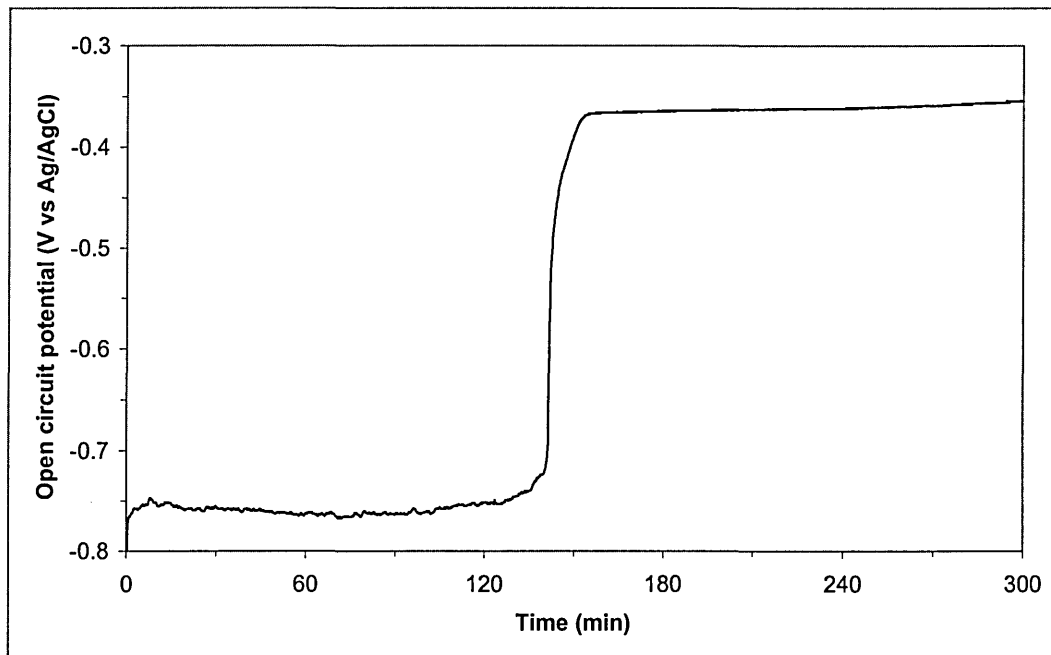


Figure 6.7. Evolution of the open circuit potential of a pure iron disc immersed in 0.05 M carbonate/0.05 M bicarbonate buffer solution. Potential measured versus Ag/AgCl electrode.

In order to correlate the evolution of the open circuit potential and the nature of the oxide, the 337-475 cm^{-1} region of the Raman spectra has been fitted and the position of the centre of the band, as well as the band width, were calculated for each spectrum. Since the fitted band can be made from a contribution of the 425 cm^{-1} from 'green rust' and the 415 cm^{-1} bands from α - and β -FeOOH, the sharp band centred around 425 cm^{-1} has been attributed to 'green rust' and a broad feature centred around 415 cm^{-1} is attributed to FeOOH. The evolution of the band width and the band position can be seen in Figure 6.8.

During the first 150 minutes of the experiment, the band appears to be sharp (50 cm^{-1} wide) and located around the 425 cm^{-1} region. It then shifts to the lower wave number and its width increases up to 80 cm^{-1} . The potential shift of the free corrosion potential, matching with the evolution of the shape and position of the bands highlight the transformation of the oxide present at the sample surface from 'green rust' to FeOOH. It is important to note that the large band width observed after 15 minutes at open

circuit potential (85 cm^{-1}) is not due to the presence of FeOOH but to the fact that the band was not intense enough to be detected. The interpretation of this high band width is confirmed by the position of the band at 429 cm^{-1} related to 'green rust'.

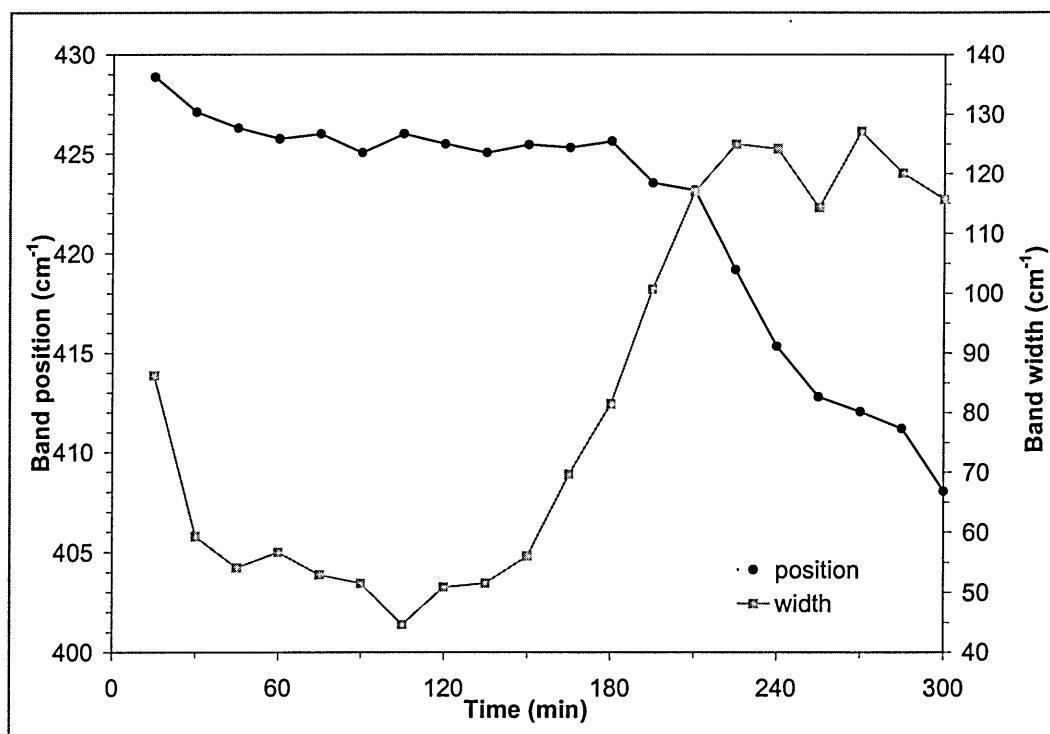
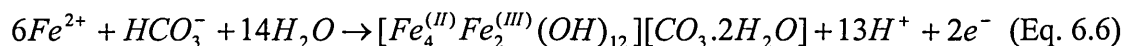
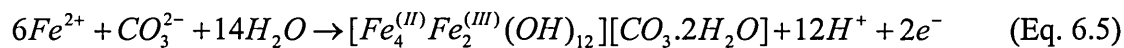


Figure 6.8. Evolution of the position and width of the $400\text{-}430 \text{ cm}^{-1}$ band with time during immersion of an iron disc in 0.05 M carbonate / bicarbonate solution at the free corrosion potential.

In a study of a new carbonate 'green rust' obtained using an electrochemical method in carbonate / bicarbonate solution, Legrand *et al.* (25) calculated the area and the ratio of the $\text{Fe}^{2+}\text{-OH}$ / $\text{Fe}^{3+}\text{-OH}$ bands to prove that the 'green rust' was made of a 1/1 ratio suggesting an iron oxidation state of 2.5. In the current study, a similar integration process has been used and shows the presence of a more conventional 'green rust' with a ratio of 2/1 as stated by Drissi *et al.* (28) suggesting a chemical composition of $[\text{Fe}_4^{(II)}\text{Fe}_2^{(III)}(\text{OH})_{12}][\text{CO}_3 \cdot 2\text{H}_2\text{O}]$.

Abdelmoula *et al.* (29) analysed the composition of the corrosion product formed on a pure iron sample in a 0.1 M NaHCO_3 solution by X-ray diffraction and Mössbauer spectroscopy. They showed that, as observed here, the corrosion product was made of carbonate-containing 'green rust'. However, if it was left in solution, the 'green rust' layer oxidised into goethite ($\alpha\text{-FeOOH}$), although they did not mention akaganeite ($\beta\text{-FeOOH}$). Moreover, Simard *et al.* (21) studied the pitting corrosion product of a 1024 mild steel in bicarbonate solution and showed that the production of 'green rust' was

preceded by the reaction of the Fe^{2+} ions with the solution to produce $Fe(OH)_2$. $Fe(OH)_2$, which is usually characterised by a band centred at 544 cm^{-1} (30), has not been observed in the current study. Therefore, the passivation process of iron in 0.05 M carbonate/bicarbonate solution starts with the oxidation of iron to Fe^{2+} , which then reacts with the carbonate ions from the solutions to form carbonate 'green rust' (equations 6.5 and 6.6). The 'green rust' is then oxidised to form the α and β - crystal structure of $FeOOH$ as shown by equation 6.7 and 6.8.



6.2.2. Cyclic polarisation

In order to increase the amount of information on the passive film grown on iron in carbonate / bicarbonate solution at open circuit potential, a set of cyclic polarisation curves have been recorded (Figure 6.9). 10 successive cycles have been recorded although only the first, fifth and tenth cycles, for clarity, are shown here.

The potentiodynamic traces are characterised by two large oxidation peaks located at -700 mV and -320 mV, a large passive region between -200 and +800 mV and two reduction peaks at -600 mV and -900 mV. Between the first and fifth cycles, the evolution of the anodic waves are similar, showing an increase of the current density. The same phenomenon can be observed on the cathodic wave suggesting that the increase of the current density during the oxidation is balanced by an increase of the reduction reaction.

Between the 5th and 10th cycles, while the current density of the second anodic wave stays constant, the one from the first anodic peak decreases from 134 to 84 $\mu\text{A}\cdot\text{cm}^{-1}$; suggesting a diminution of the first oxidation reaction due to the creation of a passive barrier.

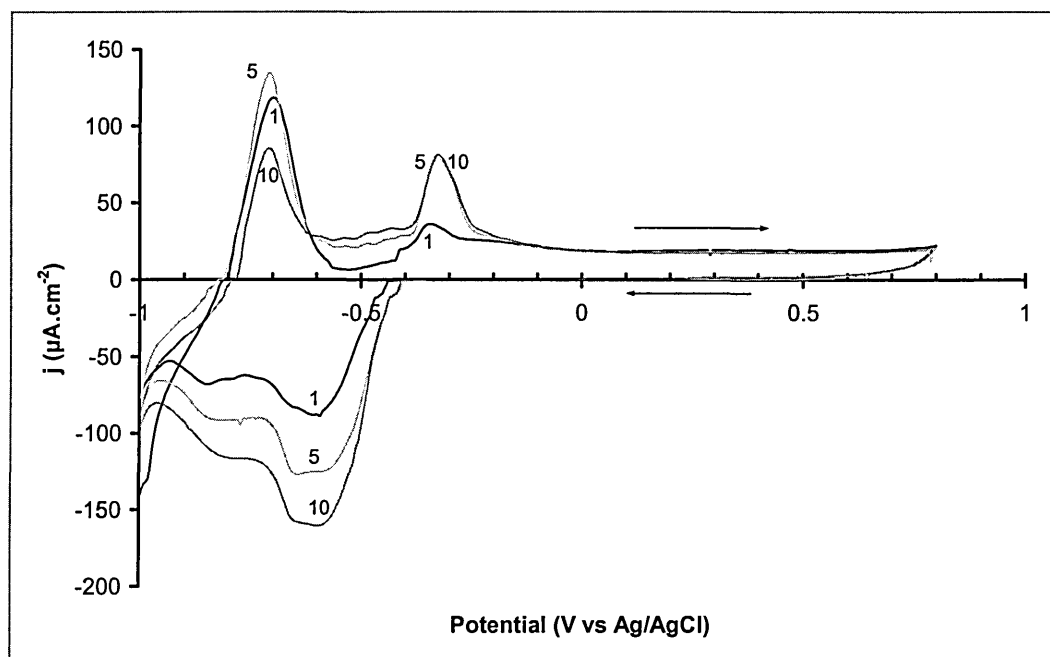


Figure 6.9. Cyclic polarisation of a 10 mm pure iron disc in 0.05 M carbonate/bicarbonate buffer solution after 1, 5 and 10 cycles. Potential switched at +0.8 V, scan rate $5 \text{ mV}\cdot\text{s}^{-1}$. The arrows indicate the scanning direction

In a paper published in 1995, Gui and Devine (22), recorded the quasi-steady-state anodic polarisation of iron in 0.15 M NaHCO_3 and 0.15 M Na_2CO_3 with a pH value of 10. They showed that the maximum oxidation rate occurred at -250 mV (vs SCE), with a maximum current density of $50 \mu\text{A}\cdot\text{cm}^{-2}$, although they did not manage to see the first anodic wave. The fact that they could not see the first anodic wave may be due to the acquisition process which consisted in increasing the potential applied by 50 mV steps and holding it for 3 minutes before recording the current. More recently Legrand *et al.* (25) recorded the voltammograms from an iron disc, immersed in a solution of 0.4 M carbonate/bicarbonate solution, at a temperature of 50°C using a $10 \text{ mV}\cdot\text{s}^{-1}$ scan rate. Whilst they recorded only 5 successive cycles, they observed the same anodic peaks at -700 and -320 mV, but with a current density 10 times higher as the one shown in Figure 6.9. The first peak was attributed to the dissolution of iron and the evolution of the current density with the increase of the number of cycles permitted the observation of the presence of a pseudo passive film, indicated by the hindering of the iron dissolution between the fourth and the fifth cycle. Moreover, they attributed the second oxidation process to the oxidation of the Fe(II)-containing species to ferric oxyhydroxides. Finally, their reverse scan shows two cathodic peaks at -520 and -700 mV suggesting that the reduction of the ferric oxyhydroxides was assumed to involve a two step process.

The fact that both cathodic waves were due to the reduction of the ferric oxyhydroxides and not to the reduction of the 'green rust' has been proved by reversing the potential at -0.42 V as shown in Figure 6.10. Even if a negative current is visible during the cathodic scan, no real cathodic waves are visible, suggesting that the two cathodic waves observed when the full cycles are recorded are due to the reduction of the ferric oxyhydroxides. Finally, the diminution of the current density of the first anodic wave has been also observed between the fifth and the tenth cycles suggesting a diminution of the corrosion rate and the creation of a 'green rust' passive film limiting the dissolution of the iron surface.

In order to understand the polarisation cycles and the reactions which were happening at each anodic and cathodic waves, the potential of the iron sample has been successively held for 2 hours at OCP, -700, -320, -600 and -1000 mV. During the polarisation, Raman spectra have been recorded every 15 minutes (Figure 6.11). The reason why a two hour polarisation period have been chosen was to avoid the natural oxidation of 'green rust' to α and β -FeOOH, as observed during the experiment conducted at open circuit potential.

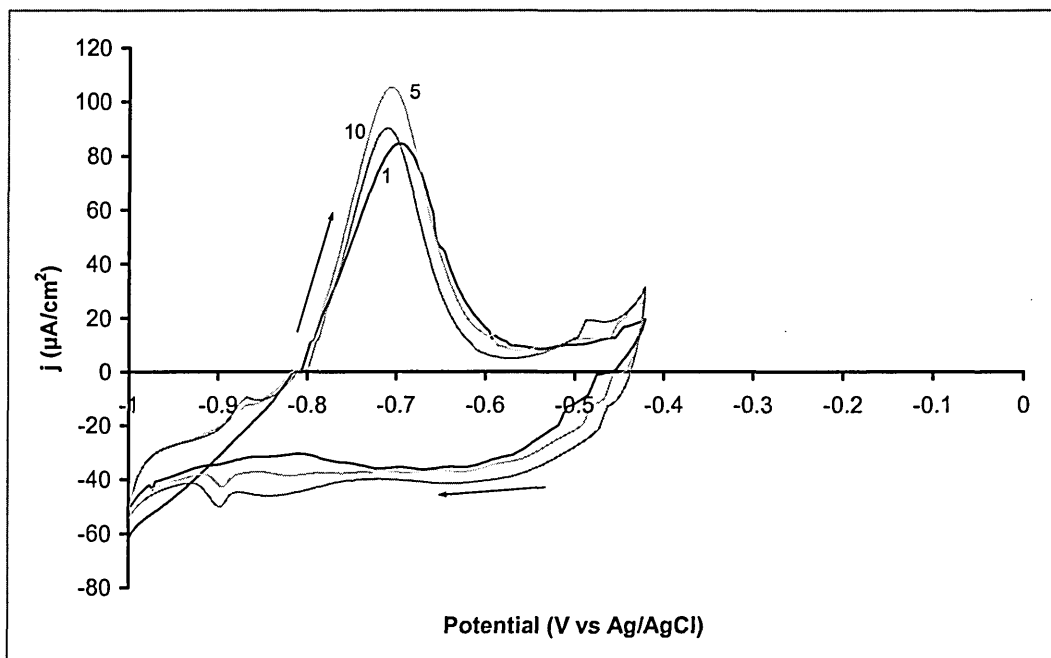


Figure 6.10. Cyclic polarisation of a 10 mm pure iron disc in bicarbonate buffer solution after 1, 5 and 10 cycles. Potential switched at -0.42 V. The arrows indicate the scanning direction

Throughout the two hours at open circuit potential, the two bands at 425 and 503 cm^{-1} increase in intensity revealing the oxidation of the iron surface to carbonate

'green rust'. After 120 minutes at OCP, the applied potential has been changed to -700 mV in order to match the first anodic wave. Like that of oxidation at open circuit potential, the two bands characteristic from 'green rust' can be seen but the shape and intensity does not appear to change with time and a slight change in the background in the 650-700 cm^{-1} seems to occur (see spectra acquired between 150 and 240 minutes.) At the end of the two hours of polarisation at -700 mV, the potential applied was changed to match the second anodic wave at -320 mV. Within 30 minutes of polarisation (Figure 6.11, c, 270 min), the transformation of 'green rust' to FeOOH, highlighted by the diminution of the intensity of the 503 cm^{-1} band and the broadening and the shift toward the lower wave number of the 425 cm^{-1} band, starts to be seen. At 300 minutes, the 503 cm^{-1} band continues decreasing and a broad feature between 625 and 750 cm^{-1} becomes visible. At 330 min, the 299 cm^{-1} band from α -FeOOH (goethite) becomes visible and the 715 cm^{-1} peak due to β -FeOOH appears to be much stronger, but is not as clearly resolved as that obtained during the experiment at open circuit potential. The fact that the akaganeite band (at 715 cm^{-1}) is not well resolved is due to the presence of an overlapping broad band on the left hand shoulder.

At 360 minutes, the potential was changed to -600 mV to match the first reduction wave. Not a lot of changes can be seen within the 30 first minutes of cathodic polarisation but the spectrum recorded at 420 min shows a diminution of the intensities of the goethite (299 cm^{-1}) and akaganeite (715 cm^{-1}) bands while the one at 503 cm^{-1} , from green, rust increases again. The band at 415 shifts back to 425 cm^{-1} and becomes sharper, showing the reduction of the mixture of α and β FeOOH and the presence of 'green rust'. Finally, the decrease in intensity of the akaganeite bands permits the separation of the shoulder to an independent peak located at 670 cm^{-1} usually attributed to magnetite (Fe_3O_4).

The spectra recorded at 450 and 480 min do not show many changes but once the applied potential was switched to -1.0 V (510 minutes), a further step in the reduction process can be seen. It is characterised by a large increase of the 503 cm^{-1} band, the shift of the 415 band toward 425 cm^{-1} , the disappearance of the 715 cm^{-1} band (from akaganeite) and a slight increase of the 670 cm^{-1} suggesting the presence of a mixture of 'green rust' and magnetite (Fe_3O_4). After 60 minutes at -1.0 V (spectrum e, 540), the 670 band from magnetite appears to be very well resolved and the two bands from 'green rust' appear to be as intense as the one observed after 90 minutes at open circuit potential. On the next spectrum (e, 570) an increase of the magnetite band is shown and

a diminution of the intensity of the 'green rust' band can be seen. A further diminution of the 425 and 503 cm^{-1} bands can be observed in the last spectrum suggesting a reduction of the 'green rust' while the intensity of the magnetite band stays constant.

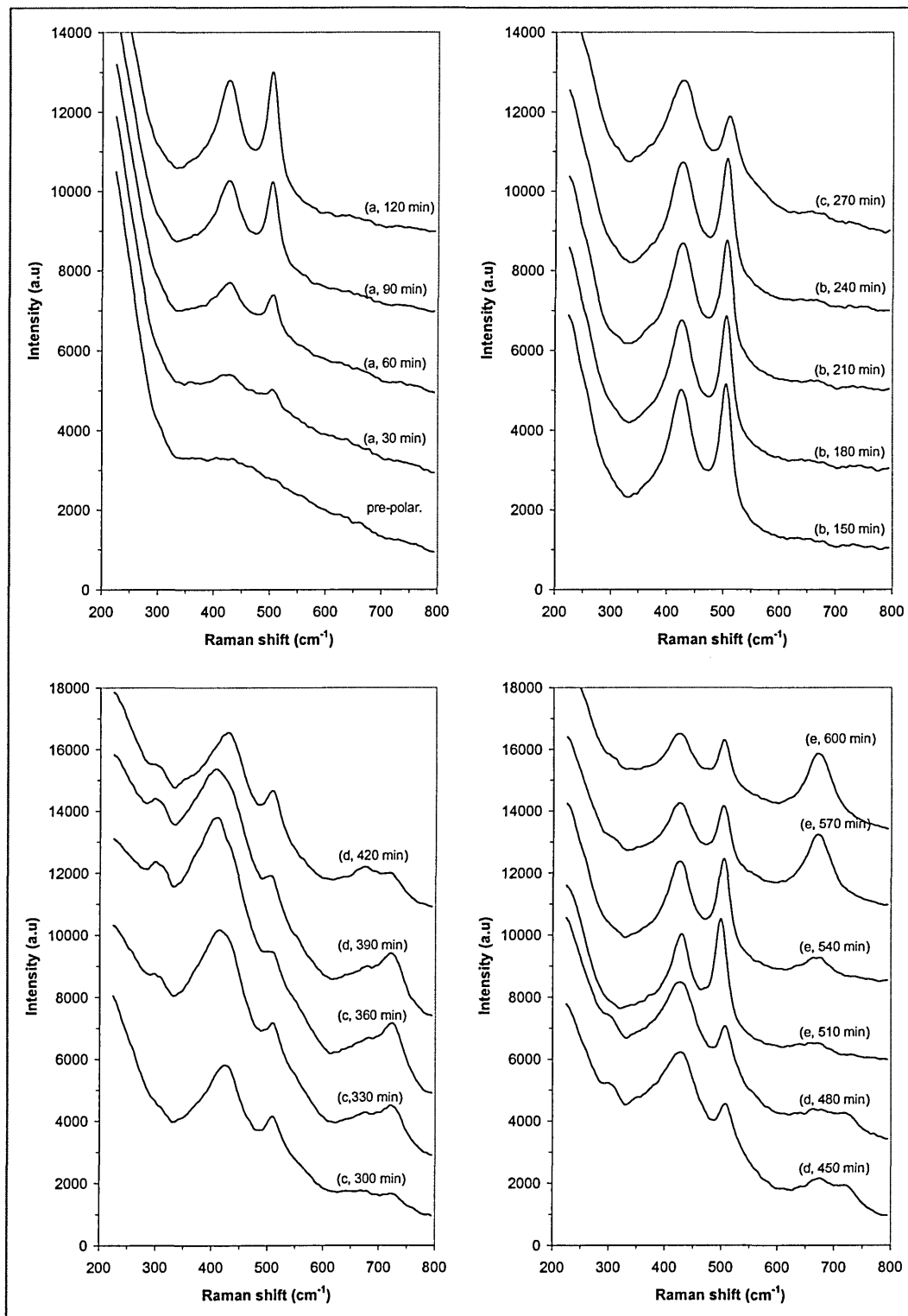


Figure 6.11. Raman spectra of the iron surface in carbonate / bicarbonate solution during successive polarisation periods of 2h at (a) open circuit potential, (b) -700 mV, (c) -320 mV, (d) -600 mV and (e) -1.0 V. The first spectrum displayed has been recorded after 30 min of pre-polarisation at -1.0 V.

To track the evolution of the broad feature located around 415-425 cm^{-1} the band has been integrated following the same process as the one used for the analysis of the OCP experiment but this time, the band position and area have been plotted versus time (Figure 6.12). During the first two hours of the experiment, at open circuit potential, the band area increases linearly, without showing a positional shift, suggesting the growth of a 'green rust' film at the sample surface. When -700 mV is applied, the band stays at the same position of 425 cm^{-1} , but does not appear to develop any further. The fact that the band intensity does not increase can be interpreted in two different ways. First, it can be due to the creation of a passive film that stops the dissolution of the iron into the solution as it has been seen in the cyclic voltamogram with the decrease of the maximum current density on the first anodic wave. Second, it can be due to the fact that the whole surface is covered by the corrosion product, showing a saturation of the detection by Raman, since the technique does not allow depth sampling of the oxide.

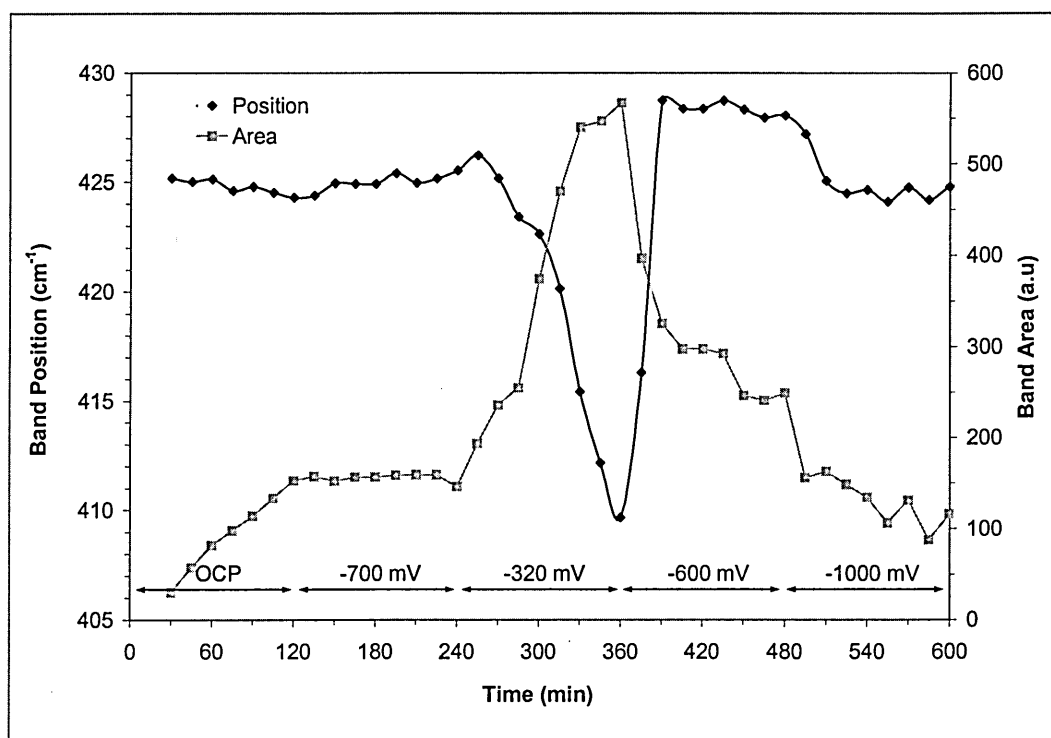


Figure 6.12. Evolution of the position and area of the 400-430 cm^{-1} band from the corrosion product grown on iron in 0.05 M carbonate during successive polarisation periods of 2h at open circuit potential, -700, -320, -600 and -1000 mV.

During the two hours at -320 mV, the 'band area' and 'position' change linearly, showing the conversion of the corrosion film from 'green rust' to ferric oxyhydroxides. As soon as the applied potential is switched to -600 mV, the reduction of FeOOH starts and the presence of 'green rust' is revealed within less than 30 minutes as shown by the

sharp shift of the ‘band position’ from 409 to 429 cm^{-1} . An equivalent phenomenon is visible on the ‘band area’ curve, showing a quick loss of intensity due to the reduction of the α - and β -FeOOH, and the detection of the inner layer of ‘green rust’. Finally, a further drop in the band intensity is observed during the polarisation at -1.0 V; which this time is explained by the reduction of the ‘green rust’ itself.

6.2.3. Anodic waves (-700 mV and -320 mV)

In order to check the relationship between the reactions that are happening at the different anodic waves, two freshly polished samples have been polarised at -700 mV and -320 mV. In both cases, the sample has been polarised for 30 minutes at -1.0 V to reduce any film that could initially be present on the sample surface. The results of both experiments are shown in Figure 6.13.

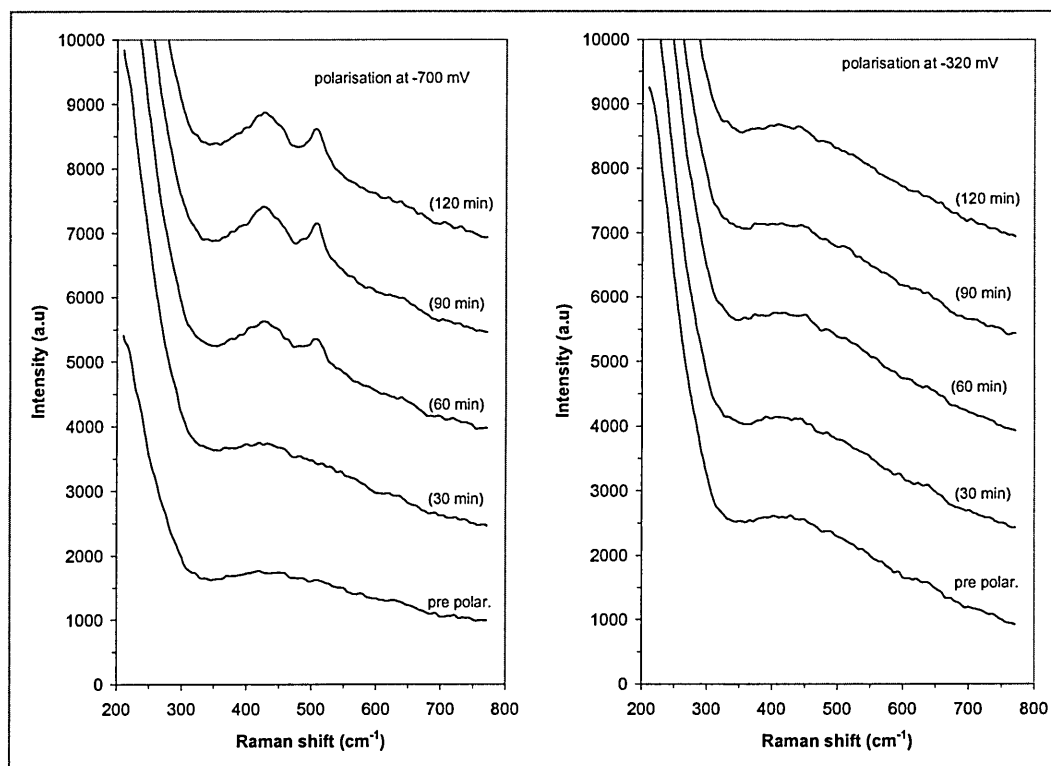


Figure 6.13. Evolution with time of the Raman spectrum of iron in 0.05 M carbonate / 0.05 M bicarbonate at -700 mV (left hand side graph) and at -320 mV (right hand side graph).

During the polarisation of ‘green rust’ at -700 mV, the Raman spectra recorded allowed the evolution of the sample surface with time to be monitored showing that, during polarisation at open circuit potential, ‘green rust’, identified by the two bands at 425 and 503 cm^{-1} , develops. It can then be concluded that the first anodic wave is due

to the dissolution of iron to Fe^{2+} which reacts with the HCO_3^- and CO_3^{2-} ions from the solution to give at 2/1 $\text{Fe}^{\text{II}}/\text{Fe}^{\text{III}}$ carbonate 'green rust' as presented in section 6.2.1.

When the sample was directly polarised at -320 mV, no bands were visible in the Raman spectra even after two hours of polarisation. It has been shown above that when the sample was polarised at -320 mV after being polarised at -720 mV, goethite (α -FeOOH) and akaganeite (β -FeOOH) develop on the sample surface. The fact that nothing is happening when the sample is directly polarised at -320 mV proves that the reaction that occurs at the second anodic wave is a further oxidation stage of the corrosion process, observed at the first anodic wave, and not an oxidation from pure iron. Without the first stage of the oxidation process, the ferric oxyhydroxides can not be developed on iron.

6.2.4. Model representation of the passive film formation

The nature of the passive film that develops on iron in carbonate/bicarbonate solution at pH= 9.4 has been studied at open circuit potential and by applying different potentials chosen according to the cyclic polarisation. The study at OCP identified that the creation of the film was due to a two step process initiated by the oxidation of the metal iron to Fe^{2+} and Fe^{3+} ions which precipitate to 'green rust', before the natural evolution to a mixture of α - and β -FeOOH. A schematic representation of the oxidation processes that may be occurring when different anodic and cathodic potentials are applied is presented in Figure 6.14.

The pre-polarisation at -1.0 V permits the reduction of any film that could have been left on the iron sample. When the sample is left at open circuit potential for less than 150 min, 'green rust' develops on the sample surface. While holding the potential at -700 mV stops the oxidation of the 'green rust' layer to ferric oxyhydroxide, the polarisation at -320 mV permits the oxidation of 'green rust' to FeOOH. Moreover, when the oxidation of the sample is allowed, the dissolution of the metal ions is limited by the creation of an inner layer of magnetite.

At -600 mV (first cathodic wave), the external layer of α and β FeOOH is reduced, allowing both the 'green rust' and the thick magnetite film formed underneath to be exposed to the solution. By pushing further the reduction process by polarising the sample at -1.0 V, the 'green rust' is reduced exposing the inner layer of magnetite.

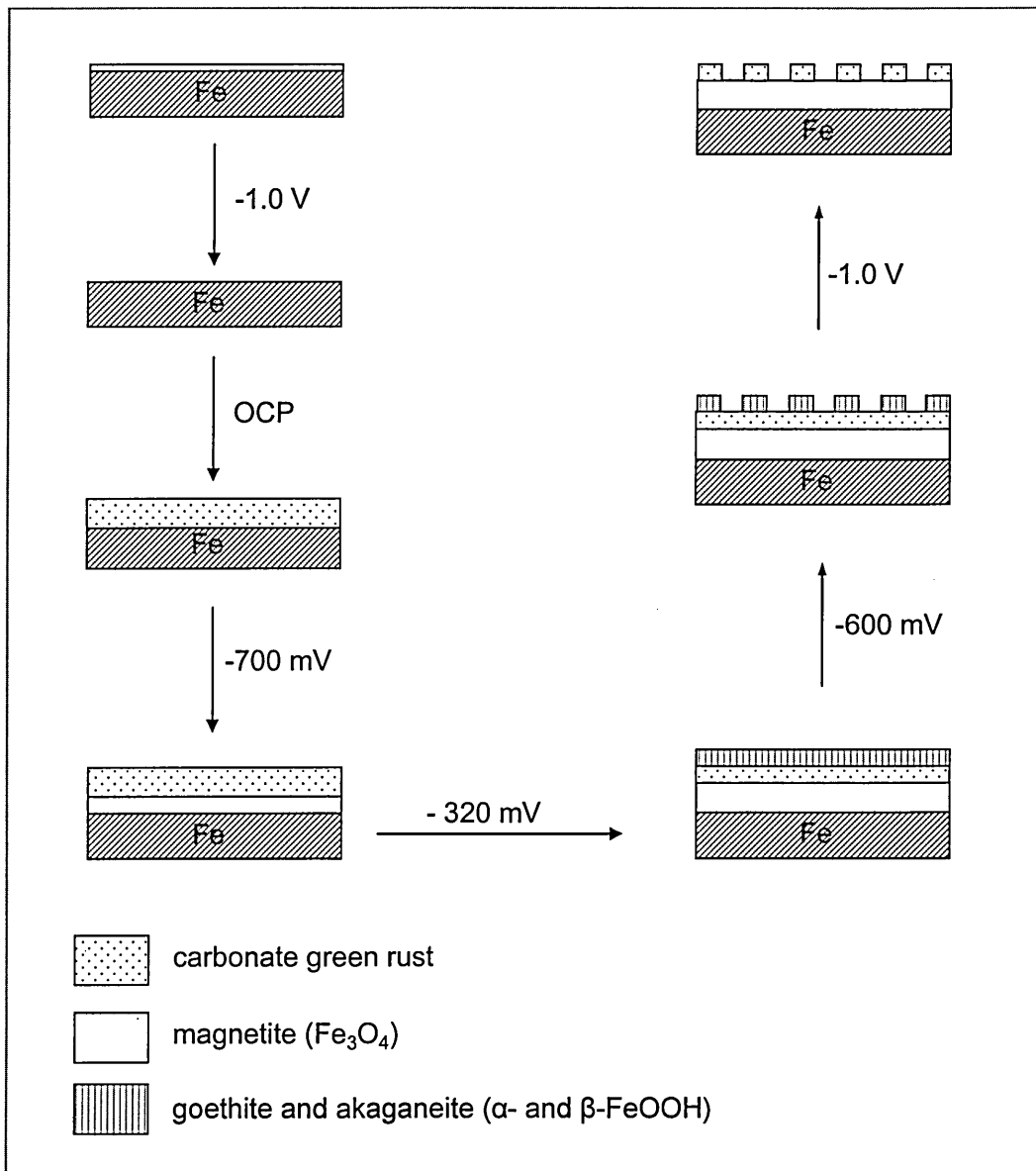


Figure 6.14. Evolution of the passive film formation on iron in 0.05 M carbonate / bicarbonate buffer solution with respect to the potential applied.

The application of successive anodic and cathodic potentials permitted the identification of the corrosion product formed on iron in carbonate/bicarbonate solution as a three layer structure. This layer comprised an inner film of magnetite, a layer of carbonate ‘green rust’ and an outer layer of a mixture of goethite (α -FeOOH) and akaganeite (β -FeOOH).

6.3. Iron in Potassium Phosphate buffer solution¹

6.3.1. Oxidation at Open Circuit Potential (OCP)

6.3.1.1. Raman data

To study the nature of the film developing at the surface of a pure iron sample immersed in a pH 7.7 phosphate buffer solution, a pure 10 mm diameter iron disc was left at open circuit potential for 6 hours. The evolution of the surface with time was monitored by Raman spectroscopy. Some of the spectra recorded during the experiment are presented in Figure 6.15.

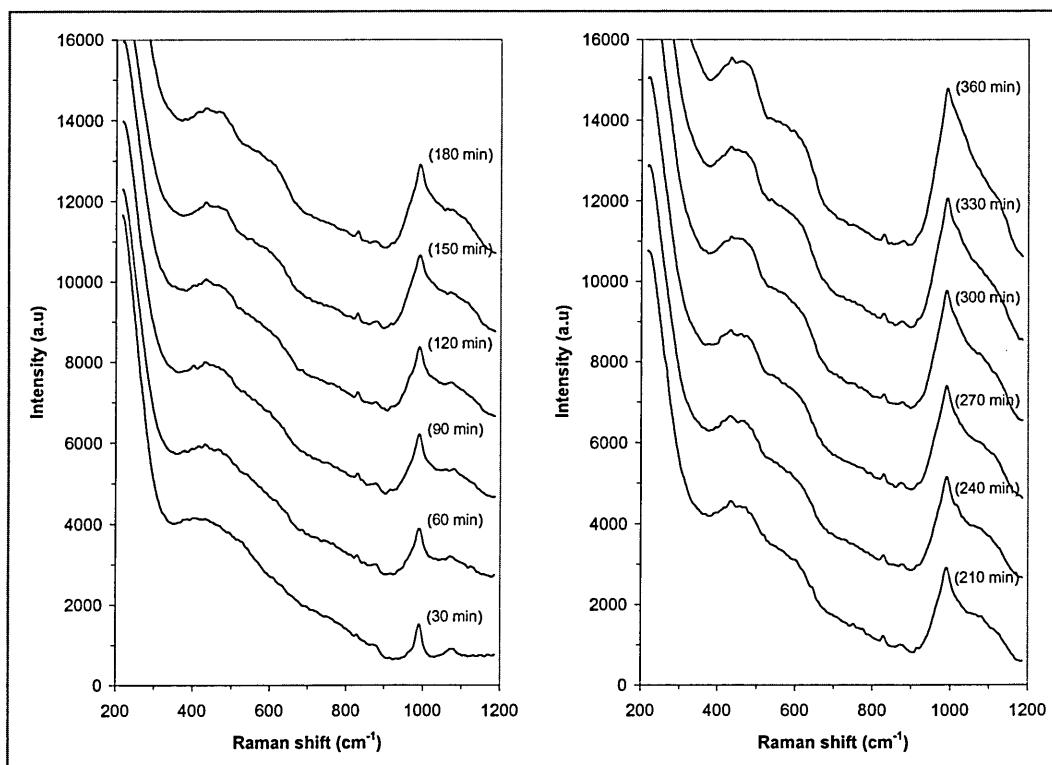


Figure 6.15. Evolution with time of the Raman spectrum of iron in phosphate buffer solution (pH 7.7) at open circuit potential after 30 minutes at -1.0 V.

After 30 minutes at open circuit potential, a broad feature located between 350 and 680 cm⁻¹ and two well resolved bands can be observed. These two bands located at 986 and 1068 cm⁻¹, visible as well on the spectra recorded during the cathodic polarisation at

¹ In the following section, the majority of the results presented are related to a pH 7.7 buffer solution made from 0.05 M KH₂PO₄ + 0.05 M NaOH. From now, it will be mentioned as a phosphate buffer solution.

-1.0 V, have been identified as the vibrational bands of the phosphate ions in solutions. Mentioned too by Melendres *et al.* (31), these bands have been attributed to the symmetric stretching modes (988 cm^{-1}) and the anti-symmetric stretching mode (1068 cm^{-1}) of the hydrogen phosphate ions in solution (HPO_4^{2-}).

After 60 min of experiment, the $900\text{-}1200\text{ cm}^{-1}$ region started to evolve, showing a large increase in the spectral background. This spectral evolution suggested the development of two broad bands overlapping with the two bands attributed to the phosphate ions in solution. Observation of the sample under the optical microscope attached to the system permitted to reveal the presence of a yellowish film covered by a white flocculent precipitate. The presence of such film was attributed to an oxide layer on the sample. According to the width and the position of the bands, it was interesting to theorise that the oxide developed at open circuit potential seemed to be highly disordered and contained absorbed PO_4^{3-} anions.

After 90 minutes, two broad bands became visible within the $360\text{-}680\text{ cm}^{-1}$ region. These two non resolved bands started to become separated to finally appear roughly resolved after 360 minutes. Due to the broadness and the position of these two bands, a clear identification could not be realised without further investigation. Similarly, the evolution of the broad feature, made from several overlapping bands located between 900 and 1200 cm^{-1} , did not allow us to make a clear interpretation of their origin but their intensities increased regularly until the end of the experiment.

6.3.1.2. Potential evolution

During the whole test, the evolution of the open circuit potential was recorded (Figure 6.16). Compared to what has been presented in section 6.2.1, no drastic change in the open circuit potential was observed. However, it could be seen that if the recorded potential was about -750 mV at the start of the experiment, it changed slightly during the first 30 minutes to reach a potential 25 mV lower and finally stay constant until the end of the test.

Even if the potential shift did not seem to be significant it was noticeable enough to suggest that a passive film started to develop at the electrode surface during the early stage of the experiment, and that its nature did not evolve with time. Such interpretation was confirmed by the observation of a film during optical analysis of the sample surface.

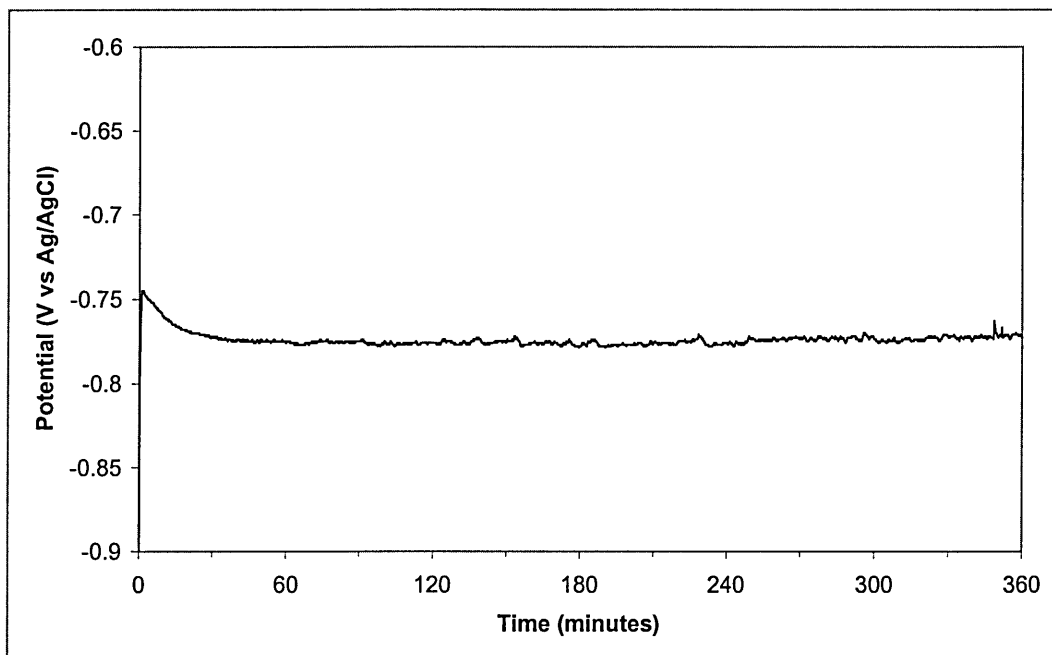


Figure 6.16. Evolution of the open circuit potential of a pure iron disc immersed in phosphate buffer solution (pH 7.7). Potential measured versus Ag/AgCl electrode.

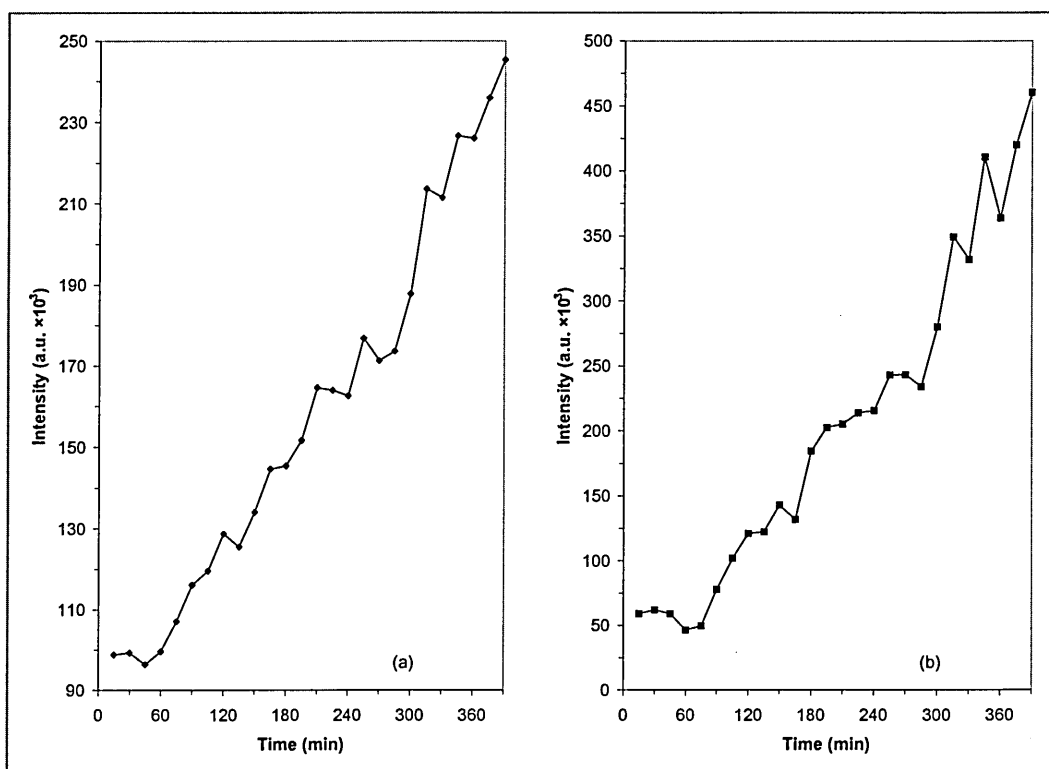


Figure 6.17. Evolution of the area of the phosphate iron compounds versus time at OCP. Integration limits (a) $370-700\text{ cm}^{-1}$ and (b) $850-1160\text{ cm}^{-1}$.

In order to correlate the information obtained from the Raman data and the potential evolution, the spectral region between $370\text{ and }700\text{ cm}^{-1}$, as well as the region between

850 and 1160 cm^{-1} , have been integrated and their results plotted against time (Figure 6.17).

The two plotted curves show a similar trend. They both stay constant during the first 45 minutes and then, their intensities increase linearly until the end of the experiment. Such observation permits us to assert that the bands present in both integrated regions are linked to the same oxide.

Moreover, the phenomenon observed during the early stage of the experiment (observed as well on the plot of the evolution of the potential with time) permit us to suppose that an incubation period precedes the formation of the oxide film on the electrode surface. A valid interpretation, that will justify the potential drop observed, may be the electro-dissolution of the iron surface liberating Fe^{nt} ions into the solution. These liberated ions react with the phosphate ions from the solution to create the passive film on the electrode surface.

6.3.1.3. Optical analysis

Every hour, an optical picture was taken from the electrode. The last picture, recorder after 6 hours at open circuit potential, is presented in Figure 6.18.

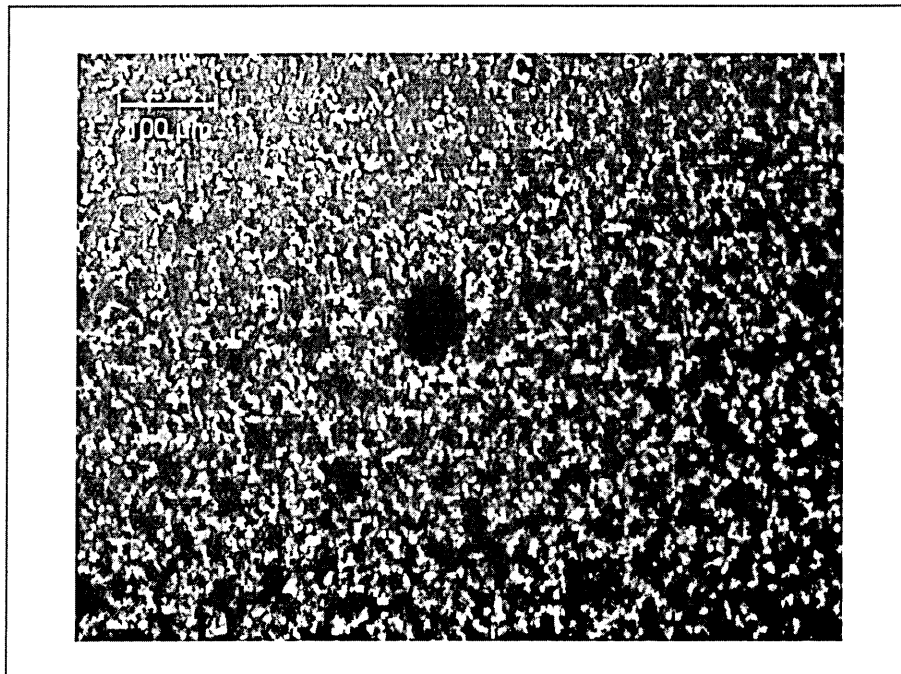


Figure 6.18. Optical picture of the pure iron disc immersed in a phosphate buffer solution for 6 hours at open circuit potential.

From this picture, two characteristics of the oxide layer can be noticed. First, a general observation of the film developed on the sample during the experiment show that the film was made of several islands of corrosion product. Second, a large corroded dot could be observed in the middle of the studied area. This circular stain, located just where the laser was focused, suggests that the laser had an effect on the kinetics of the reaction occurring at the sample surface. This phenomenon may be due to the heating effect mentioned in section 4.1.1. Even if such an effect permits us to be sure that the studied site will corrode, and that some oxide will develop under the laser source, it is then difficult to use the information given by the evolution of the band against time as a quantitative assessment about the kinetics of the reaction.

6.3.1.4. Dry sample analysis

Due to the difficulty of analysing the nature of the passive film in situ, the sample had to be removed from the solution, dried in air and studied by Raman spectroscopy. The comparison between the spectra recorded in and ex situ is presented in Figure 6.19.

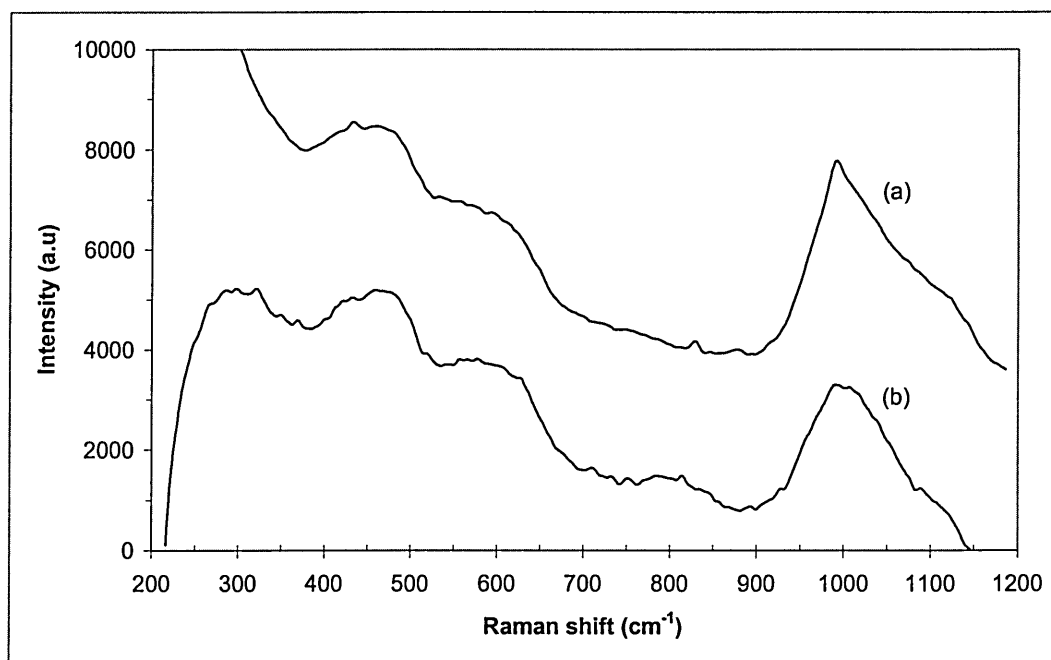


Figure 6.19. Raman spectra of the passive film grown on iron during 6 h at open circuit potential in KH_2PO_4 buffer solution. (a) spectrum recorded in situ, (b) spectrum recorded ex situ.

Despite the fact that the oxide was exposed to air before the ‘ex situ’ analysis, both spectra, recorded ‘in’ and ‘ex situ’ show similar bands, suggesting the presence of the same corrosion product on the sample. However, the presence of the solution can be easily recognised by the broad feature visible below 350 cm^{-1} (due to the Raman activity

of the water) and by the strong band centred at 987 cm^{-1} overlapping with several other bands present between 900 and 1170 cm^{-1} . Attributed previously to the free hydrogen phosphate ions in solution, the origin of the 987 cm^{-1} band can be confirmed by the fact that it is not as well resolved in the spectra recorded 'ex situ' than 'in situ'. However, the presence of such band in the spectra recorded 'ex situ' will suggest that some hydrogen phosphate ions are present in the passive film.

While in the $350\text{-}700\text{ cm}^{-1}$ region, only two broad bands could be observed from the spectrum recorded in situ, the 'ex situ' analysis permitted to reveal the presence of two overlapping band located at respectively 422 and 454 cm^{-1} . Therefore, the oxide observed 'ex situ' could be characterised by 5 broad bands located at 300 , 422 , 454 , 575 and 987 cm^{-1} .

In a previous study, Benzakour *et al.* (32) characterised the passive film on iron in phosphate medium by voltammetry and XPS measurement. The results obtained from their analysis showed that the passive layer was made of both phosphate groups and Fe^{2+} ions. They noted too that HPO_4^{2-} ions were the dominant species in the pH range used (pH 6.8) suggesting the presence of $\text{Fe}(\text{H}_2\text{PO}_4)_2$. Moreover, they showed by running a depth profiling of the phosphate groups that their concentration decreased considerably with increasing depth. This observation suggested that these species existed only on the surface of the film. Finally, the analysis at a depth of about 60 \AA revealed the existence of two iron oxides Fe_2O_3 and Fe_3O_4 . Since none of the characteristic bands of either hematite or magnetite could be observed on the Raman spectra recorded 'in' and 'ex-situ' and, since the technique does not allow the analysis of the nature of the film in depth, it was not possible here to confirm the composition of the film. However, we assume that the observed spectrum was representative of $\text{Fe}(\text{H}_2\text{PO}_4)_2$.

In a study conducted by Melendres *et al.* on the anodic corrosion and film formation on iron on phosphate solutions, the authors analysed, by Raman spectroscopy, the nature of the film developing at different pH values (31). Despite the fact that they used different solutions to cover the whole pH range, the only case in which they managed to observe the presence of magnetite was at a pH of 11.9. Even if the solution used in the current study had a pH much lower than the one used by Melendres *et al.* and even if no Raman spectra have been recorded in similar conditions, the interpretation of the

spectrum from which the presence of magnetite was identified, could be incorrect. This misinterpretation could be due to the presence of two bands assigned to the 550 and 670 cm^{-1} vibrational modes of magnetite. These two bands, showing a poor s/n ratio, could also be due to the presence of a hydrated phosphate.

By comparing the spectra presented by Melendres *et al.* with the spectrum recorded in and ex situ, it became possible to identify the origin of the different bands. Therefore, the 308, the 454 and the 560 cm^{-1} bands have been identified as originating from $\text{FePO}_4 \cdot x\text{H}_2\text{O}$. The 422 and 578 cm^{-1} bands have been identified as vibrational modes of vivianite $\text{Fe}_3(\text{PO}_4)_2 \cdot 8\text{H}_2\text{O}$. Finally, the broad feature centred around 987 cm^{-1} is due to a contribution of both iron hydrated phosphates.

Therefore, it is possible to conclude that the oxide developed at open circuit potential in pH 7.4 phosphate buffer solution is composed of both $\text{FePO}_4 \cdot x\text{H}_2\text{O}$ and $\text{Fe}_3(\text{PO}_4)_2 \cdot 8\text{H}_2\text{O}$, and that none of the $\text{Fe}(\text{H}_2\text{PO}_4)_2$, mentioned by Benzakour and Derja (32), has been observed in the studied conditions.

6.3.2. Cyclic polarisation

To understand the reactions resulting from the oxidation of iron in phosphate buffer solution, a set of 10 successive cyclic polarisation curves was recorded. The aim of running the cyclic polarisation was to identify the different anodic and cathodic waves related to the different oxidation stages and the development of the passive film. For clarity, only cycle 1, 5 and 10 are presented in Figure 6.20.

On the forward scan of the first polarisation cycle, strong ($+175 \mu\text{A} \cdot \text{cm}^{-2}$) and weak ($+25 \mu\text{A} \cdot \text{cm}^{-2}$) anodic waves could be seen at respectively -550 and -150 mV. On the reverse scan of the cycle, while two cathodic waves, associated to the observed anodic ones were expected, only one cathodic reaction could be observed at a potential of -450 mV and a new anodic wave, characterised by the strong positive ($+100 \mu\text{A} \cdot \text{cm}^{-2}$) current was observed at -550 mV.

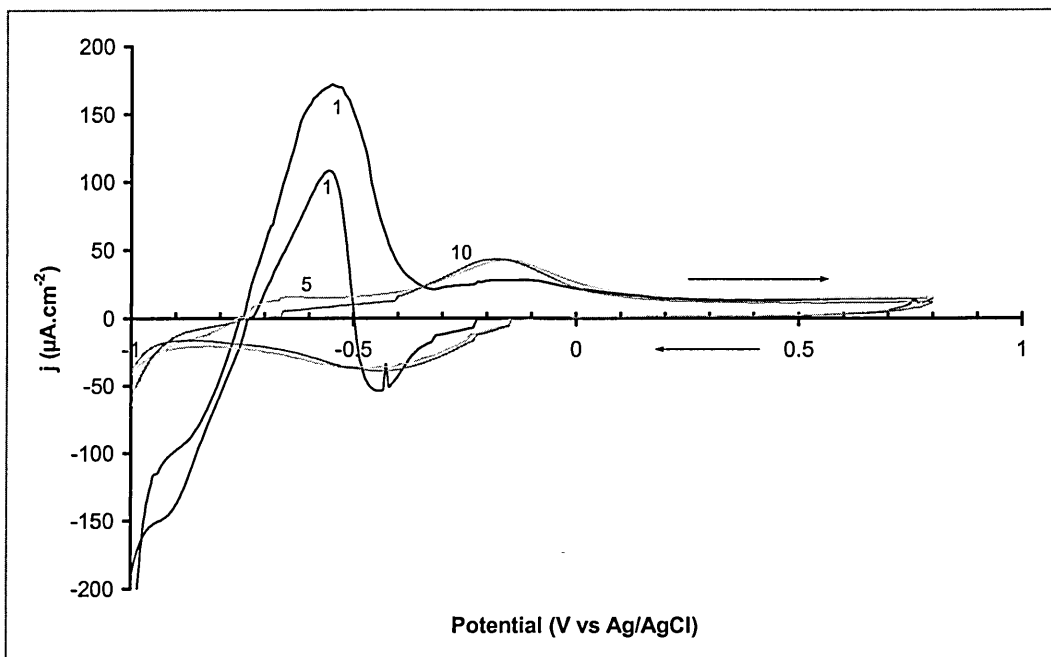


Figure 6.20. Cyclic polarisation of a 10 mm pure iron disc in pH=7.7 phosphate buffer solution after 1, 5 and 10 cycles. Potential switched at +0.8 V, scan rate 5 mV.s^{-1} . The arrows indicate the scanning direction.

Benzakour *et al.* (32), who studied the cyclic voltammograms of iron in similar conditions observed the same anodic and cathodic waves. However, they studied the effect of the sweep rate of the potential and showed that with low scan rate, the first anodic wave (-550 mV) was in fact composed of two very close peaks separated by 8 mV. They attributed the first peak to the formation of the phosphate species following the precipitation of dissolved iron with phosphate ions in the solution (eq. 6.9). The second peak was attributed to the formation of magnetite (Eq. 6.10).



Finally, they explained the presence of the anodic wave, located at -150 mV, to the oxidation of magnetite to hematite as shown by equation 6.11. However, if the theoretical potential they calculated was close to the observed potential for the two first reactions described, the potential calculated for the oxidation of magnetite to hematite did not match at all with the measured potential. They tried to explain the difference between the theoretical value and the experimental one by the strong local artificial acidity which was greater than the acidity of the solution itself. They also claimed that

the presence of magnetite (Fe_3O_4), which partially passivated the electrode, lead to a positive shift of the potential.

The fifth cyclic polarisation recorded here showed an entirely different behaviour to the one observed on the first cyclic polarisation. The first anodic wave, located at -550 mV, was not visible anymore and the intensity of the second anodic one was almost twice as intense than that during the first cyclic polarisation. On the reverse scan, only one cathodic reaction was visible, and was probably associated with the oxidation happening at -150 mV. The fact that the first anodic wave, associated to the electro-dissolution of the iron to Fe^{n+} ions, was not visible anymore was probably due to the presence of a passive film on the sample surface. This prevented a further dissolution of the iron substrate into the solution. Then, since the iron dissolution was not visible during the fifth cycle, the reactivation of the iron dissolution observed during the cathodic scan of the first cycle could not be expected anymore. This could be explained by the presence of a strong passive film on the sample surface.

Between the fifth and the tenth cycle, no real changes between the voltammograms could be observed, suggesting that no evolution of the nature of the oxide could happen once the passive film was grown on the sample.

6.3.3. Anodic waves identification.

6.3.3.1. Raman data

To confirm the origin of the anodic waves observed during cyclic polarisation, a pure 10 mm diameter iron disc was immersed in phosphate solution and successively polarised, for three hours periods, at -550, -150, and -450 mV. To make sure that no oxide was present at the sample surface prior the start of the experiment, the iron disc was polished and pre polarised at -1.0 V for 30 minutes.

Throughout the experiment, the Raman spectra were recorded 'in situ'. The collected spectra are presented in Figure 6.21

As observed during the analysis realised at open circuit potential, the spectrum recorded during the pre-polarisation shows only the separated band due to the hydrogen phosphate ions in solution, suggesting no presence of any kind of oxide at the sample surface. Then, during the polarisation at -550 mV, the evolution of the collected spectra with time showed the presence of the same oxide which started to develop at open

circuit potential. However, the two broad bands, located around 450 and 575 cm^{-1} were not as well resolved as during the OCP experiment, suggesting a lower iron dissolution and film formation of $\text{Fe}_3(\text{PO}_4)_2 \cdot 8\text{H}_2\text{O}$ and $\text{FePO}_4 \cdot x\text{H}_2\text{O}$.

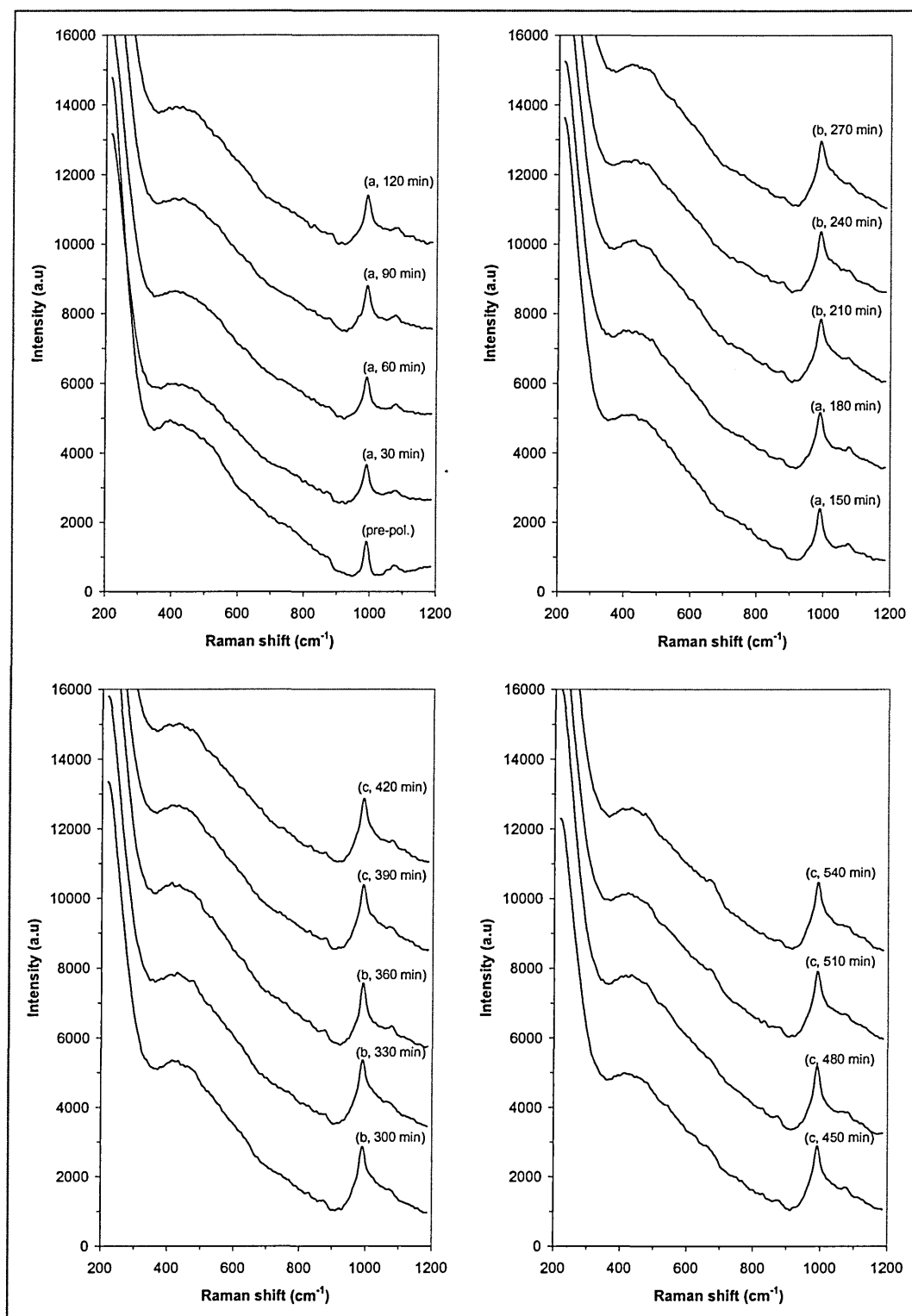


Figure 6.21. Raman spectra of iron in KH_2PO_4 buffer solution during successive polarisation periods of 3 hours at (a) -550 mV , (b) -150 mV and (c) -450 mV . The first spectrum was recorded after 30 min of pre-polarisation at -1.0 V .

After the three hours at -550 mV, the potential applied had been switched to -150 mV to match with the potential of the second anodic wave. Once again, the shape of the spectra recorded during the second polarisation period did not change, suggesting that no different oxide was developing on the electrode surface. The spectrum recorded after three hours of polarisation at -150 mV (fig. 6.21, b, 360 min) was similar to the one recorded at the end of the first polarisation period (fig. 6.21, a, 180 min).

Despite the fact that no noticeable changes were observed during the second polarisation stage, the potential was switched back to -450 mV to match with the cathodic reduction wave described in section 6.3.2. At this potential, the reverse reaction happening at -150 mV was expected and a diminution of the bands related to the oxide film present on the sample was expected. The spectra recorded did not allow us to observe such phenomenon and it was therefore impossible to identify the cathodic reaction. However, on the last spectrum recorded, a small band, centred at 660 cm^{-1} was observed. One of the possible explanations of the presence of such band could be due to the reduction of the outer layer of iron phosphate oxide, exposing the inner layer of magnetite mentioned by Benzakour (32) and Melendres (31) to the laser.

6.3.3.2. Band integration

To follow the growth of the oxide on the substrate, the $930\text{-}1160\text{ cm}^{-1}$ region has been integrated and the result plotted against time. The resulting trace is shown in Figure 6.22. After the 30 first minutes of experiment (during the prepolarisation at -1.0 V), the band area stayed constant, showing that no oxide was developing when a large negative potential was applied. Then, as soon as the applied potential was switched to -550 mV, the band area started to increase linearly, suggesting the development of an oxide layer at the sample surface. After three hours of polarisation, the potential was switched to -150 mV (on the second anodic wave) and the band area appeared to stop increasing. The band evolution even started to show a slow decay between during the cathodic polarisation at -450 mV.

Even if the graph plotted above appears to show the evolution of the oxide band as a function of the potential applied, it is important to note that the observation may not be representative of the real film formation/reduction process happening at the sample surface. A decrease in the growth of the band area could also be due to the saturation of the surface exposed under the laser, as shown by the optical picture shown in Figure 6.18

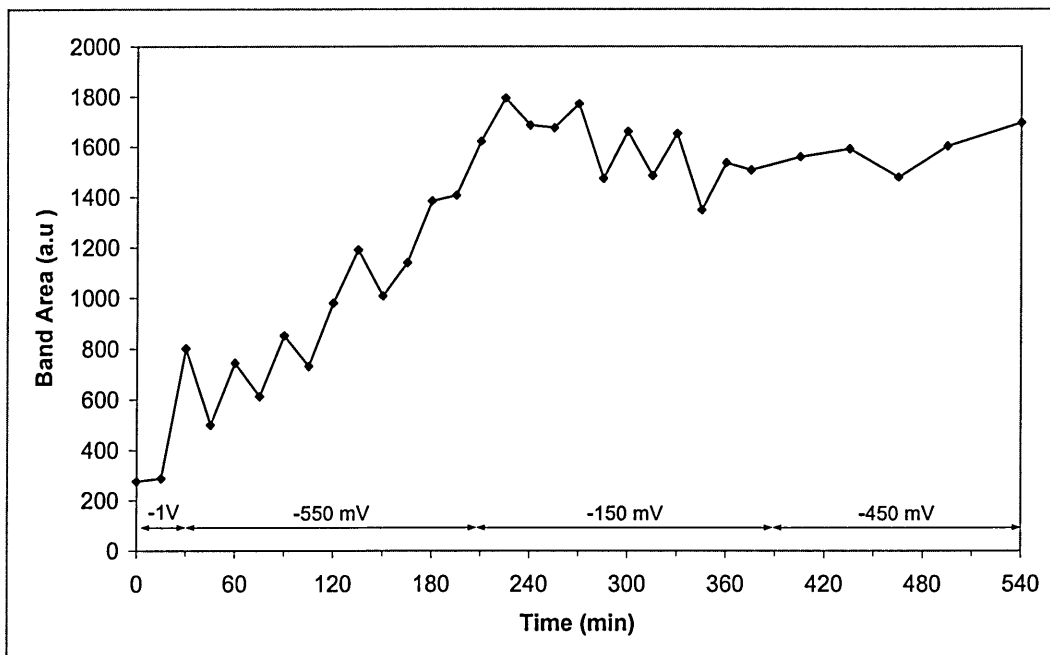


Figure 6.22. Evolution of the area of the $930\text{-}1160\text{ cm}^{-1}$ band from the corrosion product grown on iron in KH_2PO_4 buffer solution during 30 minutes of pre-polarisation at -1.0 V and successive periods of 3 hours at -550 , -150 and -450 mV .

6.3.3.3. Current evolution

To complete the information given by Raman spectroscopy, during the successive polarisation experiment, the current flowing between the counter electrode and the working electrode (iron disc) was recorded. First, it can be seen (fig. 6.23) that a strong negative current ($-250\ \mu\text{A}\cdot\text{cm}^{-2}$) was flowing between the electrodes during the pre-polarisation, suggesting a strong cathodic activity. As soon as the potential was switched to -550 mV , the current increased up to $+125\ \mu\text{A}\cdot\text{cm}^{-2}$ and quickly dropped to $5\ \mu\text{A}\cdot\text{cm}^{-2}$. Even if the strong positive current could be related to the activation of the anodic reaction and particularly to the iron dissolution, the high value reached was more due to an ‘overshooting effect’ due to the potentiostat than to the oxidation reaction itself. The same phenomenon was observed when the potential was switched to -150 mV but, this time, the recorded current was less intense and dropped quicker than when the potential was switched from -1000 mV to -550 mV . As expected, either a reactivation of the electrode surface or a different oxidation reaction happened at -150 mV , but the results obtained by Raman did not allow us to follow the evolution of the surface. Finally, when the potential was changed to -450 mV to match with the cathodic wave observed in Figure 6.20, a negative current was observed. After the overshooting effect

mentioned above, the current quickly became close to zero, suggesting that no real reduction was happening at such potential.

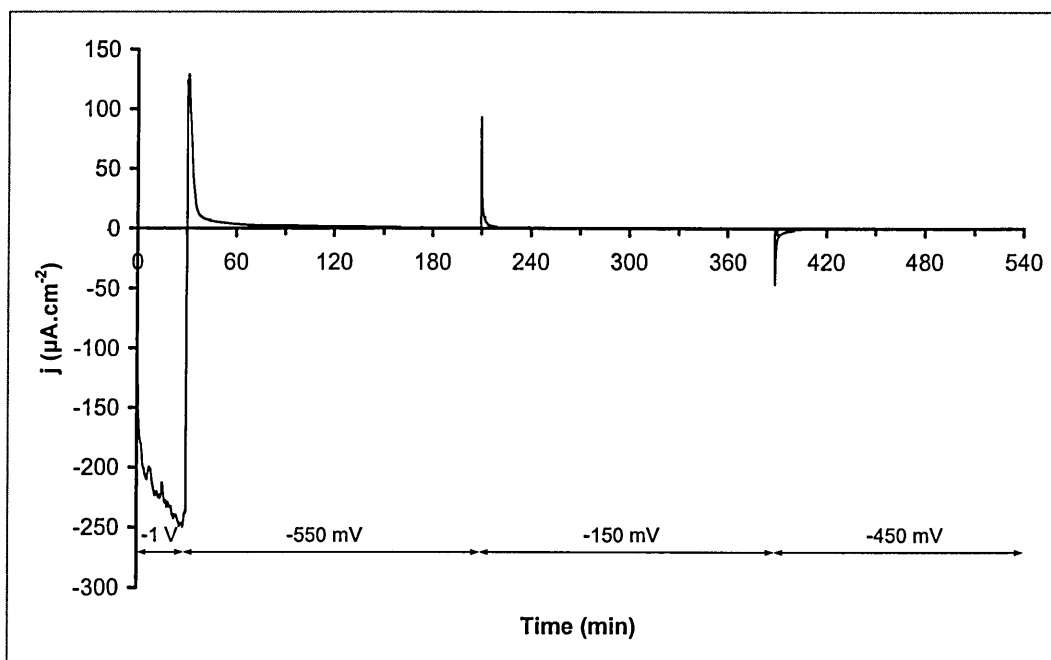


Figure 6.23. Evolution of the current density of pure iron in KH_2PO_4 buffer solution during 30 minutes of pre-polarisation at -1.0 V and successive periods of 3 hours at -550 , -150 and -450 mV .

Therefore, the evolution of the current recorded with time, showed that no real oxidation or film reduction was happening at the sample, once the phosphate passive film was formed.

6.3.4. Pitting experiment

To test the resistance of the passive film grown on the iron sample immersed in phosphate buffer solution, a set of pitting tests were carried out.

The resulting potentiodynamic polarisation curves are illustrated in Figure 6.24. While the first curve (a) shows the cyclic polarisation of iron in phosphate buffer solution, recorded straight after a 30 seconds pre-polarisation period at -1.0 V , the second curve (b) shows the cyclic polarisation recorded in similar conditions but this time, after two hours at open circuit potential. The potential scan was started at -1000 mV and stopped once the current density reached the reverse value of $500\text{ }\mu\text{A.cm}^{-2}$. Once the reverse current had been attained, a 30 s pause was made before the potential was reversed. The scan was finally stopped when the current density reached a value of 1 nA .

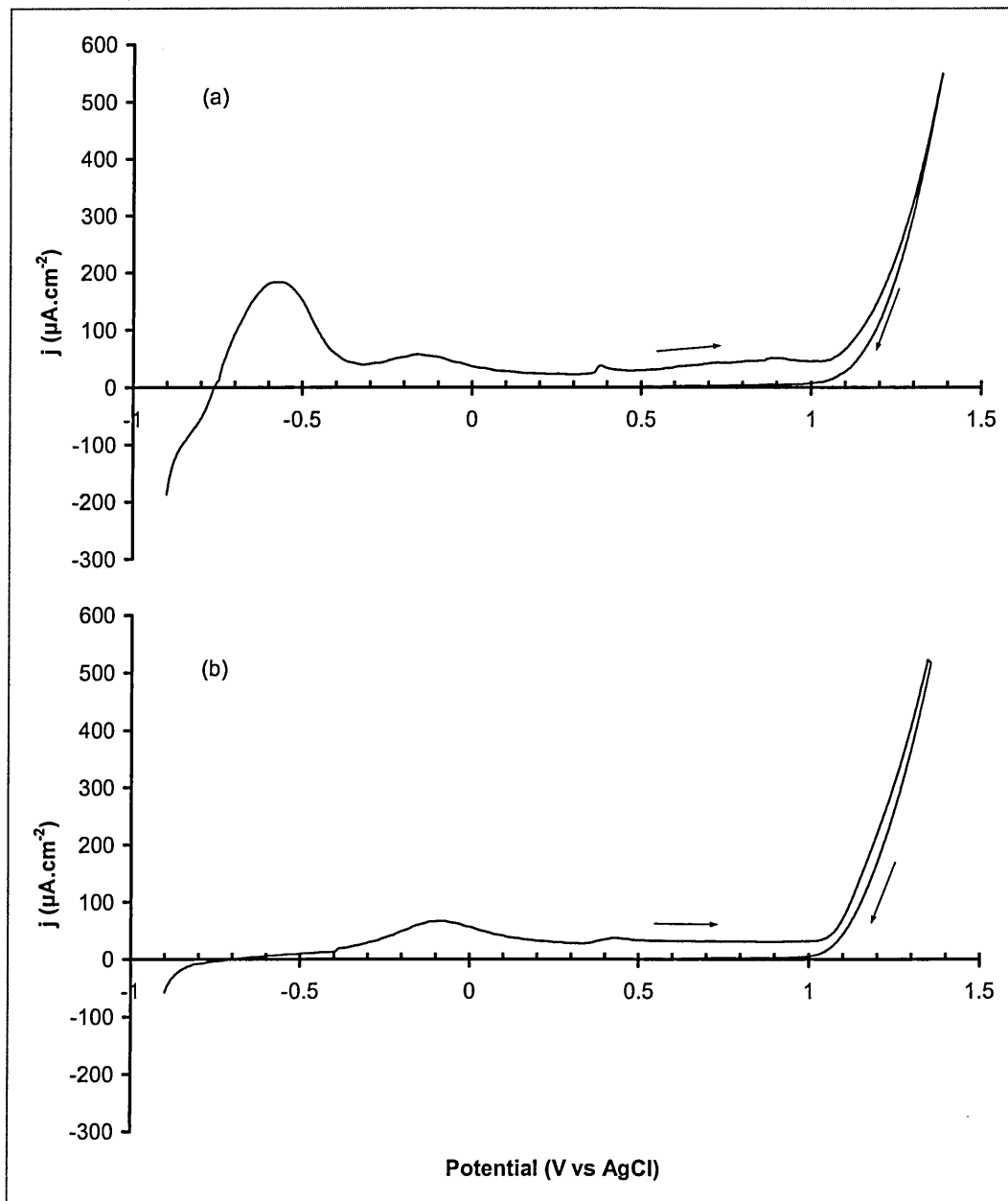


Figure 6.24. Potentiodynamic polarisation curves for iron in (a) KH_2PO_4 buffer solution, (b) following 2h at OCP in KH_2PO_4

When the sample was exposed directly to phosphate buffer solution (a), two anodic waves at respectively -550 and -150 mV and a large passive region (1000 mV wide), which stops when the transpassive dissolution occurs at a potential of 1050 mV, can be seen on the potentiodynamic scan. The main feature observed, reaching a maximum of $180 \mu\text{A}\cdot\text{cm}^{-2}$, is the first anodic wave and is related to the electro-dissolution of Fe(0) to Fe(II). The Fe(II) reacts with the phosphate ions from the solution, as observed during the cyclic polarisation (Figure 6.20). It can also be seen that the protection potential (see section 3.3.3 for definition) is higher than the transpassive dissolution potential suggesting that first; iron in phosphate buffer solution will have a very low tendency to

pit, and second; that the passive film redevelops at the sample surface as soon as the applied potential is lowered.

When the sample is left at open circuit potential for two hours (b), a similar polarisation curve can be observed except that the anodic wave due to the electro-dissolution of iron is not visible anymore. The absence of the first anodic wave is due to the presence of the passive film that acts as a barrier between the iron substrate and the solution. Hence, only the second anodic wave at -150 mV, is visible. It is interesting to note that the maximum current density reached before the potential is reversed is $50 \mu\text{A}\cdot\text{cm}^{-2}$ lower after the two hours at OCP, than when the sample is not polarised prior the potentiodynamic scan. As seen during the analysis of the passive film grown at OCP, the intensity of the Raman bands due to the passive layer increased with time suggesting an increase of the thickness of the iron phosphate film present on the sample surface. The growth of the passive film did not have any effect on the value of the transpassive dissolution potential but the faster decrease of the current density suggests that the repassivation of the exposed sample happens more quickly than without passivation at OCP.

Figure 6.25 shows the same type of potentiodynamic scans as the one presented above but this time the first curve (a) has been recorded just after the addition of 0.15 M NaCl to the phosphate buffer solution. In the second case (b), the sodium chloride has been added just before the start of the potentiodynamic scan, after a 2 hour immersion period at open circuit potential.

When the sample is not left at open circuit potential before starting the potentiodynamic scan (a), the anodic wave due to the electro-dissolution of iron is visible as shown in Figure 6.25.(a) but reaches a maximum current density of $2000 \mu\text{A}\cdot\text{cm}^{-2}$. The rise of the maximum current density suggests that the presence of chloride ions augments the electro dissolution of the iron substrate. Also, in the presence of 0.15 M NaCl, the passive region is now only 250 mV wide and the transpassive dissolution occurs at -81 mV instead of +1050 mV. Once the potential is reversed, the protection potential was much lower than it was in the experiment without added chloride. This phenomenon highlights the fact that not only the dissolution of the passive film occurs, but that pitting of the iron substrate is happening too. In addition, an increase of the current density around -500 mV can be explained by the reactivation of the iron dissolution and the start of the general corrosion process.

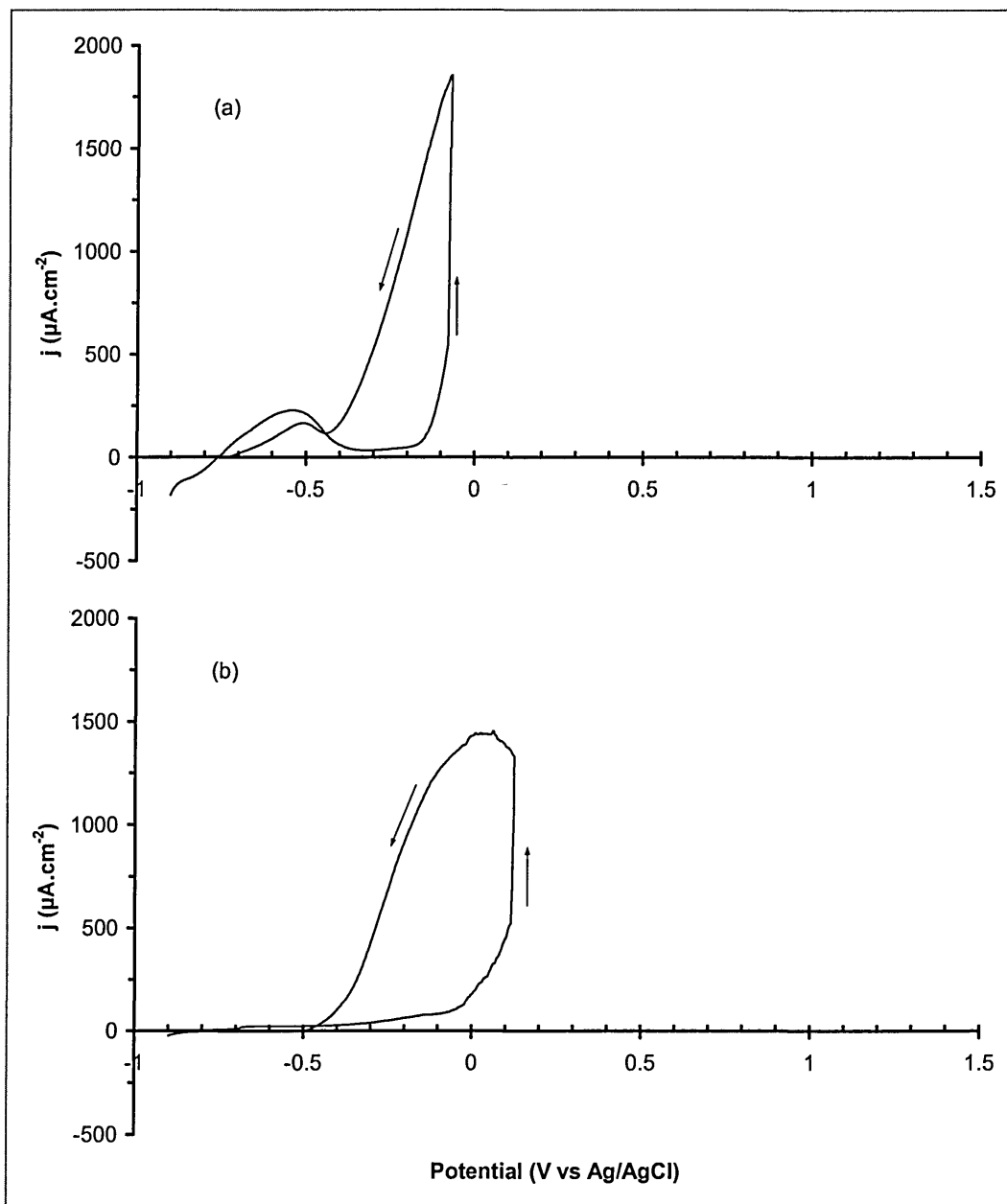


Figure 6.25. Potentiodynamic polarisation curves for iron in (a) Phosphate buffer + 0.15 M NaCl solution and (b) following 2h at OCP in KH_2PO_4 with + 0.15 M NaCl added at the beginning of the sweep.

In Figure 6.25 (b), slightly different behaviour of the sample can be observed due to the two hour immersion period at OCP. As expected, and according to the previous experiment (section 6.3.2), the anodic wave at -550 mV can not be seen anymore, confirming the presence of the film grown during the polarisation at OCP. Moreover, pitting occurs at a potential 200 mV higher ($E_{\text{pit}} = +117$ mV) than during the experiment without passivation. Additionally, the maximum current density reached during the 30 second delay before the reverse of the potential is much lower (by ~ 400 μA) once the iron sample has been passivated. This phenomenon shows that the passive film

increases the resistance of the sample to pitting even if chloride ions are present in the solution.

The pitting experiments described above permitted to demonstrate the efficiency of the passive film developed on iron in phosphate buffer solution. To complete the results obtained during the pitting test, a further investigation of the oxide developing inside the pits could be achieved by Raman spectroscopy. Even is similar work has been already presented by Simard et al. (21) few guidelines will be given in chapter 7.

6.4. Summary

In the current chapter, the nature, the kinetics and the oxidation processes associated with the passive film grown on iron, in three different solutions, at different potentials have been studied. Even if the initial experimental conditions where chosen to give comparable results, entirely different oxides were observed, depending on the environment used.

The work on iron on pH 7.7 borate buffer solution showed that it was not possible to monitor the evolution of iron using conventional Raman spectroscopy. Even if some others have shown by SERS that the film was composed of $\text{Fe}(\text{OH})_2$ and Fe_3O_4 , the results presented in the current work did not allow us to confirm the presence of such materials on the iron surface. One of the reasons why these two well know oxides, usually easily identified by Raman, were not observed here could be due to the thinness of the passive film grown during the polarisation. Such interpretation is doubtful since the oxide present at the iron surface was clearly visible by eye and it did not have the black characteristic colour of magnetite. It is then possible to suppose that the presence of magnetite on the film observed in such conditions could be due to the presence of silver deposited on the electrode to run the SERS analysis. Therefore, it is important to note that the SERS technique is not suitable for in situ corrosion studies of iron in borate buffer solution.

The analysis of the film grown in carbonate/bicarbonate buffer solution allowed us to identify the different oxides present on the iron substrate and to identify the different oxidation processes, and relate them to the anodic and cathodic curves observed during the cyclic voltammetric studies. We have shown that 'green rust' developed on the iron substrate during the early stage of the oxidation processes. Later, an inner film of

magnetite was developed between the 'green rust' layer and the iron substrate and finally, an amorphous layer made of a mixture of α and β -FeOOH was covering the whole oxide structure developed during the oxidation. The film developed either at open circuit potential or at the different applied potential, could be reduced when a cathodic current was applied between the electrodes.

The last system studied (iron in phosphate solution), showed that a strong passive film could be identified as a mixture of $Fe_3(PO_4)_2 \cdot 8H_2O$ and $FePO_4 \cdot xH_2O$. An attempt to study the kinetics of the oxidation processes was achieved, but no valid results could be obtained. This was due to, the difficulty to follow the different oxidation stages, to the fact that the laser had an effect on the sample, increasing the corrosion rate. However, the pitting experiment confirmed that the film developed under such conditions increased the resistance to pitting of the material.

A discussion on the results, the interest and the limitations of using the Raman spectroscopy technique to follow the evolution of the corrosion phenomenon (and some suggestion for improving the results) are presented in chapter 7.

6.5. References

- (1) Bonin PML, Jedral W, Odziemkowski MS, Gillham RW. Electrochemical and Raman spectroscopic studies of the influence of chlorinated solvents on the corrosion behaviour of iron in borate buffer and in simulated groundwater. *Corrosion Science* 2000 11; 42 (11): pp. 1921-1939.
- (2) Bonin PML, Odziemkowski MS, Gillham RW. Influence of chlorinated solvents on polarization and corrosion behaviour of iron in borate buffer. *Corrosion Science* 1998 AUG; 40 (8): pp. 1391-1409.
- (3) Oblonsky LJ, Devine TM. A surface enhanced Raman spectroscopic study of the passive films formed in borate buffer on iron, nickel, chromium and stainless-steel. *Corrosion Science* 1995 JAN; 37 (1): pp. 17-41.
- (4) Gui J, Devine TM. In situ vibrational spectra of the passive film on iron in buffered borate solution. *Corrosion Science* 1991; 32 (10): pp. 1105-1124.
- (5) Gui J, Devine TM. Obtaining surface-enhanced Raman spectra from the passive film on iron. *Journal of the electrochemical society* 1991; 138 (5): pp. 1376-1384.
- (6) Sato N, Noda T, Kudo K. Thickness and structure of passive films on iron in acidic and basic solution. *Electrochimica Acta* 1974 8; 19 (8): 471-475.
- (7) Diez-Perez I, Gorostiza O, Sanz F, Muller C. First stage of electrochemical growth of the passive film on Iron. *Journal of the electrochemical society* 2001; 148 (8): pp. B307-B313.

- (8) Bhardwaj RC, Gonzalez-Martin A, Bockris JOM. In-situ scanning tunnelling microscopy studies on passivation of polycrystalline iron in borate buffer. *Journal of electrochemical society* 1991; 138 (7): pp. 1901-1908.
- (9) Sato N, Kudo K, Nishimura R. Depth analysis of passive films on iron in neutral borate solution. *Journal of the electrochemical society* 1976: pp. 1419-1977.
- (10) O'Grady WE. *Journal of electrochemical society* 1980; pp. 129:555.
- (11) Oblonsky LJ, Davenport AJ, Ryan MP, Isaacs HS, Newman RC. In situ X-ray absorption Near Edge structure study of the potential dependence of the formation of the passive film on iron in borate buffer. *Journal of the Electrochemical society* 1997; 144 (7): pp. 2398-2404.
- (12) Nagayama M, Cohen M. *Journal of the Electrochemical society* 1962; 109: pp. 781.
- (13) Odziemkowski MS, Schuhmacher TT, Gillham RW, Reardon EJ. Mechanism of oxide film formation on iron in simulating groundwater solutions: Raman spectroscopic studies. *Corrosion Science* 1998; 40 (2-3): pp. 371-389.
- (14) Simpson LJ, Melendres CA. Temperature dependence of the surface enhanced Raman spectroelectrochemistry of iron in aqueous solutions. *Electrochimica Acta* 1996; 41 (10): pp. 1727-1730.
- (15) Boucherit N, Hugot-Le Goff A, Joiret S. Raman studies of corrosion films grown on Fe and Fe-6Mo in pitting conditions. *Corrosion Science* 1991; 32 (5-6): pp. 497-507.
- (16) Rubim JC, Dunnwald J. Enhanced Raman scattering from passive film on silver-coated iron electrodes. *Journal of electroanalytical chemistry* 1989; 258: pp. 327-344.
- (17) Mahomey MR, Howard MW, Cooney RP. Carbon dioxide conversion to hydrocarbons at silver electrode surfaces : Raman Spectroscopic evidence for surface carbon intermediates. *Chemical Physics Letters* 1980; 71 (1): pp. 59-63.
- (18) Cooney RP, Mahomey MR, Howard MW. Intense Raman spectra of surface carbon and hydrocarbons on silver electrodes. *Chemical Physics Letters* 1980; 76 (3): pp. 448-452.
- (19) Howard MW, Cooney RP, McQuillan AJ. *Journal of Raman spectroscopy* 1980; 9: pp. 273.
- (20) Thanos ICG. In situ Raman and other studies of electrochemically oxidized iron and iron-9% chromium alloy. *Electrochimica Acta* 1986 7; 31 (7): pp. 811-820.
- (21) Simard S, Odziemkowski MS, Irish DE, Brossard L, Menard H. In situ micro-Raman spectroscopy to investigate pitting corrosion product of 1024 mild steel in phosphate and bicarbonate solutions containing chloride and sulfate ions. *Journal of Applied Electrochemistry* 2001 AUG; 31 (8): pp. 913-920.
- (22) Gui J, Devine TM. A SERS investigation of the passive films formed on iron in mildly alkaline solutions of carbonate/bicarbonate and nitrate. *Corrosion Science* 1995 8; 37 (8): pp. 1177-1189.
- (23) Refait P, Memet J-, Bon C, Sabot R, Génin JMR. Formation of the Fe(II)-Fe(III) hydroxysulphate green rust during marine corrosion of steel. *Corrosion Science* 2003; 45 (4): pp. 833-845.

- (24) Legrand L, Abdelmoula M, Gehin A, Chausse A, Génin JMR. Electrochemical formation of a new Fe(II)-Fe(III) hydroxy-carbonate green rust: characterisation and morphology. *Electrochimica Acta* 2001 3/30; 46 (12): pp. 1815-1822.
- (25) Legrand L, Sagon G, Lecomte S, Chausse A, Messina R. A Raman and infrared study of a new carbonate green rust obtained by electrochemical way. *Corrosion Science* 2001 SEP; 43 (9): pp. 1739-1749.
- (26) Boucherit N, Delichere P, Joiret S, Hugot-Le Goff A. Passivity of iron and iron alloys studied by voltammetry and Raman Spectroscopy. *Material science forum* 1989; 44&45: pp. 51-62.
- (27) Nauer G, Strecha P, Brindakonopik N, Liptay G. Spectroscopic and thermo-analytical characterization of standard substances for the identification of Reaction-Products on iron. *Journal of thermal analysis* 1985; 30 (4): pp. 813-830.
- (28) Drissi SH, Refait P, Abdelmoula M, Génin JMR. The preparation and thermodynamic properties of Fe(II)-Fe(III) hydroxide-carbonate (green rust 1); Pourbaix diagram of iron in carbonate-containing aqueous media. *Corrosion Science* 1995; 37 (12): pp. 2025-2041.
- (29) McMurray HN, Worsley DA. Scanning electrochemical techniques for the study of localised metallic corrosion. *Research in chemical kinetics* 1997; 4: pp. 149-202.
- (30) Baek W-, Kang T, Sohn H-, Kho YT. In situ surface enhanced Raman spectroscopic study on the effect of dissolved oxygen on the corrosion film on low carbon steel in 0.01 M NaCl solution. *Electrochimica Acta* 2001 4/30; 46 (15): pp. 2321-2325.
- (31) Melendres CA, Camillone I, N., Tipton T. Laser Raman spectroelectrochemical studies of anodic corrosion and film formation on iron in phosphate solutions. *Electrochimica Acta* 1989; 34 (2): pp. 281-286.
- (32) Benzakour J, Derja A. Characterisation of the passive film on iron in phosphate medium by voltammetry and XPS measurements. *Journal of Electroanalytical Chemistry* 1997; 437: pp. 119-124.

Chapter 7. General discussion

The main objective of the work presented here was to assess the feasibility of using the Raman spectroscopy technique to evaluate corrosion processes. Since numerous studies had already been published by a large number of research groups (section 3.7), the questions that needed to be answered were more concerned with the limitations of the technique itself and, about the conditions in which Raman spectroscopy could be employed to make the most of the results. It is apparent from the literature review that, most of the previous work in this area is concerned with samples removed from the solution, and analysed in the dehydrated condition or, by using the surface enhanced Raman spectroscopy (SERS) technique.

Unfortunately, the two analytical methods listed above ('ex situ' and SERS) could not really be considered truly representative of a study of the corrosion processes since they may have an effect on the nature of the oxide studied during the analysis. Removing the solution in which the sample had been corroded and therefore, exposing the corrosion products to air, induces a modification of the structure of the oxide developed in situ. Thus, the results obtained from the analysis of such modified oxides did not reflect the true oxidation processes happening at the sample/solution interface. Moreover, depositing islands of silver, gold, copper or other metals used to enhance the Raman signal during the SERS studies may, apart from affecting the sample surface during the deposition process, create a galvanic cell and affect the corrosion processes. Other examples of the limitations of the SERS technique are presented in section 3.7.4 and 6.1.2.3.

Therefore, the objective of the current work was to evaluate the *feasibility of using conventional Raman spectroscopy for 'in situ' corrosion studies*. To achieve this objective it was first necessary to *identify the potential advantages* and the *limitations of the technique* itself. Once these had been identified (chapter 4), it was necessary to *assess the technique* through different experimental tests, as presented in chapters 5 and 6.

7.1. Potential advantages of the Raman technique

Due to the origin of the Raman effect (section 2.2) and to the fact that it is directly linked to the vibrational modes of the molecules, the information given by Raman spectroscopy is equivalent to a 'molecular fingerprint' and it allows the *identification of particular molecular species* present on the sample under study. Moreover, since this molecular probe has a scattering cross section directly proportional to the concentration of the studied element, Raman spectroscopy offers up the *possibility of studying the kinetics* of the formation and /or the conversion of particular molecular species. This advantage is complimented by the fact that a relatively good spectrum can be recorded in a short period of time. Also, since the technique can be considered as *non intrusive*, no alteration of the sample will be induced by the technique. Therefore, the corrosion processes happening at the sample surface will not be affected. Besides, since no *particular sample shape, size or preparation* is needed, the sample under investigation can be studied with no major limitations. Additionally, the ability to analyse the sample *in situ* allows temporal evolution of the sample reactions to be made without risk of damaging the products developed during the oxidation processes. Such oxide modifications have often been observed when the corrosion product had to be dried in air or exposed to low pressure. Finally, due to the use of a microscope to focus the laser onto the surface being investigated, *the corrosion processes can be followed on a microscopic scale*.

7.2. Challenges of using Raman spectroscopy

However, if the use of Raman spectroscopy offers a large number of advantages, a certain number of limitations have to be identified and evaluated.

First, as has been observed that the use of the laser source employed to excite the molecules under investigation produces a *localised heating effect*. For example, the heating effect producing, oxidation of magnetite to hematite, has been observed (section 4.1.1.2) and calculated using Raman spectroscopy (section 4.1.1.3). Even if the temperature calculated for the hematite powder (120°C) was far below the temperature at which the oxidation of magnetite to hematite started to occur (200°C) the temperature change could not be neglected since it had a clear effect on the sample studied. This phenomenon has also been observed during the investigation of the passive layer

developing on iron in phosphate buffer solution (section 6.3.1.3) where the oxidation reaction was clearly accelerated under the laser source.

Second, the experimental used to evaluate the heating effect highlighted the tendency of the coloured oxide to be subject to *resonance Raman enhancement* (section 2.1.3). This phenomenon was seen to produce a change in the intensities of the studies species, thereby restricting the ability to follow accurately the kinetics of the reaction. Therefore it became impossible to prepare a calibration system to run PCA and PLS tests and evaluate the amount of individual oxides present on the sample surface at different stages of the oxidation processes (section 4.1.2). However, it did not prevent obtaining several valid results from which the kinetics of the oxidation processes could be assessed (chapter 5 and 6).

The reason why SERS had been used so often by different research groups was to improve the quality of the signal measured from a studied sample. Such alternative had to be taken into consideration due to the *weakness of the Raman scattering effect* which does not allow the identification of thin films. This was confirmed by the inability to identify the thin passive film grown on iron in a borate buffer solution (section 6.1). However, adopting a SERS approach was not considered necessary since, in numerous cases, good Raman spectra were obtained. The Resonance Raman effect observed on oxides such as hematite and magnetite probably helped us to detect accurately the presence of thin oxide film which could not have been detected if there were not subject to resonance enhancement.

Another well known phenomenon often associated with Raman spectroscopy is the increase of the spectral background due to *fluorescence* (2.1.4). Fluorescence limits the observation and identification of Raman bands and can be difficult to eliminate. Since it is often originating from the colour of the sample studied or the environment in which it is studied (e.g. aqueous solution), the use of coloured solution with Raman is difficult. One possible solution to reduce the phenomenon is to select a different laser source.

In addition, even if depth profiling can be conducted by Raman on transparent materials, the high visible absorption of the oxides observed during the corrosion studies did not allow a depth profile survey of the corrosion layer. This inability to study the evolution of the film grown in depth reduced the information on the evolution of the film. It often became difficult to identify with certainty the corrosion processes

occurring between the substrate and the upper oxide layer. However, it was still possible by applying different electrode potentials, to reduce the oxide layers one after another and identify the structure of the oxide film.

Finally, the combination between the small size of the area studied over the whole exposed surface and the fact that the sample surface is always susceptible to change with time increased the *difficulty in obtaining reproducible results*. This was illustrated, in the case of the ECCS, by the fact that the laser could be initially focused on a site that could either react as a cathode or as an anode (section 4.1.5) and therefore be subject to entirely different chemical reactions and Raman response.

7.3. Study of pure iron oxidation processes in different solutions.

Despite the fact that particular attention had to be taken to overcome the different challenges met during the preliminary work, it was possible, by conducting various Raman investigations, to identify the nature of the corrosion product and study the kinetics of the oxidation of iron under different conditions.

7.3.1. Iron in Sodium Chloride solution

7.3.1.1. Simple iron wire model system

The work performed on a pure iron wire immersed in 3.5 % NaCl solution at open circuit potential showed that the oxide layer was composed of lepidocrocite (γ -FeOOH). The production of such oxide was preceded by an initiation period confirmed by the evolution of the free corrosion potential with time. It had not been possible to identify the nature of the initiation reaction due to a large degree of fluorescence.

During the initial stage of the oxidation of iron polarised at -300 mV, no fluorescence effect was observed rather two bands, attributed to 'green rust' were detected. Then, magnetite (Fe_3O_4), goethite (α -FeOOH) and lepidocrocite (γ -FeOOH) were successively observed. From this the structure of the oxide developed on iron is presented in figure 5.4. However, since in the final few spectra recorded, all oxides except green rust were still visible, the only certain conclusion was that the oxide was made of a multi layer structure and was not homogeneous. One possibility of improving the chances of growing a homogeneous passive film on the iron substrate would be to use a rotating

electrode. However the operator will have to be aware that the electrode rotation will create some perturbation in the solution which will lead to difficulties in focusing the laser onto the sample, through the solution. To confirm the presence of a layered film it would be interesting to, once the sample has been polarised for several hours to grow the passive film, polarise cathodically the sample in order to reduce the whole oxide layer and study by Raman the evolution of the surface. It will as well permit an identification of the reverse reactions and identify the corrosion processes and kinetics.

Thus, since no fluorescence could be observed on an iron substrate immersed in 3.5 % chloride solution and polarised at -300 mV, yet could be observed in similar conditions at open circuit potential, it is now possible to conclude that the fluorescence was due to either the solution or the iron substrate. Therefore, we can conclude that the fluorescing species originated on the iron substrate at open circuit potential. Hence, the reduction in fluorescence was due to a covering of the fluorescing layer by lepidocrocite and not to the fact that it could be burned out by the long exposing time.

7.3.1.2. **Twin iron model system**

The analysis conducted on the twin iron model system permitted the isolation of the anodic and the cathodic reactions sites. The in situ analysis showed that, while the cathode remained unreacted, the oxidation of the anode consisted of a two step process. It began with the growth of a layer of magnetite onto the iron substrate and was followed by the development of an outer layer of lepidocrocite. The value of the potential difference applied had a non negligible effect: the higher the potential difference, the thicker was the magnetite layer and the longer it took before it was covered by lepidocrocite.

The optical analysis conducted either in or ex situ permitted to show that the oxide layer was first not homogeneously spread on the cathode (due to the proximity of the anode / cathode, i.e., short diffusion path) and second that different oxides, which were not observed during the in situ analysis, were present on the surface. It was concluded that the presence of such oxides (green rust, $\text{Fe}(\text{OH})_3$, and $\beta\text{-FeOOH}$) was due to the fact that an outer layer had been removed from the sample by the rinsing process, thereby exposing an inner layer or that the lepidocrocite layer was oxidised on exposure to air. Consequently it is important to realise that the results obtained in and ex situ may be entirely different and that it is necessary to use a technique that allows in situ

analysis to obtain accurate information on the corrosion processes. It has been shown here this could be achieved by Raman spectroscopy.

7.3.2. Iron in borate buffer solution

Due to the large number of studies realised on iron in borate buffer solution, it was decided to use a similar system to validate the feasibility of running in situ corrosion studies by conventional Raman. It appeared that, due to a lack of Raman activity, none of the Raman spectra recorded over time, at open circuit potential, permitted us to identify the nature of the passive film. However, the evolution of the potential with time allowed us to confirm that the passivation of iron in borate solution consisted of a single stage process. It has also been identified that one possible explanation for the lack of Raman activity was the thin nature of the oxide film. Therefore, different attempts to identify the oxide layer on the iron surface were unsuccessful (although it could be done by SERS). However, despite the fact that some oxide could be identified by SERS, and not by conventional Raman spectroscopy, we showed that the use of SERS could influence the corrosion reactions.

7.3.3. Iron in carbonate buffer solution

The analysis, by cyclic voltammetry and Raman spectroscopy, permitted the identification of the structure of the oxide developing at open circuit potential and, the correlation between the anodic/cathodic potential cycles and the electrochemical reaction occurring on the iron in the carbonate buffer solution. It has been shown that at open circuit potential, the iron substrate starts to oxidise forming Fe^{n+} ions. Liberated into the solution, these free ions react with the carbonates anions from the solution and give a II/I ratio carbonate green rust: $[Fe_4^{(II)}Fe_2^{(III)}(OH)_{12}][CO_3 \cdot 2H_2O]$. Once the green rust layer covers the surface of the electrode, it naturally evolves into goethite (α -FeOOH) and akaganeite (β -FeOOH). The polarisation experiments showed that the oxidation reactions were reversible and that an inner layer of magnetite developed between the green rust layer and the iron substrate. It was concluded that the passive film was composed of a superposition of layers of magnetite (Fe_3O_4), carbonate green rust and a mixture of α - and β -FeOOH. Through this set of experiments, it has been possible to prove that Raman spectroscopy can be used to follow both the formation and the conversion of particular molecular species.

7.3.4. Iron in phosphate buffer solution

The evolution of the Raman spectra recorded with time at open circuit potential permitted us to show that an amorphous passive layer was developing at the iron surface. The 'ex situ' analysis first showed, that the passive layer was stable and was not subject to any chemical modification once exposed in air and second, that it was composed of a mixture of $Fe_3(PO_4)_2 \cdot 8H_2O$ and $FePO_4 \cdot xH_2O$. An attempt to study the kinetics of the passive film was made however, due to the modification of the corrosion rate by the laser source, it was not possible to obtain a quantitative result. Finally, several pitting corrosion tests showed that, when no aggressive ions were introduced into the solution, the exposed substrate became passive as soon as the potential was reduced. In addition, the introduction of chloride ions into the solution showed that the passive film had a true protection effect and that it reduced the iron's tendency to pit. Finally, no Raman investigations of the corrosion product developing inside the pits have been realised. However, some preliminary test permitted to show that the spectrum acquisition was not straightforward since some difficulties were encountered. First, it appeared that the resulting product of the oxidation of the iron exposed to chloride ions was precipitating into the solution making it difficult to focus the laser onto the oxide. Second, the development in depth of the pit during the experiment made it difficult to focus the laser onto the bottom of the pit and hence acquire data. One possible way to analyse the nature of the oxide will be to initiate the pits by imposing a potential above that of the pitting potential. Once the pits are initiated and the oxide developed, the potential can be reduced thereby avoiding further growth. It will be then possible to analyse, in situ, the nature of the oxide produced.

7.4. Future work

The utilisation of the pure iron model systems allowed us to evaluate the capability and identify the different limiting factors of the Raman spectroscopy technique applied to corrosion studies. Even if we managed to obtain good results and identify the film developing on iron in different conditions, it has to be kept in mind that such basic systems are rarely used in everyday applications. Even if further work has to be achieved to complete what has been started here, it is important now, to try to apply the technique to study the different types of corrosion in the different practical systems.

7.4.1. Sample heterogeneity

It appeared difficult in some cases to obtain reproducible results due to the lack of homogeneity of the sample studied and to the fact that corrosion was initiated on a microscopic scale. However, as shown by the study using a twin iron wire system, it is possible to record Raman spectra from two well separated sites by using a computerised 2D stage. The use of a computerised mapping stage, linked to a spectrometer equipped with a CCD detector, permits also the realisation of maps and images which are representative of a whole area. The Raman mapping technique can be widely applied to corrosion studies since it will give information on what is happening elsewhere on the surface. It can be used for example to study the galvanic corrosion processes where two different materials are in contact. Unfortunately, mapping a surface takes time and the results obtained from a system in constant evolution may not be representative of the corrosion at one specific time and could not be considered as a 'snapshot' of the corrosion state during the analysis. Therefore, it will be necessary to find the best compromise between spectra quality, size of the area studied and acquisition time. However, imaging, with a shorter acquisition time can be one solution to faster acquisition and might be therefore appropriate for corrosion studies. This might be achieved only if the collected signal is sufficient.

7.4.2. Study of Stress corrosion cracking

Due to the possibility to study in situ, on a microscopic scale, the corrosion processes of a system, it may be possible to investigate, by Raman, the phenomenon of stress corrosion cracking. This can be achieved by using an appropriately designed rig that will allow the application of a stress either in tension or compression. Combined with mapping and imaging, it should be therefore possible to study the initiation and development of stress corrosion cracking.

7.4.3. Study of alternative conversion coatings for aluminium.

Cr(VI) compounds, mainly chromates, are widely applied as corrosion inhibitors in the form of conversion coatings or as pigments in paints. A wide range of metals and alloys, such as iron, steels, aluminium alloys, zinc, copper, lead and others, can be protected using chromates. Their high efficiency/cost ratio has made them standard corrosion inhibitors. Despite their high efficiency and established industrial application,

environmental laws in many countries have imposed severe restrictions on the use of chromate, due to its high toxicity (carcinogen) and consequent environmental hazards.

Regarding the protection of aluminium alloys, in recent years, more ecological alternatives have been investigated to replace chromates in their different fields of application. Lanthanide compounds are among the substances that have been investigated as an alternative to chromates; both as cathodic inhibitors and in the development of conversion coatings. Furthermore, lanthanides can be considered as economically competitive products because, as elements, some of them are relatively abundant in nature; cerium, for instance, is as plentiful as copper.

7.4.4. Coupling of Raman spectroscopy and ESEM

Due to the type of information given by Raman spectroscopy (qualitative and quantitative) it is a complementary tool for corrosion studies. Therefore, associated with other techniques such as the environmental scanning electron microscopy (ESEM), it will offer the possibility to study pitting and cracking corrosion processes happening during wet/dry corrosion cycles. This could be achieved by coupling a Raman spectrometer to an ESEM, holding a constant pressure into the cell and changing the sample temperature using a Pelletier stage to condense/evaporate a solution onto the sample surface. Raman spectroscopy will then offer the possibility to obtain information from the sample during the wet periods (which is not possible by ESEM) and complete the optical information obtained during the dry periods.